THE UNIVERSITY OF MICHIGAN

7692-2-Q

Electromagnetic Coupling Reduction Techniques

Second Quarterly Report
15 February 1966 - 14 May 1966

By

J.A.M. Lyon, N.G. Alexopoulos, D.R. Brundage,
A.G. Cha, C.J. Digenis, M.A.H. Ibrahim
and Y.K. Kwon

May 1966

Contract No. AF 33(615)-3371
Project 4357, Task 435709

Prepared for

Air Force Avionics Laboratory
United States Air Force, AFSC
Wright-Patterson AFB, Ohio 45433

TABLE OF CONTENTS

LIST OF FIGURES

LIST OF FIGURES
(continued)

LIST OF FIGURES
(continued)

ABSTRACT

A detailed analysis is presented of a flush-mounted impedance strip which lies between a magnetic line source and a field point locating the aperture of a receiving antenna. In this analysis, the assumption has been made that the line source, and the impedance strip are each of infinite length. This analysis shows the influence of the surface impedance of the strip upon the coupling between the assumed magnetic source and a field point on the ground plane beyond the strip. The analysis clearly shows the desirability of having the surface impedance with a capacitive reactance characteristic. Some verification of this analysis has been obtained experimentally through the use of a flush-mounted corrugated metal obstacle between two antennas.

In this report, information is presented on the influence on radiation pattern of a given antenna, such as a slot or horn in the near presence of absorbing material. In some cases, the absorbing material is contained within the flare of the antenna. In other cases, the absorbing material is mounted flush in the surrounding ground plane. In still other cases, the absorbing material protrudes above the ground plane.

Results are reported upon a series of experiments using rectangular slot antennas where one or both of the antennas is surrounded by a choke trench. The trenches were circular in form. The depth of the trenches was chosen so as to offer a given type of reactance.

Work has continued during this period, on providing simple absorbing materials whose electrical characteristics can be varied according to a specific need for isolation. A large number of mixes of absorbing materials were made and the electrical characteristics were obtained for each mix.

I
INTRODUCTION

In the next section, a detailed mathematical account is given of the analysis of a flush-mounted impedance strip. The problem is considered as a two dimensional one. It is recognized that the mathematical model can be confirmed only in part by experimental analysis. However, it is believed that the results of this analysis indicate some of the important influences of an absorbing layer between two antennas. The analysis is based upon the assumed knowledge of the surface impedance. Introducing this as a factor, analysis then indicates the amount of attenuation obtained as a wave passes over such a strip from one antenna to another. The required character of this surface impedance is explored in this analysis and the advantage of capacitive reactance is apparent. The dependence of the coupling level on the spacing between antennas and the intervening impedance strip is shown in this analysis.

A series of measurements has been made using both E-secotral and H-sectoral horns. Radiation patterns were obtained on such horns both with and without small wedges of absorbing material inserted within the horns. Such absorbing material did not have a marked influence on the directivity of the main beam of such horns. However, a substantial reduction in the efficiency of the horn as a radiator took place and therefore, a much reduced gain in the direction of the main beam was observed. Such radiation pattern results are important in considering any reduced coupling associated with insertion of absorber. The coupling has only been reduced approximately in proportion to the reduction of gain. This can be considered a rather undesirable way of reducing coupling. Similar experiments were made with horns for absorber mounted on the ground plane near the horn in question. The absorber on the ground plane was relatively effective in reducing coupling; a reduction in coupling level of approximately 20 db was observed.

The use of a circumferential choke surrounding a rectangular slot antenna has been observed to produce a change in coupling of the order of 3 db. A second such choke trench around the other antenna would result in another 3 db change of coupling. The use of choke trenches increased the directivity of a rectangular slot antenna as observed by the radiation patterns of such antennas.

During this report period, the experiments dealing with slots and intervening layers of absorbing material were continued. The sensitivity of the decoupling effect of such slabs was observed as a function of frequency during these tests. Such tests were made in the anechoic chamber and represent a refinement over earlier tests reported. Various thicknesses of the slab of absorber were used. The radiation patterns of both E and H-planes were measured for the slots as used in conjunction with such slabs of absorber.

A series of studies was made for the coupling between two slots with an intervening metal corrugated section in between the slots. In the first attempt, the metal corrugations were mounted above the ground plane and in this way one antenna was obscured optically from the other by the corrugated section acting as an obstacle; up to 28 db increased isolation was observed with the metal corrugation so used. In a second series of experiments on the coupling between two slots, the corrugated metal section was mounted flush between the two slots. The depth of the trenches between the metal surfaces was kept constant. The effect on coupling was observed as a function of frequency of operation. It was found that the corrugated metal surface was very frequency sensitive. Such experiments have been helpful in indicating the direction for further work in using metal corrugations. In order to obtain broadband characteristics, different depths of corrugations will be helpful. Likewise, different separations between corrugations will be useful.

In order to expedite the work on increasing the isolation between antennas, readily fabricated artificial materials have been studied. Several mixes of paraffin wax, carbon black, powdered iron, and powdered aluminum, have been made. The electrical characteristics of some of these mixes has been ascertained. At the present time, additional electrical measurements must be made so that the characteristics can be carefully catalogued to indicate the exact mix necessary to give desired electrical characteristics.

II

ANALYSIS OF FLUSH-MOUNTED IMPEDANCE STRIP

2.1 Detailed Formula

The effect of a flush-mounted impedance strip on the field distribution is investigated. The model to be considered is shown in the Fig. 2-1. The strip is infinitely long. In general, rigorous analysis of the model becomes extremely difficult if the width "w" of the strip is comparable with the wavelength, and, if the field point of interest and the source point are near the strip edge. Therefore, the approach taken in this report is strictly on the basis of a first order approximation and the following assumptions are made:

i) The width of the impedance strip is larger than wavelength, i.e. $w >> \lambda$.

ii) The surface impedance Z_s of the strip is not large.

iii) Both the field point and source are located far from the nearest edges of the impedance strip.

The assumptions (i) and (ii) are necessary purely because the integrations involved have to be performed by the steepest descent or stationary phase method and the assumption (iii) is to avoid involvement with extremely complicated integral equations.

If the magnetic line source is given by

$$\bar{M}(\bar{r}) = \hat{x}_o M \delta(\bar{\rho} - \bar{\rho}_o) \tag{2.1}$$

the non-vanishing component of magnetic fied H_x satisfies the two-dimensional wave equation

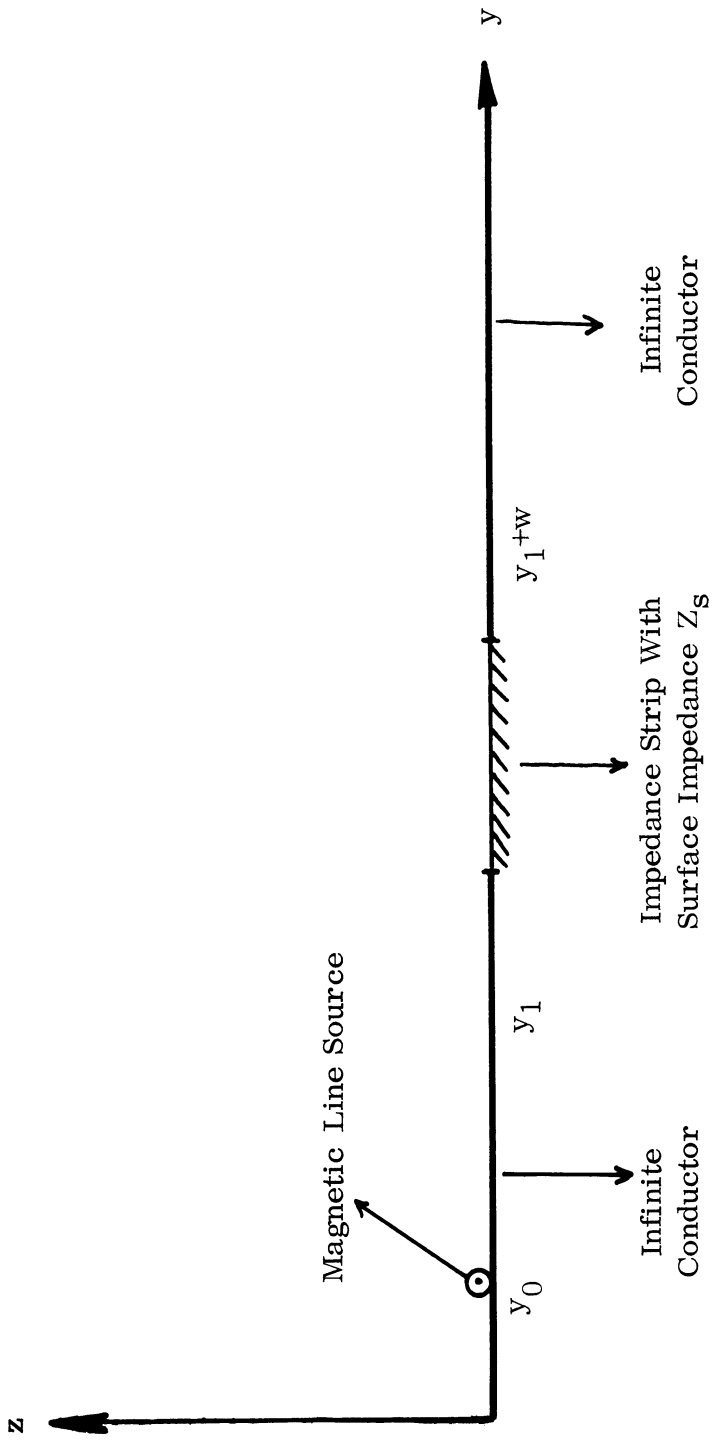

FIG. 2-1: THE MATHEMATICAL MODEL FOR THE PROBLEM.

$$(\nabla^2 + k^2) H_x(\bar{\rho}) = j\omega\epsilon M \delta(\bar{\rho} - \bar{\rho}_o) \quad , \quad \text{with} \tag{2.2}$$

$$\frac{\partial}{\partial x} = 0, \quad \bar{\rho} = (y, z), \quad \bar{\rho}_o = (y_o, o) \quad .$$

The non-vanishing electric field components E_x and E_z are given in terms of H_x by

$$E_y = \frac{1}{j\omega\epsilon} \frac{\partial H_x}{\partial z} \quad , \quad E_z = \frac{1}{-j\omega\epsilon} \frac{\partial H_x}{\partial y} \quad . \tag{2.3}$$

The solution H_x of Eq. (2.2) must satisfy the radiation condition at $|\rho| \longrightarrow \infty$.

When there is no impedance strip, the solution of the Eq. (2.2) is immediate:

$$H_x = -\frac{\omega\epsilon}{2} M H_o^{(2)} \left(k\sqrt{(y-y_o)^2 + z^2}\right) \tag{2.4}$$

$$E_y = j\frac{1}{2} M \frac{\partial}{\partial z} H_o^{(2)} \left(k\sqrt{(y-y_o)^2 + z^2}\right) \tag{2.5}$$

and

$$E_z = -j\frac{1}{2} M \frac{\partial}{\partial y} H_o^{(2)} \left(k\sqrt{(y-y_o)^2 + z^2}\right) \tag{2.6}$$

In order to introduce approximation, consider the model shown in Fig. 2-2, where the impedance strip is extended from $y = y_1$, to $y = \infty$. Since one is only interested in the field at $y > y_1$, the field can be viewed as arising from an equivalent magnetic current distribution $M_x = -E_z$ flowing on a perfectly conducting plane at $y = y_1$ (Fig. 2-3). To obtain the Green's function for this condition, it is convenient to introduce a new coordinate y_A defined by

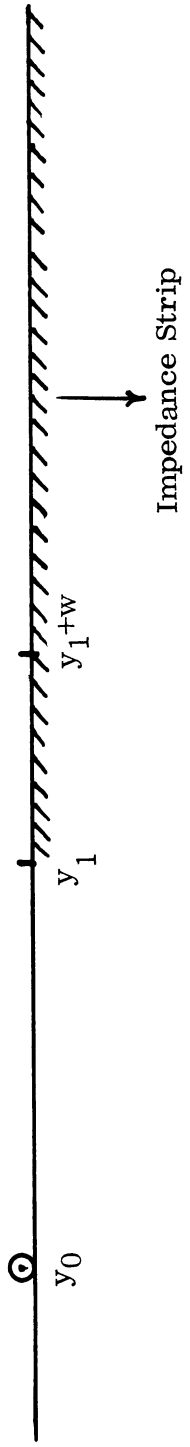

FIG. 2-2: SIMPLIFIED MODEL TO CALCULATE FIELD ON IMPEDANCE STRIP.

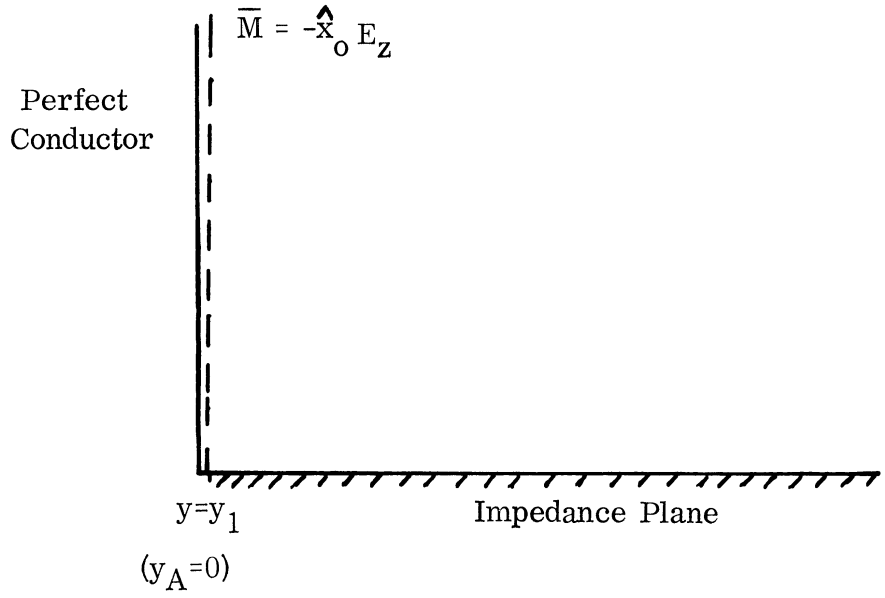

FIG. 2-3: MODEL EQUIVALENT TO FIG. 2-2.

$$y_A = y - y_1 \tag{2.7}$$

Then, the Green's function for the quarter-space is given by

$$G(y_A, z, o, z') = -\frac{j}{2\pi}\int_{-\infty}^{\infty} d\beta \frac{e^{-j\beta y_A}}{\sqrt{k^2-\beta^2}} \left[e^{-j\sqrt{k^2-\beta^2}\,|z-z'|} - \Gamma(\beta)\, e^{-j\sqrt{k^2-\beta^2}\,(z+z')}\right] \tag{2.8}$$

where

$$\Gamma(\beta) = \frac{kZ_1 - \sqrt{k^2-\beta^2}}{kZ_1 + \sqrt{k^2-\beta^2}}$$

and

$$Z_1 = Z_s \Big/ \cdot \sqrt{\frac{\mu}{\epsilon}} \tag{2.10}$$

By introducing $\rho(\beta)$ defined by

$$\Gamma(\beta) = 1 - \rho(\beta) \tag{2.11}$$

$$\rho(\beta) = \frac{2\sqrt{k^2-\beta^2}}{kZ_1 + \sqrt{k^2-\beta^2}} \tag{2.12}$$

G can be written as

$$G(y_A, z:o, z')$$

$$= -\frac{j}{2\pi}\int_{\infty}^{\infty} d\beta \frac{e^{-j\beta y_A}}{\sqrt{k^2-\beta^2}}\left[e^{-j\sqrt{k^2-\beta^2}\,|z-z'|} - e^{-j\sqrt{k^2-\beta^2}\,|z+z'|}\right.$$

$$\left. + \rho(\beta)e^{-j\sqrt{k^2-\beta^2}\,(z+z')}\right] \qquad (2.13a)$$

$$= -\frac{j}{2}\left[H_o^{(2)}\left(k\sqrt{y_A^2+(z-z')^2}\right) - H_o^{(2)}\left(k\sqrt{y_A^2+(z+z')^2}\right)\right]$$

$$-\frac{j}{2\pi}\int_{-\infty}^{+\infty} d\beta \frac{e^{j\beta y_A}}{\sqrt{k^2-\beta^2}}\rho(\beta)e^{-j\sqrt{k^2-\beta^2}\,(z+z')} \quad . \qquad (2.13b)$$

The path of integration is shown in Fig. 2-4. However, if one chooses the branch cuts as in Fig. 2-5 the imaginary part of $\sqrt{k^2-\beta^2}$ becomes always negative on entire top sheet of the two-sheeted Riemann surface. The singularities of $\rho(\beta)$ in Eq. 2.13 are simple poles at:

$$\sqrt{k^2-\beta^2} = -kZ_1 = -k(R_1 + jX_1) \qquad (2.14a)$$

$$\beta_p = \pm k\sqrt{1-Z_1^2} \qquad (2.14b)$$

$$Z_1 = R_1 + jX_1 \qquad R_1 \geq 0 \qquad (2.14c)$$

One notes from Eq. (2.14a) that the poles β_p lie on the top sheet only when

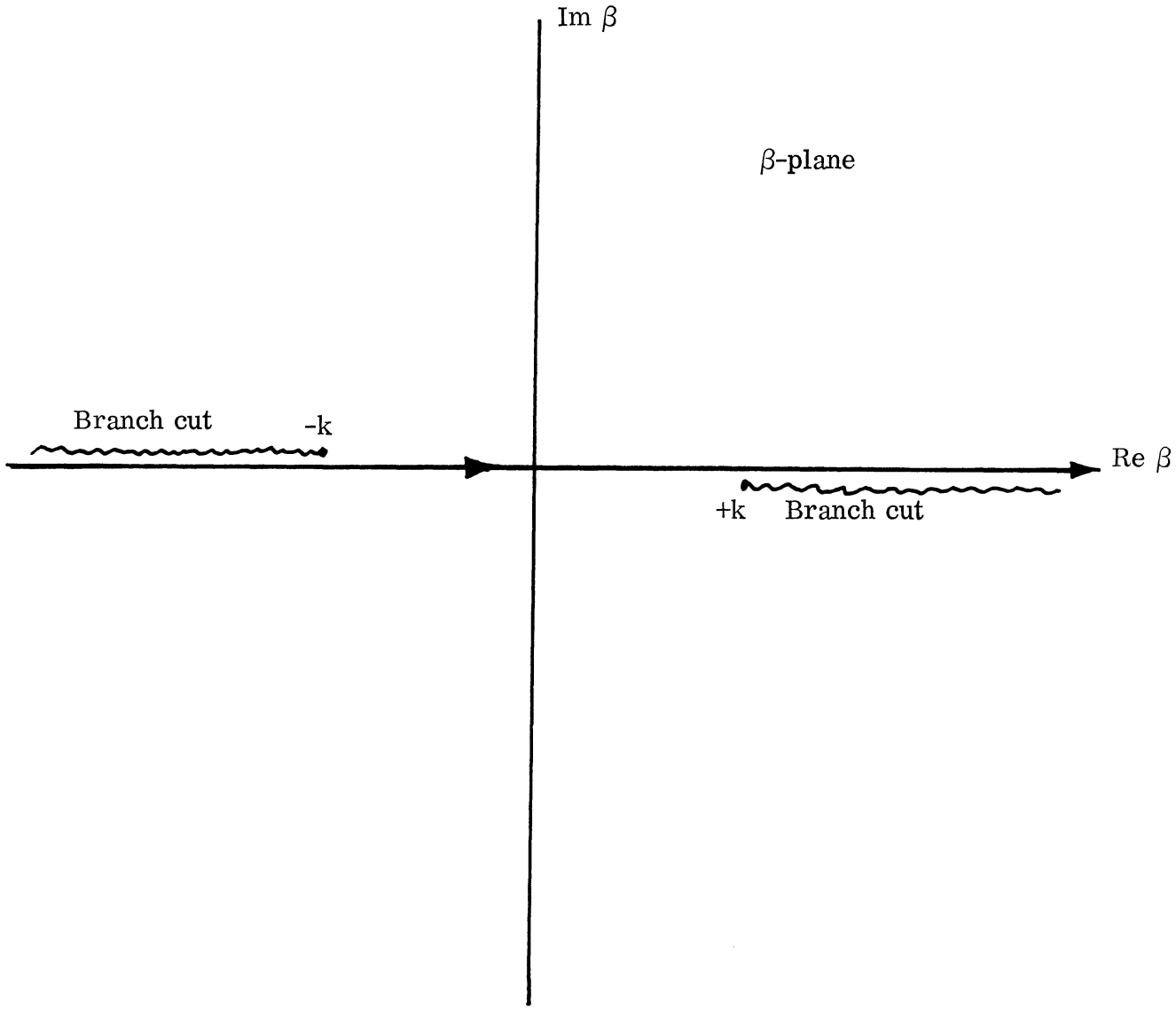

FIG. 2-4: THE PATH OF INTEGRATION FOR EQ. (2.13b)

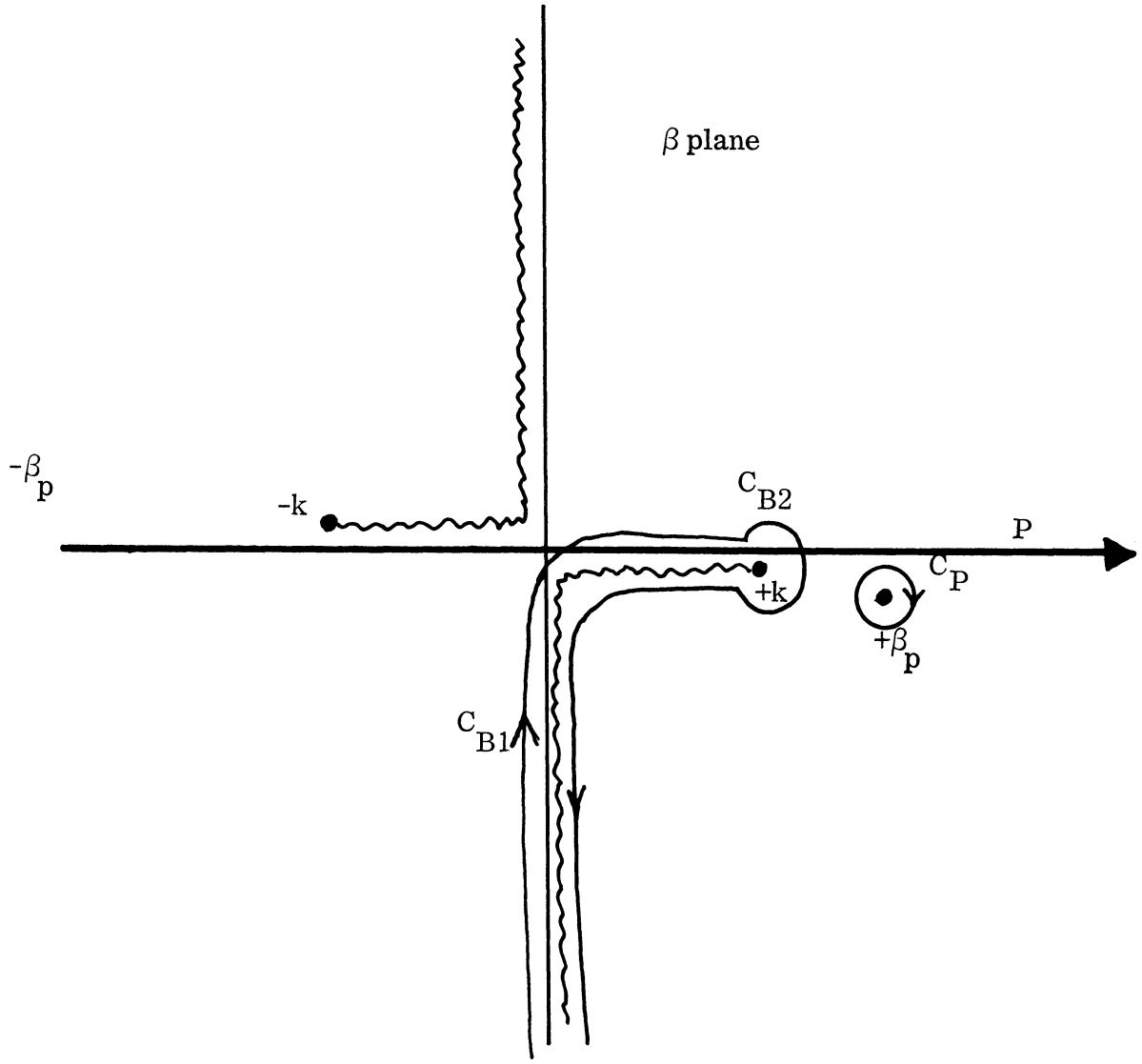

FIG. 2-5: ALTERNATE INTEGRAL PATH FOR EQ. (2.13b).

imaginary part of $Z_1 > 0$, in which case they are located in the 4th and 2nd quadrants. Then, the contour P can be deformed into the contour $C_{B_1} + C_{B_2} + C_p$. It can be easily proved that the contribution from the integration over C_{B_2} vanishes as the radius of the circle C_{B_2} goes to zero. Then Eq. (2.13a) becomes:

$$G(y_A\, z : o,\, z')$$

$$= -\frac{j}{2\pi} \int_{C_{B_1}} d\beta \, \frac{e^{-j\beta y_A}}{\sqrt{k^2 - \beta^2}} \left[e^{-j\sqrt{k^2 - \beta^2}\,|z - z'|} - \Gamma(\beta) e^{-j\sqrt{k^2 - \beta^2}\,(z+z')} \right] d\beta$$

$$+ 2 \frac{Z_1}{\sqrt{1 - Z_1^2}} e^{-jk\sqrt{1 - Z_1^2}\, y_A} e^{jkZ_1(z+z')} U(I_m Z_s) \qquad (2.15)$$

where

$$U(x) = \begin{cases} 1 & \text{when } x > 0 \\ o & x \leqslant 0 \end{cases} \qquad (2.16)$$

Upon introducing change of variable

$$\zeta = \sqrt{k^2 - \beta^2}, \qquad \beta d\beta = -\zeta d\zeta \qquad (2.17)$$

in the integral over C_{B_1}, one notes that ζ is real and varies from $+\infty$ to $-\infty$ as β moves along C_{B_1} in the direction shown in Fig. 2-5. Thus, Eq. (2.13a) transforms into

$$G(y_A, z; o, z') = -\frac{j}{2\pi}\int_{-\infty}^{\infty} d\zeta \frac{e^{-j\beta\sqrt{k^2-\zeta^2}\, y_A}}{\sqrt{k^2-\zeta^2}}\left[e^{-j\zeta(z-z')} - \frac{kZ_1-\zeta}{kZ_1+\zeta}e^{-j\zeta(z+z')}\right]$$

$$+ 2\frac{Z_1}{\sqrt{1-Z_1^2}} e^{-jk\sqrt{1-Z_1^2}\, y_A} e^{jkZ_1(z+z')} U(I_m Z_s) \qquad (2.18)$$

The replacement of $|z-z'|$ by $(z-z')$ in the integrand is justified by noting that the part of the integral containing the $\exp(-i\zeta(z-z'))$ term is insensitive to the algebraic sign of $(z-z')$.

The magnetic field in the quarter-space in Fig. 2-3 can be expressed in terms of the Green's function just obtained as:

$$H_x = -j\omega\epsilon\int_o^{\infty} dz' M_x(o, z') G(y_A, z; o, z') dz$$

$$= +j\omega\epsilon\int_o^{\infty} dz' E_z(o, z') G(y_A, z; o, z') dz' \quad . \qquad (2.19)$$

If values of M_x or E_z at $y_A = 0$ are known, the H_x in the quarter space is uniquely determined using the above equation. Since, unfortunately, this is not the case, one approximates that

$$E_z \cong E_z^{(inc)}$$

where $E_z^{(inc)}$ is given by Eq. (2.6). The assumption (ii) in the beginning of this chapter is to justify this approximation. Under the approximation (2.20), one can write Eq. (2.19) as:

$$H_x = \frac{1}{2}\omega\epsilon \int_o^\infty dz' \left[\frac{\partial}{\partial y} H_o^{(2)}\left(k\sqrt{(y-y_o)^2+z'^2}\right)\right]_{y=y_1} G(y_A, z; o, z') \tag{2.21}$$

or, by using Eq. (2.18) for G, one gets:

$$\begin{aligned} H_x = & -\frac{j}{4\pi}\omega\epsilon \int_o^\infty dz' \left[\frac{\partial}{\partial y} H_o^{(2)}\left(k\sqrt{(y-y_o)^2+z'^2}\right)\right]_{y=y_1} \\ & \cdot \int_{-\infty}^{\infty} d\zeta \frac{e^{-j\sqrt{k^2-\zeta^2}\, y_A}}{\sqrt{k^2-\zeta^2}} \left[e^{-j\zeta(z-z')} - \frac{kZ_1-\zeta}{kZ_1+\zeta} e^{-j\zeta(z+z')}\right] \\ & + \omega\epsilon \frac{Z_1}{\sqrt{1-Z_1^2}} e^{-jk\sqrt{1-Z_1^2}\, y_A} e^{jkZ_1 z} U(X_1) \\ & \cdot \int_o^\infty e^{jkZ_1 z'} \left[\frac{\partial}{\partial y} H_o^{(2)}\left(k\sqrt{(y-y_o)^2+z'^2}\right)\right]_{y=y_1} \end{aligned} \tag{2.22}$$

Next, consider the physical configuration shown in Fig. 2-6. The incident wave is assumed to be given by Eq. (2.22). As in the previous case, a new coordinate y_B is introduced, which is defined by $y_o = y - (y_1 + w)$. Now, one considers only the region S wherein $y_B > o$, and $z > o$. In this region, H_x satisfied the equation

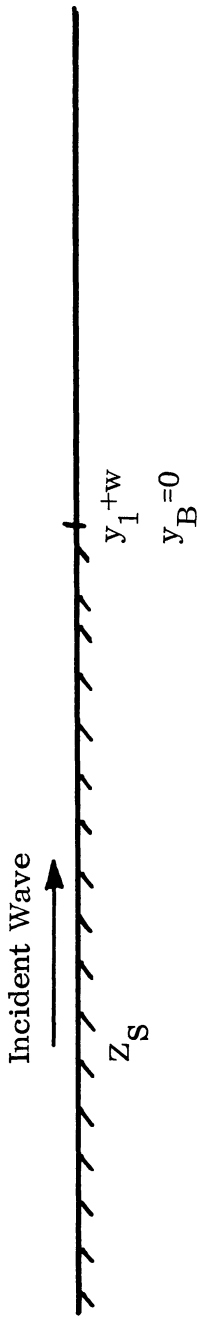

FIG. 2-6: SIMPLIFIED MODEL FOR EVALUATING FIELDS.

$$\nabla^2 H_x + k^2 H_x = 0 \tag{2.23}$$

Subject to, in addition to the radiation condition,

$$\frac{\partial H_x}{\partial y} = 0 \qquad \text{on} \quad z = 0 \qquad (y_B > 0) \quad . \tag{2.24}$$

Correspondingly one chooses a Green's function

$$G(y_B, z: y'_B, z')$$

satisfying

$$(\nabla^2 + k^2)\, G = -\delta (y_B - y_{B'})\, \delta (z - z') \tag{2.25}$$

subject to a boundary condition

$$\frac{\partial G}{\partial z} = 0 \qquad \text{on} \qquad z = 0 \quad (y_B > 0) \tag{2.26}$$

and the radiation condition.

By using the two-dimensional Green's theorem one gets:

$$H_x(y^{(B)}, z) = -\int_o^\infty \left[G \frac{\partial}{\partial y'_B} H_x(y', z') - H_x \frac{\partial}{\partial y'_B} G \right]_{y'_B = 0} dz' \quad . \tag{2.27}$$

As the Green's function, one chooses

$$G = -\frac{j}{4\pi} \int_{-\infty}^{\infty} d\zeta \, \frac{e^{-j\zeta (y_B - y'_B)}}{\sqrt{k^2 - \zeta^2}} \left[e^{-j\sqrt{k^2 - \zeta^2}\,|z - z'|} \right.$$

$$+e^{-j\sqrt{k^2-\zeta^2}\,(z+z')}\Big] \quad . \tag{2.28}$$

The path of integration is the same as the one shown in Fig. 2-4. One can avoid a cumbersome integration difficulty involving $z-z'$ by deforming the path of integration around the singularities as demonstrated in one previous case. The result is

$$G = -\frac{j}{4\pi}\int_{-\infty}^{\infty} d\xi\, \frac{e^{-j\sqrt{k^2-\xi^2}\,\left|y_B - y'_B\right|}}{\sqrt{k^2-\xi^2}}\left[e^{-j\xi(z-z')}+e^{-j\xi(z+z')}\right] \tag{2.29}$$

Now, once again, assume that H_x and $\frac{\partial}{\partial y}(H_x)$ in Eq. (2.27) can be approximated by the value of $H_x^{(inc)}$ and $\frac{\partial}{\partial y}(H_x^{(inc)})$, where $H_x^{(inc)}$ is given by Eq. (2.22). Under the approximation, the integrand of Eq. (2.27) is given by:

$$G\,\frac{\partial}{\partial y'_B} H_x(y'_{B'}, z')\Big|_{y'_B = 0}$$

$$= +j\,\frac{1}{(4\pi)^2}\,\omega\epsilon\left\{\int_0^{\infty} dz''\left[\frac{\partial}{\partial y} H_0^{(2)}\left(k\sqrt{(y-y_o)^2+z''^2}\right)\right]_{y=y_1}\right\}$$

$$\cdot\left\{\int_{-\infty}^{\infty} d\zeta\, e^{-j\sqrt{k^2-\zeta^2}}\, w\left[e^{-j\zeta(z'-z'')} - \frac{kZ_1-\zeta}{kZ_1+\zeta}\, e^{-j\zeta(z'+z'')}\right]\right\}$$

$$\cdot \left\{ \int_{-\infty}^{\infty} d\xi \, \frac{e^{-j\sqrt{k^2-\xi^2}}}{\sqrt{k^2-\xi^2}} \; y_B \left[e^{-j\xi(z-z')} + e^{-j\xi(z+z')} \right] \right\}$$

$$- \frac{k\omega\epsilon}{4\pi} Z_1 e^{-jk\sqrt{1-Z_1^2}\, w} e^{jkZ_1 z'} \qquad U(X_1)$$

$$\left\{ \int_0^{\infty} dz'' \, e^{jkZ_1 z''} \left[\frac{\partial}{\partial y} H_o^{(2)}\left(k\sqrt{(y-y_o)^2+z''^2}\right) \right]_{y=y_1} \right\}$$

$$\cdot \left\{ \int_{-\infty}^{\infty} d\xi \, \frac{e^{-j\sqrt{k^2-\xi^2}}}{\sqrt{k^2-\xi^2}} \; y_B \; e^{-j\xi(z-z')} + e^{-j\xi(z+z')} \right\} \qquad (2.30)$$

$$H_x \frac{\partial}{\partial y'_B} G \Big|_{y'_B = 0}$$

$$= - \frac{j}{(4\pi)^2} \omega\epsilon \left\{ \int_0^{\infty} dz'' \left[\frac{\partial}{\partial y} H_o^{(2)}\left(k\sqrt{(y-y_o)^2+z''^2}\right) \right]_{y=y_1} \right\}$$

$$\left\{ \int_{-\infty}^{\infty} d\zeta \, \frac{e^{-j\sqrt{k^2-\zeta^2}}}{\sqrt{k^2-\zeta^2}} \; w \left[e^{-j\zeta(z'-z'')} - \frac{kZ_1-\zeta}{kZ_1+\zeta} e^{-j\zeta(z'+z'')} \right] \right\}$$

$$\cdot \left\{ \int_{-\infty}^{\infty} d\xi\, e^{-j\sqrt{k^2-\xi^2}\; y_B} \left[e^{-j\xi(z-z')} + e^{-j\xi(z+z')} \right] \right\}$$

$$+ \frac{\omega\epsilon}{4\pi} \frac{Z_1}{\sqrt{1-Z_1^2}}\, e^{-jk\sqrt{1-Z_1^2}\; w}\, e^{jk Z_1 z'}\, U(X_1)$$

$$\cdot \left\{ \int_{0}^{\infty} dz''\, e^{jk Z_1 z''} \left[\frac{\partial}{\partial y} H_o^{(2)}\left(k\sqrt{(y-y_o)^2+z''^2}\right) \right]_{y=y_1} \right\}$$

$$\cdot \left\{ \int_{-\infty}^{\infty} d\xi\, e^{-j\sqrt{k^2-\xi^2}\; y_B} \left[e^{-j\xi(z-z')} + e^{-j\xi(z+z')} \right] \right\} \qquad (2.31)$$

Substituting Eqs. (2.30) and (2.31) into Eq. (2.27) and performing the indicated integrations by the steepest descent method, one gets $H_z(y, o)$ on the ground plane as:

$$H_x(y, z=o) = -\frac{1}{2}\omega\epsilon\, H_o^{(2)}\left(k\left[y-y_o\right]\right)$$

$$+ \frac{1}{2}\,\omega\epsilon \sqrt{\frac{2}{\pi k(y-y_o)}}\, e^{-j\left[k(y-y_o)-\frac{\pi}{4}\right]}$$

$$\cdot \left[1 + j\frac{1}{8}\frac{1}{k(y_1-y_o+w)}\right] \left[1 + j\frac{1}{8}\frac{1}{ky_B}\right]$$

$$+\frac{1}{2}\frac{\omega\epsilon}{Z_1}\, e^{-jk\sqrt{1-Z_1^2}\, w}\left[\frac{1}{\sqrt{1-Z_1^2}}+1\right]$$

$$\cdot\sqrt{\frac{2}{\pi k(y_1-y_o)}}\sqrt{\frac{2}{\pi k y_B}}\, e^{-j\left[k(y_1-y_o+y_B)-\frac{\pi}{2}\right]}$$

$$\cdot\left[1+j\frac{1}{8}\frac{1}{k(y_1-y_o)}\right]\left[1+j\frac{1}{8}\frac{1}{k y_B}\right] \qquad U(X_1)\ , \qquad (2.32)$$

where

$$y = (y_1-y_o)+w+y_B$$

$$Z_1 = R_1 + jX_1 = Z_s\Big/\sqrt{\frac{\mu}{\epsilon}}$$

$$U(X_1) = \begin{cases} 1 & \text{if} \quad X_1 > 0 \\ 0 & \text{if} \quad X_1 \geqslant 0 \end{cases}$$

The first term in Eq. (2.32) is the radiation field when there is no impedance strip. (compare with Eq. (2.4). The second term is the disturbance in the radiation field due to the impedance strip. It may be strange, at first sight, that no impedance factor Z_1 appears in the radiation disturbance term. Actually, when $z = o$, the Z_1 - factor is associated with the second term, but as $z > o$, the factor drops out. The third term is the field generated by the surface wave created in the impedance strip. This term appears only if the strip is the inductive type ($X_1 > o$). The capacitive type impedance strip ($X_1 < o$) cannot support surface waves.

Now, if one expands $H_o^{(2)}(k(y-y_o))$ into the asymptotic form:

$$H_o^{(2)}\left[k(y-y_o)\right] = \sqrt{\frac{2}{\pi k(y-y_o)}}\left[1+j\frac{1}{8}\frac{1}{k(y-y_o)}\right]e^{-j\left[k(y-y_o)-\frac{\pi}{4}\right]}$$

The dominant part of the first two terms of Eq. (2.32) cancels out and $H_x(y,\ z=o)$ is reduced to:

$$H_x(y_1,\ z=o) \doteqdot +j\frac{1}{16}\omega\epsilon\sqrt{\frac{2}{\pi k(y-y_o)}}\,e^{-j\left[k(y-y_o)-\frac{\pi}{4}\right]}$$

$$\cdot\left[\frac{1}{ky_B}+\frac{1}{k(y_1-y_o+w)}-\frac{1}{k(y-y_o)}\right]$$

$$+\frac{1}{2}\frac{\omega\epsilon}{Z_1}e^{-jk\sqrt{1-Z_1^2}\,w}\left[\frac{1}{\sqrt{1-Z_1^2}}+1\right]$$

$$\cdot\sqrt{\frac{2}{\pi k(y_1-y_o)}}\sqrt{\frac{2}{\pi ky_B}}\,e^{-j\left[k(y_1-y_o+y_B)-\frac{\pi}{2}\right]}$$

$$\cdot\left[1+j\frac{1}{8}\left\{\frac{1}{ky_B}+\frac{1}{k(y_1-y_o)}\right\}\right]\qquad U(X_1)\qquad (2.33)$$

2.2 Conclusions on Strip Analysis

The comparison of Eq. (2.33) with the field at the same point without impedance strip, namely,

$$H_x^{(o)} = -\frac{1}{2}\omega\epsilon H_o^{(2)} k(y-y_o)$$

$$\doteqdot -\frac{1}{2}\omega\epsilon \frac{2}{\pi k(y-y_o)} e^{-jk(y-y_o)-\frac{\pi}{4}} \qquad (2.34)$$

shows that a substantial reduction in field intensity (hence coupling) can be attained as $(y-y_o)$, y_B, and (y_1-y_o+w) become large.

Though no numerical calculation has yet been made, some qualitative interpretations of physical interest can be extracted from Eq. (2.33). For illustration, assume the distance between the source and the field point is fixed, namely,

$$y-y_o = d \quad . \qquad (2.35)$$

i) Suppose that a capacitive impedance strip is used. Then, the second term of Eq. (2.33) (surface wave term) vanishes. In this case, the field is independent of the width of the impedance strip, since

$$y_1-y_o+w = d-y_B \quad ,$$

and hence

$$\frac{\left|H_x\right|^2}{\left|H_x^{(o)}\right|^2} = \frac{1}{64}\left[\frac{1}{ky_B}+\frac{1}{k(d-y_B)}-\frac{1}{kd}\right]^2 \quad . \qquad (2.36)$$

ii) Consider the case where inductive impedance strip is used and the surface wave term is much greater than the pure radiation term (the first term). Noting that

$$\sqrt{1-Z_1^2} = \sqrt{1-(R_1+jX_1)^2} = \sqrt{(1+X_1^2-R_1^2)^2+2jR_1X_1}$$

$$\doteqdot (1+X_1^2-R_1^2)+j\frac{R_1X_1}{(1+X_1^2-R_1^2}\quad ,$$

one obtains

$$\frac{|H_x|^2}{|H_x^{(o)}|^2} = \frac{1}{(R_1^2+X_1^2)}\left[1+\frac{(1+X_1^2-R_1^2)\left[2(1+X_1^2-R_1^2)+1\right]}{(1+X_1^2-R_1^2)^4+R_1^2X_1^2}\right]$$

$$\cdot\ \frac{d}{(d-w-y_B)}\ \frac{2}{\pi k y_B}\exp\left[-\frac{2kwR_1X_1}{(1+X_1^2-R_1^2)}\right] \quad . \qquad (2.37)$$

For a good absorber (R_1 large, yet $X_1 > R_1$), the exponential term dominates other increasing factors and the reduction of the field intensity can be achieved. However, an increase of field intensity would result using ordinary dielectric (R_1 and X_1 small), thus causing guided wave phenomena.

III

EXPERIMENTAL DECOUPLING PROCEDURES

3.1 Decoupling Two Slots on a Common Ground Plane by Means of Chokes

The type of slot that was examined is the open ended waveguide. Such slot antennas are often found flush mounted in close proximity. In such cases the low directivity which characterizes this type of antenna gives rise to a strong interference which is due to the mainlobe of the pattern and not just weak sidelobes.

When a slot antenna is radiating the ground plane supports a traveling wave. To prevent propagation of a surface wave, the surface reactance must be capacitive (Elliott, 1954).

A single, circumferential choke was used to create such a capacitive impedance (see Fig. 3-1). The width of this choke was very small compared to both the depth and the free-space wavelength so that higher order modes would be attenuated.

Results obtained by another worker (Hurd, 1954) for the case of corrugations with infinitely thin walls indicate that for small groove widths the cutoff depth is between $\lambda/4$ and $\lambda/2$ or any multiple of $\lambda/2$ deeper. To test the validity of this statement in the case of the single groove, two slot antennas of a transmitter-receiver system each surrounded by a single choke of depth equal to a quarter wavelength at 8.0 GHz were manufactured and tested at X-band frequencies. The coupling measured was compared with the one in the case of two slots without chokes in the same geometry. It was found that maximum decoupling (approximately 9 db) occured at 8.2 GHz, the lowest frequency used in the measurements. At 10 GHz, however, the decoupling was reduced to approximately 4 db.

In the case where only one of the two slots had a choke it was found that the decoupling was not dependent upon whether the choke was on the transmitter or the receiver. The decoupling observed was equal to 50 per cent of that observed when both antennas were equiped with chokes.

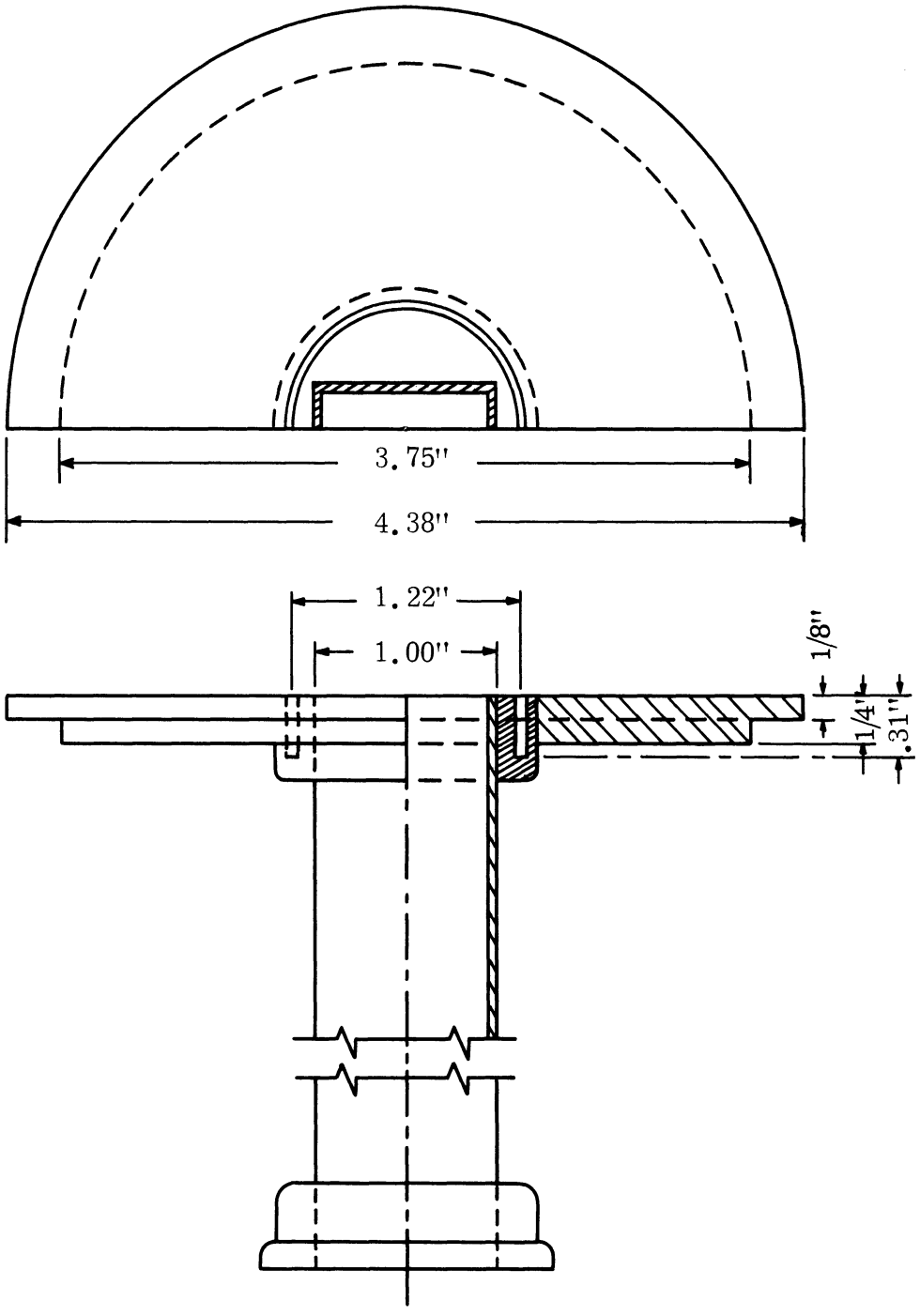

FIG. 3-1: SLOT ANTENNA WITH CHOKE.

In order to examine the behaviour of the choke at lower frequencies, the groove depths of the transmitter and receiver were modified so that they would be equal to a quarter wavelength at 10.0 GHz and 9.2 GHz respectively. This was realized by the addition of two copper rings which were covered with silver paint.

The E- and H-plane coupling versus frequency for this case is shown in Fig. 3-2. In the same figure the coupling of two plain slots, in the same geometry, is given as a reference. The following data apply in this case:

Center-to-center distance:	$D = 11.43$ cm
Groove depths:	$d_t = 0.75$ cm
	$d_r = 0.82$ cm
Groove width:	$g = 0.16$ cm (1/16")
Slot dimensions:	2.29 x 1.01 cm (0.900 x 0.400 inches)

Patterns of coupling when one slot was fixed and the other rotated by 360^{o} were taken for the cases of E- and H-plane coupling (geometry shown in Fig. 3-3), and compared with similar patterns for two plain slots. Such patterns are shown in Figs. 3-4 and 3-5 for a frequency of 10.03 GHz. Figure 3-4 shows that, for E-plain coupling, the decoupling obtained with the choke is practically constant, i.e., independent of the relative orientation of one slot with respect to the other. In the case of H-plane coupling (Fig. 3-5) although the maximum coupling is reduced with the chokes, the nulls are deeper in the case of the plain slots. This, however, could be due to mechanical imperfections since the coupling levels in question were 80 db below direct coupling. More accurately machined chokes which are going to be used in planned experiments will help clarify this point. It should be noted that similar patterns were taken for five different frequencies covering the whole X-band but are not presented here because they did not contain any additional information beyond that already presented.

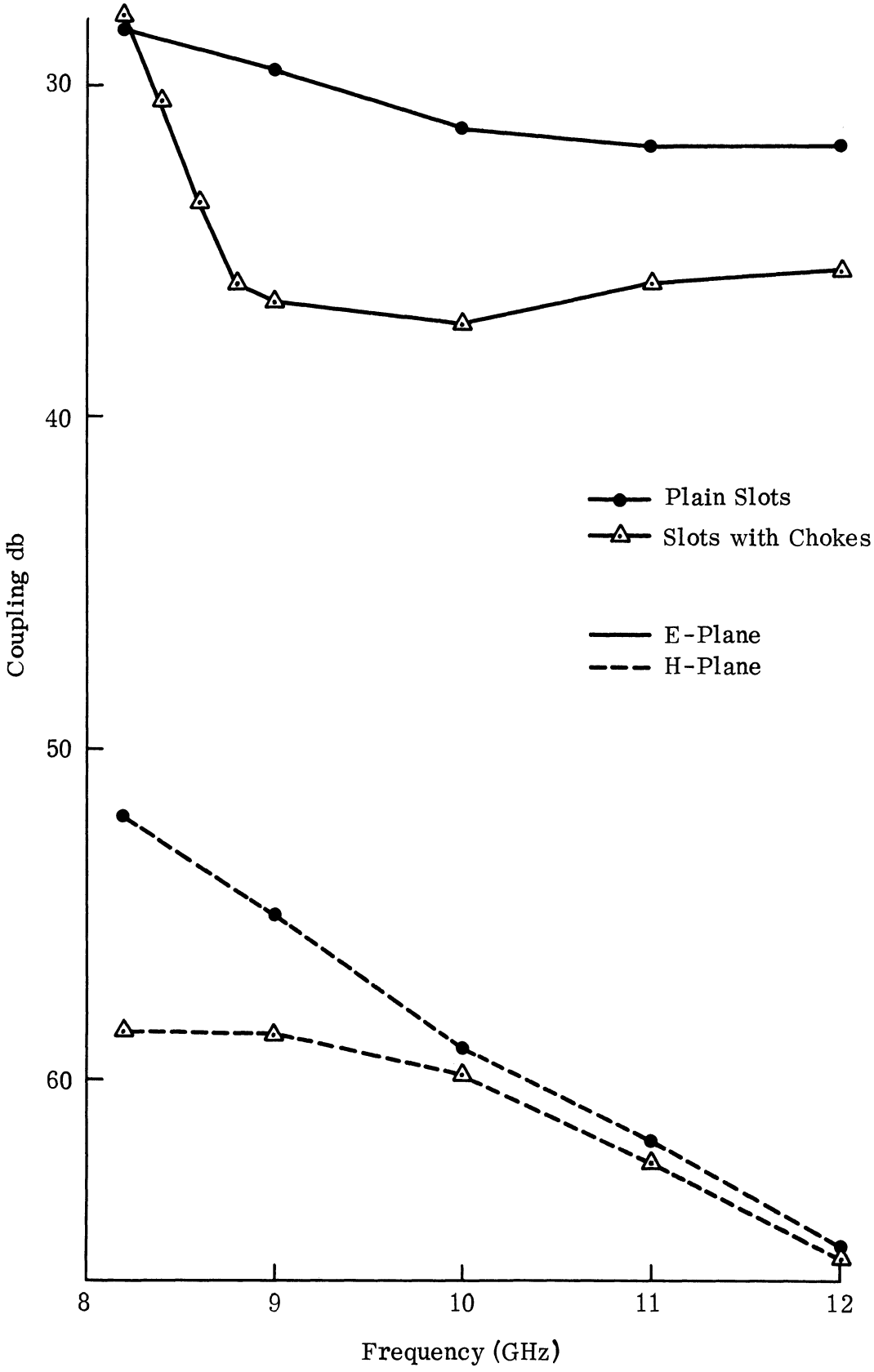

FIG. 3-2: E- AND H-PLANE COUPLING VERSUS FREQUENCY FOR TWO SLOTS ON A COMMON GROUND PLANE. D = 11.43 cm.

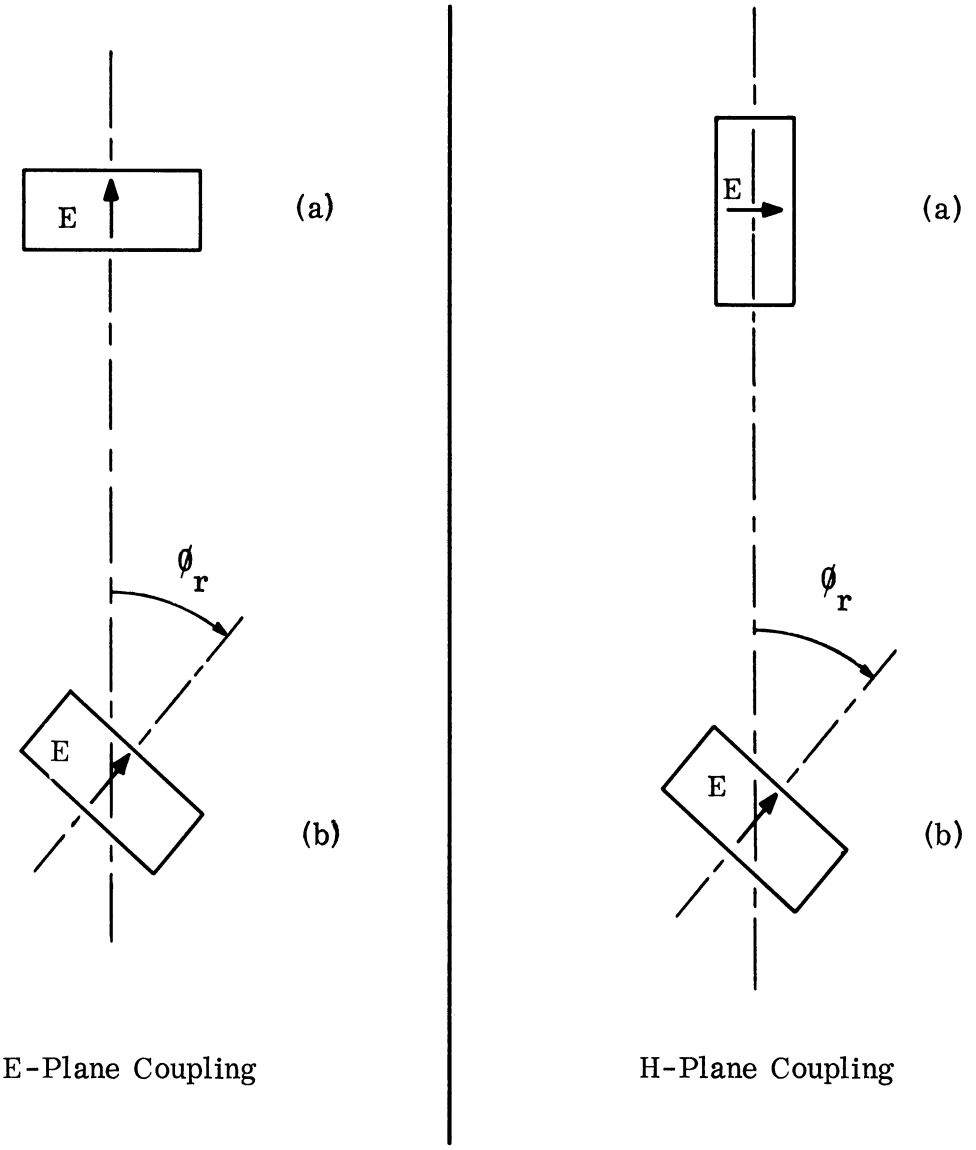

FIG. 3-3: GEOMETRY OF TWO SLOT ANTENNAS SHOWING E- AND H-PLANE COUPLING. (a) TRANSMITTER-FIXED POSITION (b) RECEIVER-ROTATABLE.

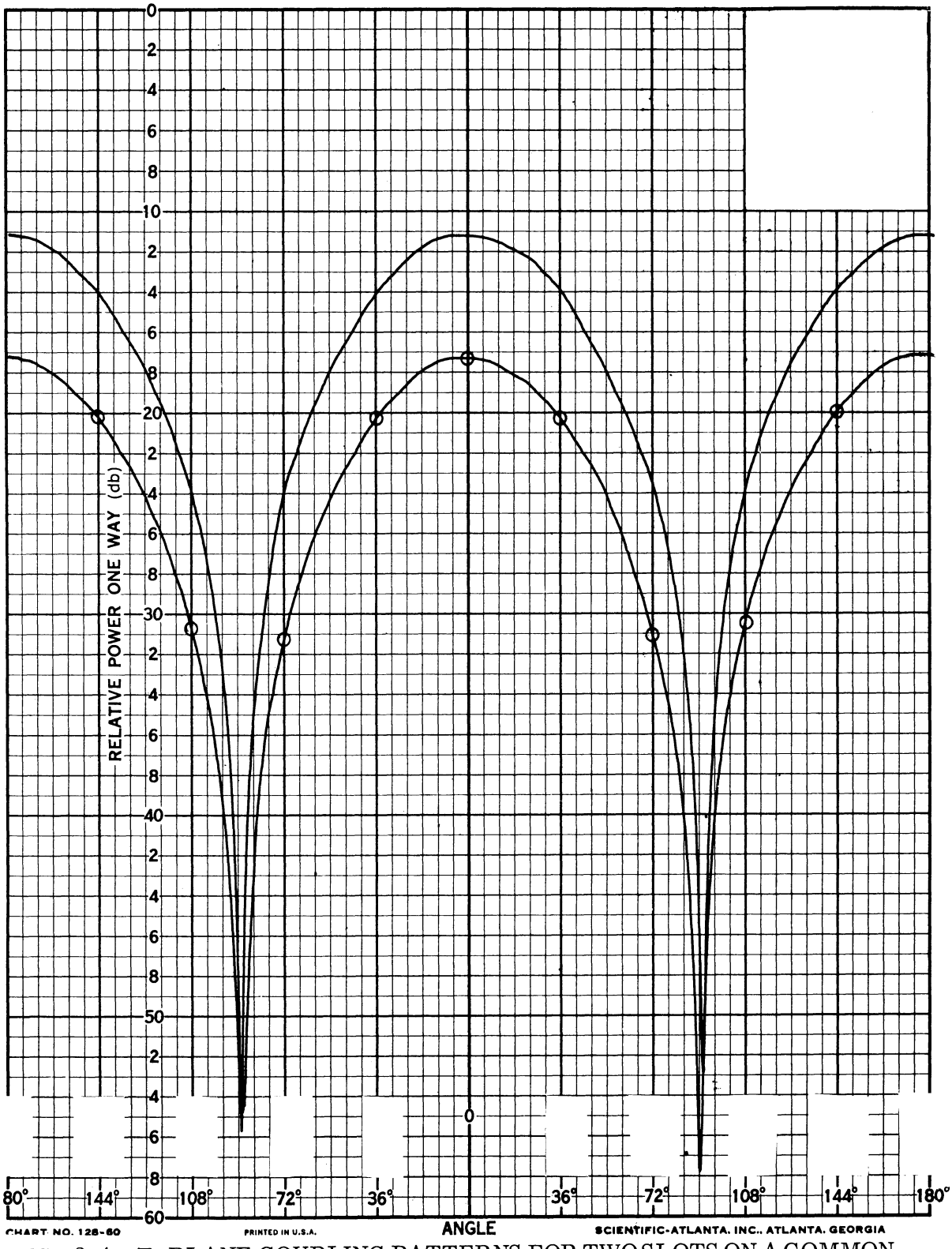

FIG. 3-4: E-PLANE COUPLING PATTERNS FOR TWO SLOTS ON A COMMON GROUND PLANE, (—) plain slots; (-o-) slots surrounded by chokes. f = 10.030 GHz, D = 11.43 cm, 0 = -20 db.

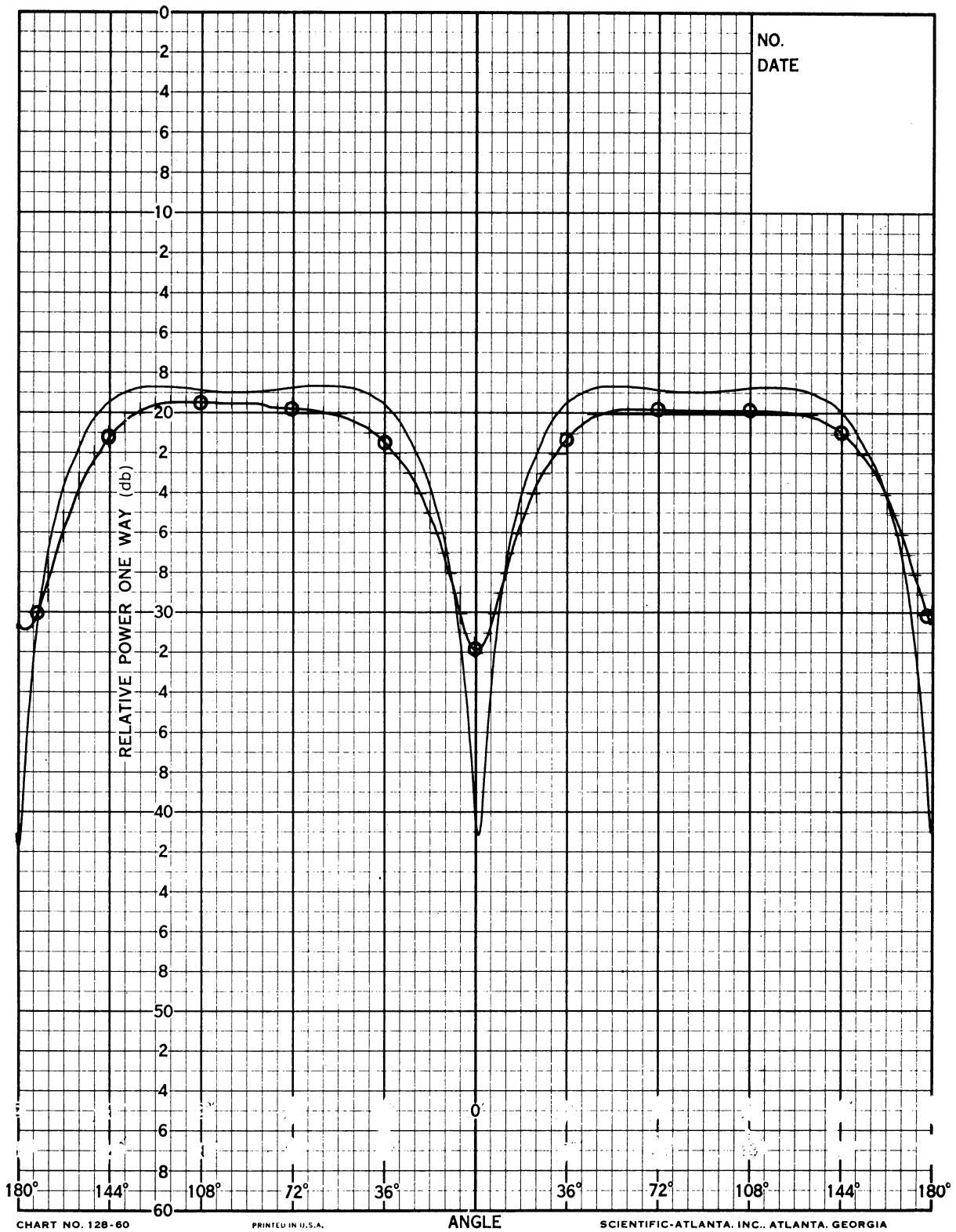

FIG. 3-5: H-PLANE COUPLING PATTERNS FOR TWO SLOTS ON A COMMON GROUND PLANE, (—) plain slots; (-o-) slots surrounded by chokes. f = 10.030 GHz, D = 11.43 cm, 0 = -40 db.

An investigation would not be complete without radiation patterns. Such patterns were taken and are shown in Figs. 3-6 to 3-8 for three different frequencies. Again the corresponding patterns for a plane slot antenna, taken with the same reference, are superimposed on the same page for easy comparison.

These figures show that although the shape of the H-plane radiation pattern is very little affected, the shape of the E-plane pattern is greatly affected and shows a substantial improvement in gain (for frequencies 10.03 GHz and 12.03 GHz) and a great improvement in directivity. At the frequency of 8.23 GHz, however, which is outside the cutoff frequency range, the antenna gain is reduced.

From the above the following conclusions can be made:

1) The choke does exhibit a cutoff region defined by $\lambda/4 < d < \lambda/2$ (d = trench depth). Operating in this region increases the antenna gain, decreases the sidelobes and consequently decreases coupling to adjacent antennas.

2) Operating at a frequency such that $d < \lambda/4$ affects coupling and gain little, either favorably or adversely depending upon the deviation from $d = \lambda/4$. This imposes a restriction on the possibility of broadbanding by placing a number of chokes of different depths around a slot antenna.

3) Two chokes are twice as effective as one in decoupling.

In view of these conclusions, a new slot antenna with four circumferential grooves has been designed with a depth d fulfilling the condidtion

$$\lambda/4 < d < \lambda/2 \text{ for } 8.2 \text{ GHz} < f < 12.4 \text{ GHz}.$$

Tests on this antenna will be conducted in the immediate future.

3.2 Decoupling E- and H-Sectoral Horns on a Common Ground Plane by Means of Absorbing Materials

Two different approaches were tried (1) the nonparallel walls of the horns were lined with absorbing material cut in the shape of wedges; (2) a slab of absorbing

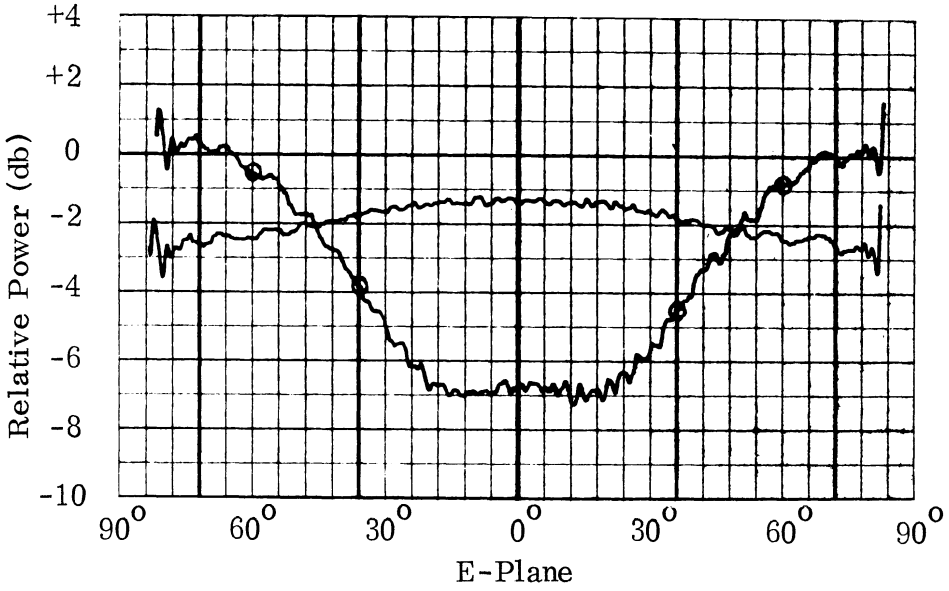

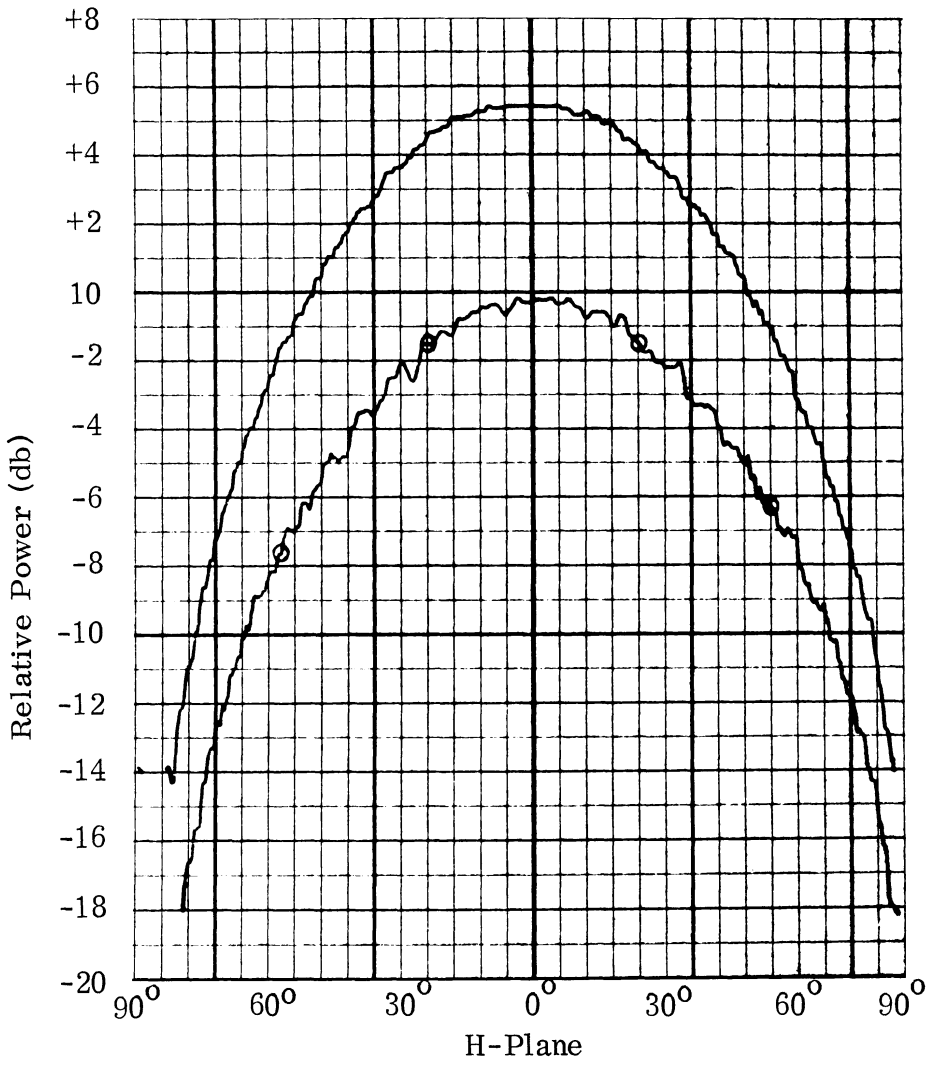

FIG. 3-6: E- AND H-PLANE PATTERNS OF PLANE SLOT (——) AND THE SLOT SURROUNDED BY A CHOKE (—o—) AT 8.23 GHz.

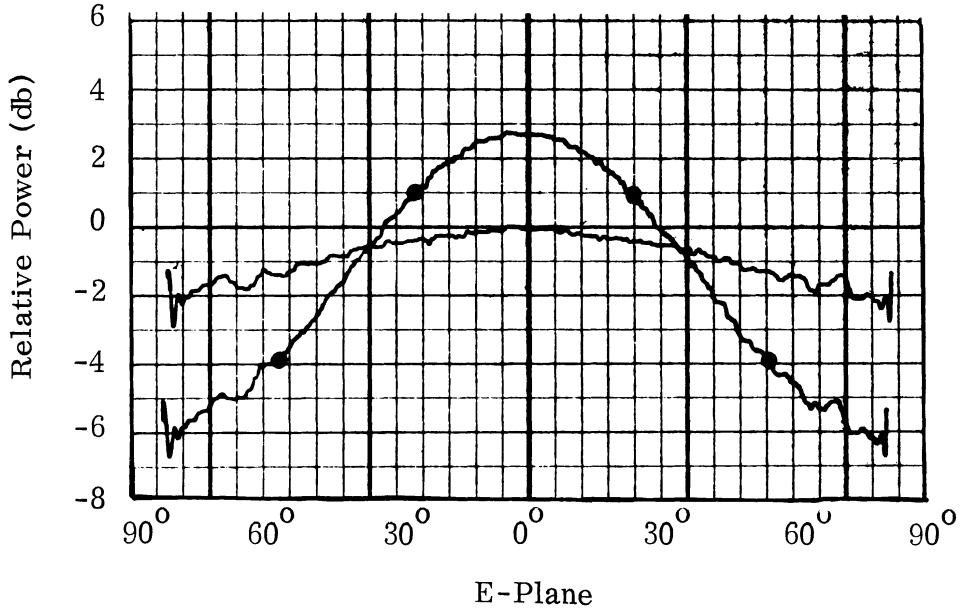

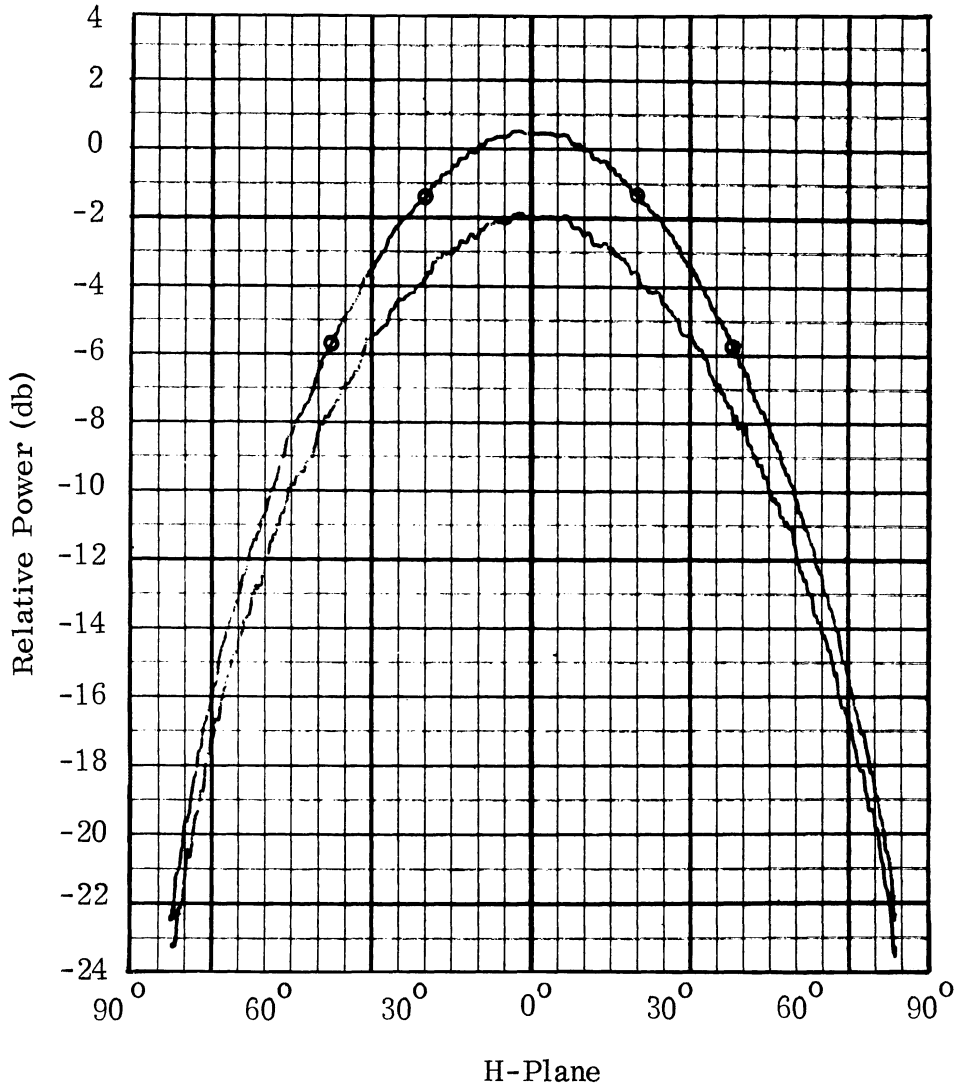

FIG. 3-7: E- AND H-PLANE PATTERNS OF PLANE SLOT (——) AND THE SLOT SURROUNDED BY A CHOKE (-●-) AT 10.03 GHz.

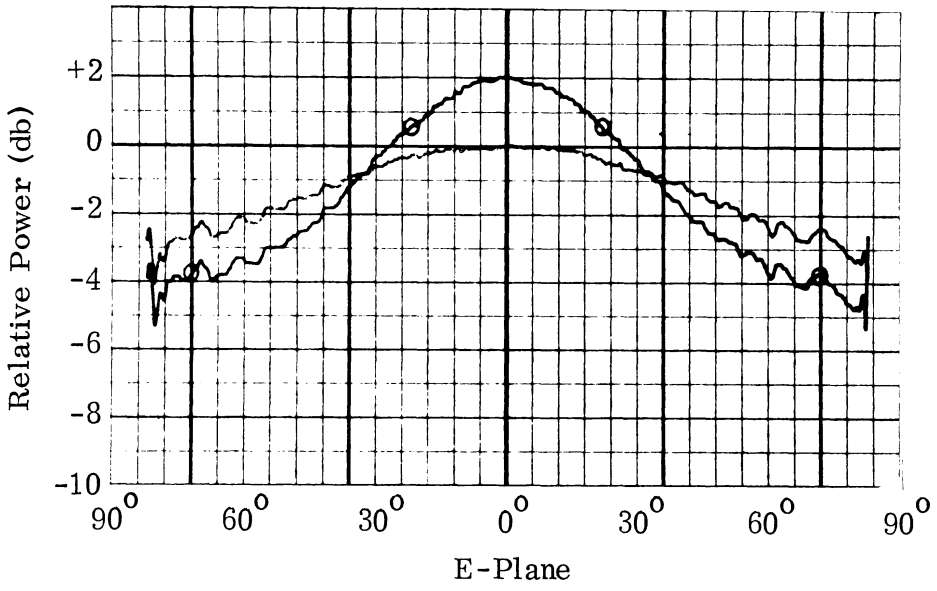

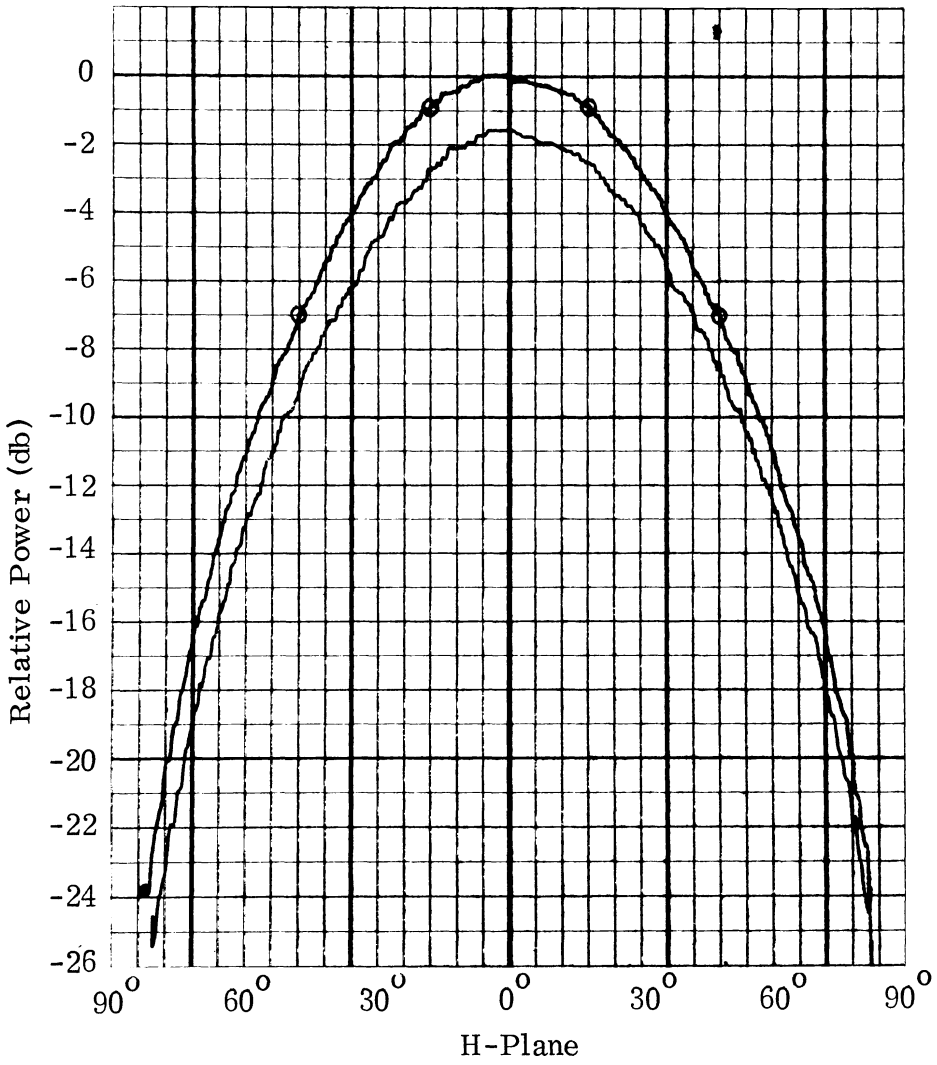

FIG. 3-8: E- AND H-PLANE PATTERNS OF PLANE SLOT (——) AND THE SLOT SURROUNDED BY A CHOKE (-o-) AT 12.03 GHz.

material was placed on the ground plane between the two horns. In both cases the absorbing material used was Emerson and Cuming's Eccosorb-CR.

3.2.1 H-Sectoral Horns

The use of absorber wedges affected coupling very little. The maximum decoupling observed was 3 db. This was considered unsatisfactory and the method was abandoned.

An absorber slab of dimensions 7.8 x 7.8 x 1.8 cm (1.8 cm being the height above the ground plane) placed on the ground plane between the two antennas produced a decoupling of 20 db. This situation is described as follows: H-sectoral horns, flare angle 70^{o}, center-to-center distance 11.43 cm, frequency 10.03 GHz, initial E-plane coupling -28 db, and final E-plane coupling with absorber -48 db.

3.2.2 E-Sectoral Horns

For this type of antenna, absorber wedges placed inside the horn (see Fig. 3-9) proved to be very effective in reducing coupling. Curves of E- and H-plane coupling versus frequency are shown in Fig. 3-10. In this figure the coupling between two absorber lined horns is compared with the coupling of two sets of control horns; one set with flare angle of 45^{o} and the other with flare angle of 20^{o}.

The variation of coupling for various orientations of the receiving antenna was also studied at different X-band frequencies. Typical patterns, taken at a frequency of 10.030 GHz, are shown in Figs. 3-11 and 3-12. The relative orientation of the two antennas is the same as in the case of slots (Fig. 3-3). In this case a "slot" should be interpreted as the waveguide termination. The center-to-center distance of the two antennas is denoted by D.

Radiation patterns taken (Figs. 3-13 and 3-14) for the absorber lined horn and a control horn indicate a loss in maximum gain of 11 db. This loss in gain is mainly due to antenna efficiency decrease since the radiation patterns indicate a small

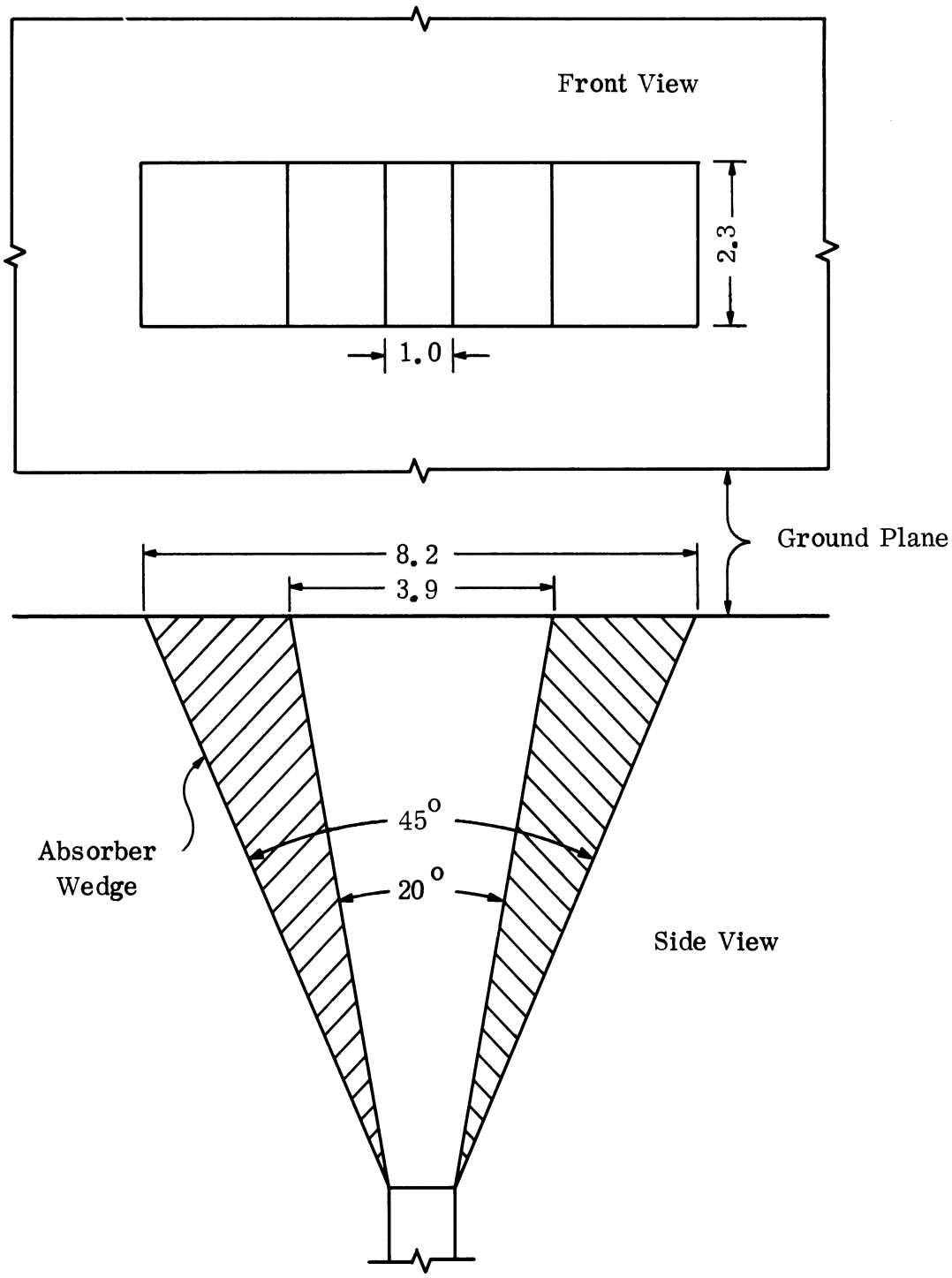

FIG. 3-9: FRONT AND SIDE VIEW OF E-SECTORAL HORN WITH ABSORBER WEDGES (DIMENSIONS IN cm)

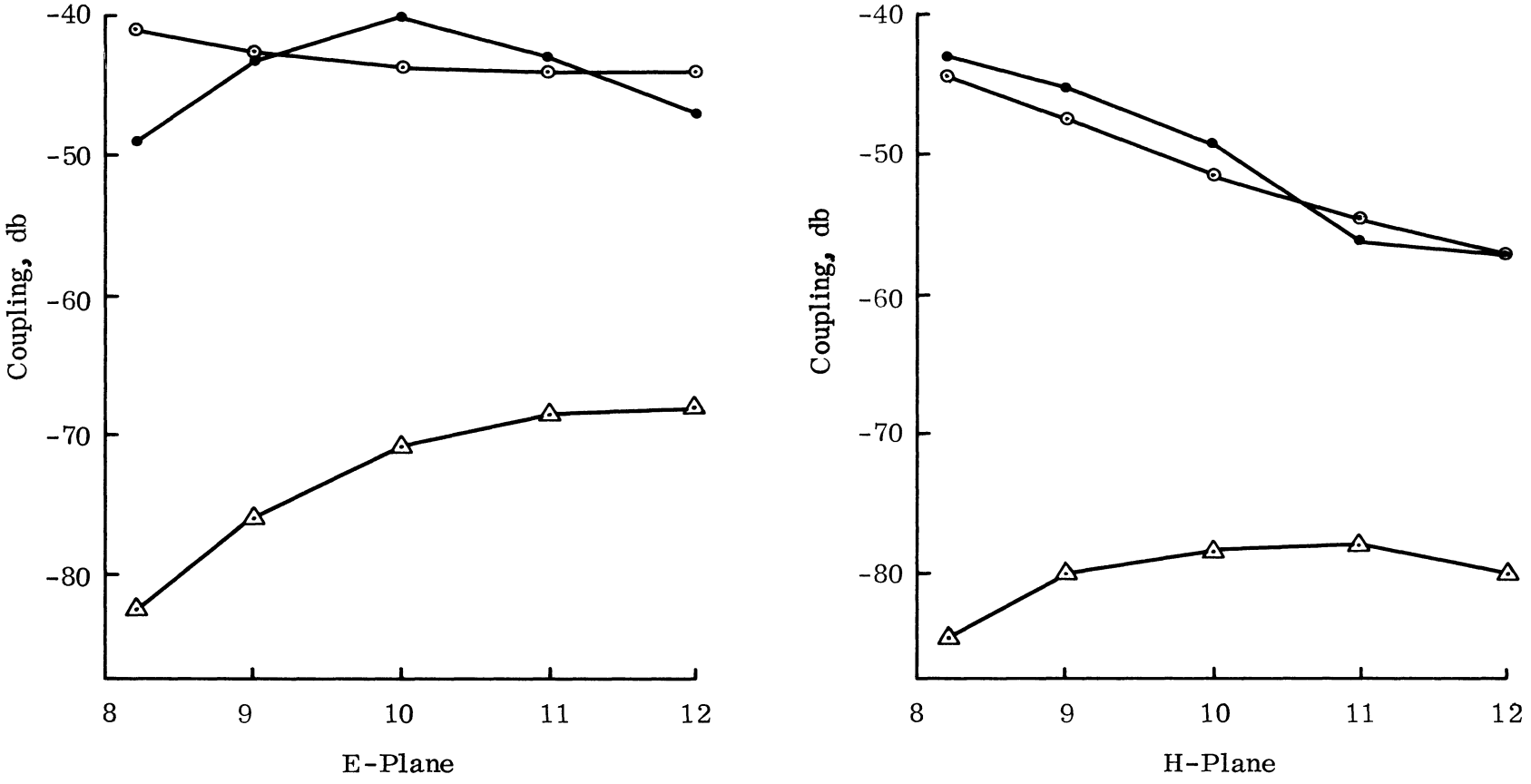

FIG. 3-10: E- AND H-PLANE COUPLING VERSUS FREQUENCY FOR TWO IDENTICAL E-SECTORAL HORNS FLUSH MOUNTED ON A COMMON GROUND PLANE. CENTER-TO-CENTER DISTANCE 11.43 cm. FLARE ANGLES: (—●—) 20^{o}; (—⊙—) 45^{o}; (—△—) 45^{o} MODIFIED TO 20^{o} BY THE USE OF ABSORBER WEDGES.

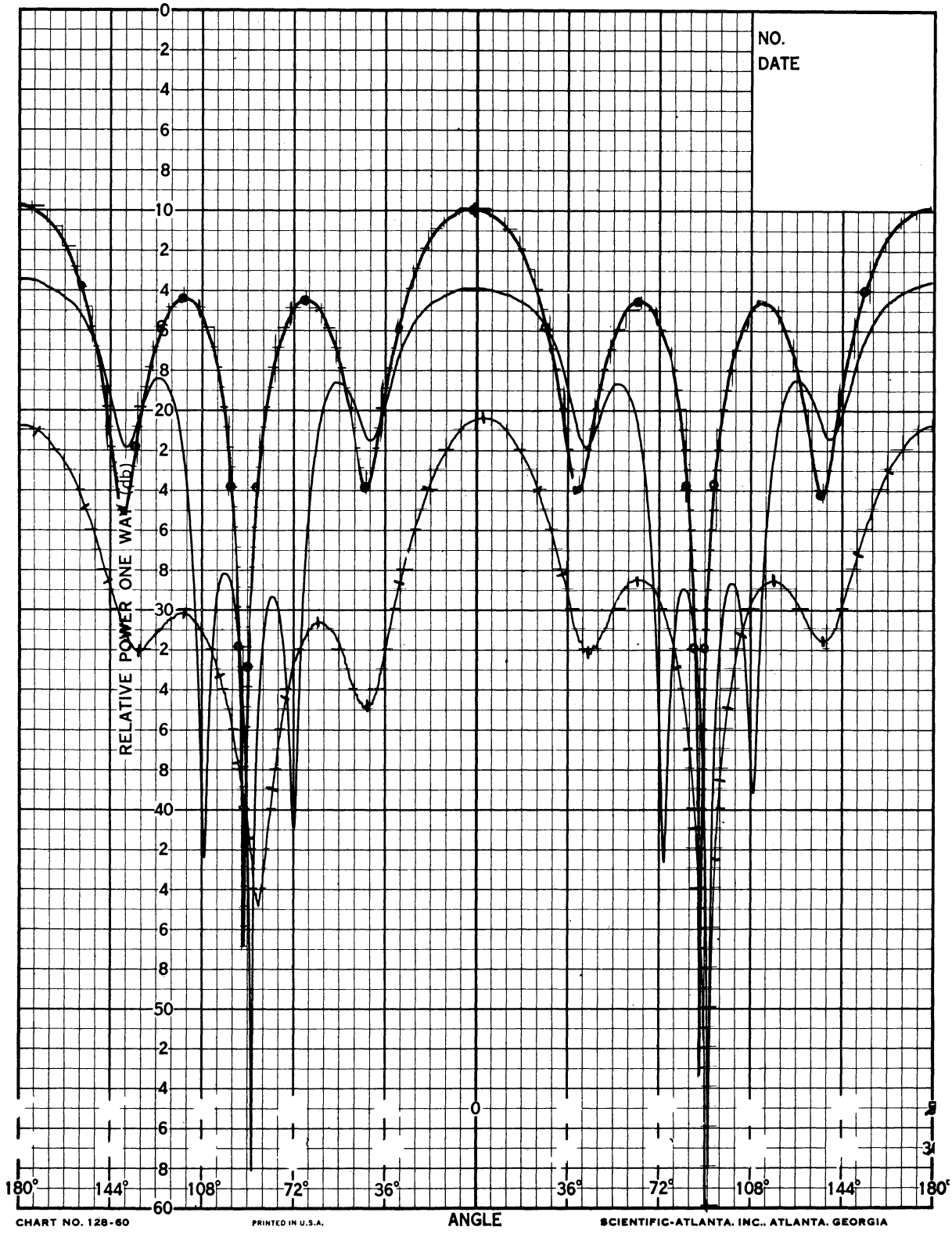

FIG. 3-11: E-PLANE COUPLING VERSUS RECEIVING ANTENNA ORIENTATION (-180^{o} to 180^{o}) FOR TWO E-SECTORAL HORNS ON A COMMON GROUND PLANE AT 10.030 GHz, D = 11.43 dm. ZERO REFERENCE LEVEL AND FLARE ANGLE: (——) -30 db, 45^{o}; (—o—) -30 db, 20^{o}; (—+—) -50 db, 45^{o}, WITH ABSORBER WEDGES

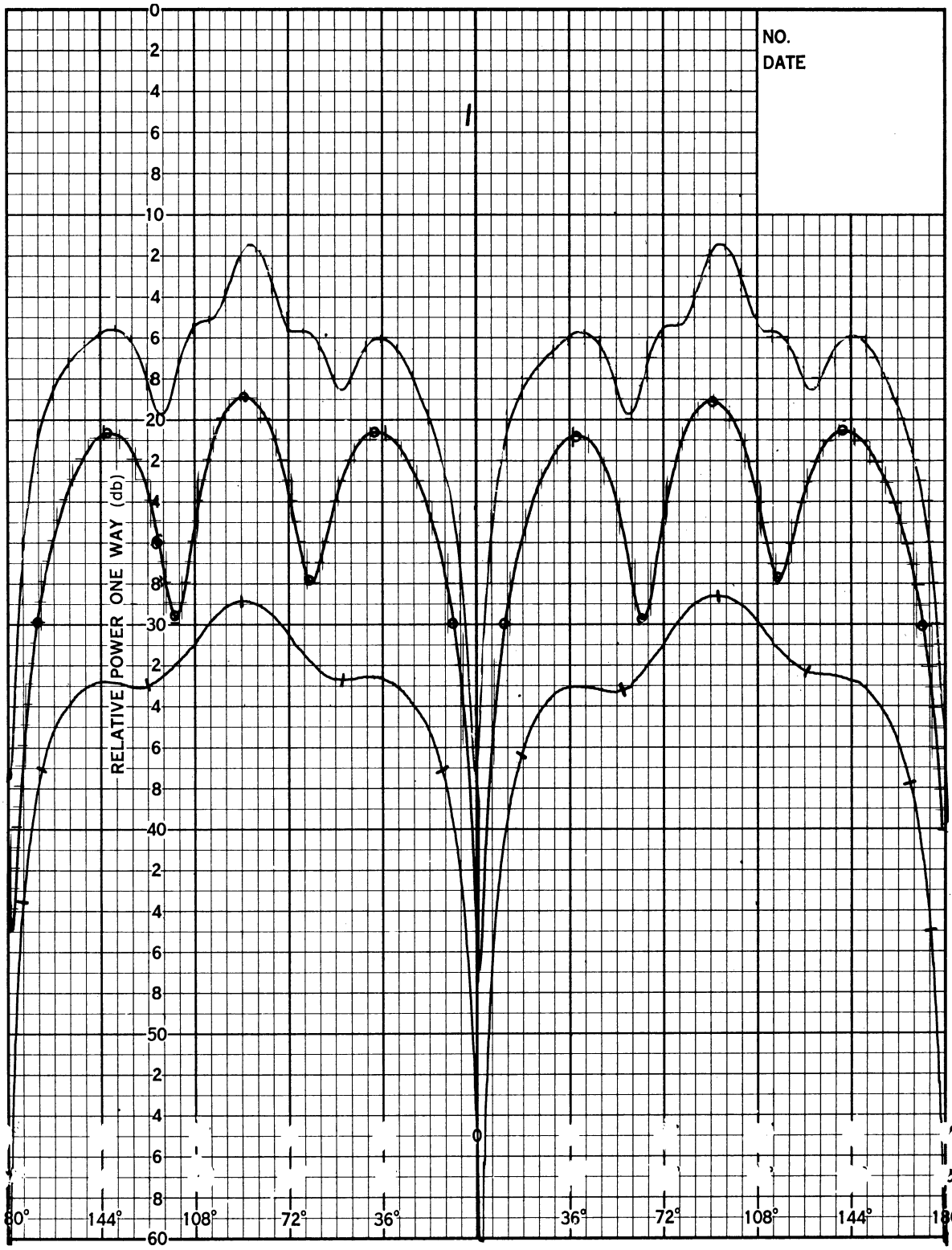

FIG. 3-12: H-PLANE COUPLING VERSUS RECEIVING ANTENNA ORIENTATION (-180^{o} to 180^{o}) FOR TWO E-SECTORAL HORNS ON A COMMON GROUND PLANE AT 10.030 GHz. D = 11.43 cm ZERO REFERENCE LEVEL AND FLARE ANGLE: (——) -40 db, 45^{o}; (—o—) -30 db, 20^{o}; (—+—) -50 db, 45^{o}, WITH ABSORBER WEDGES.

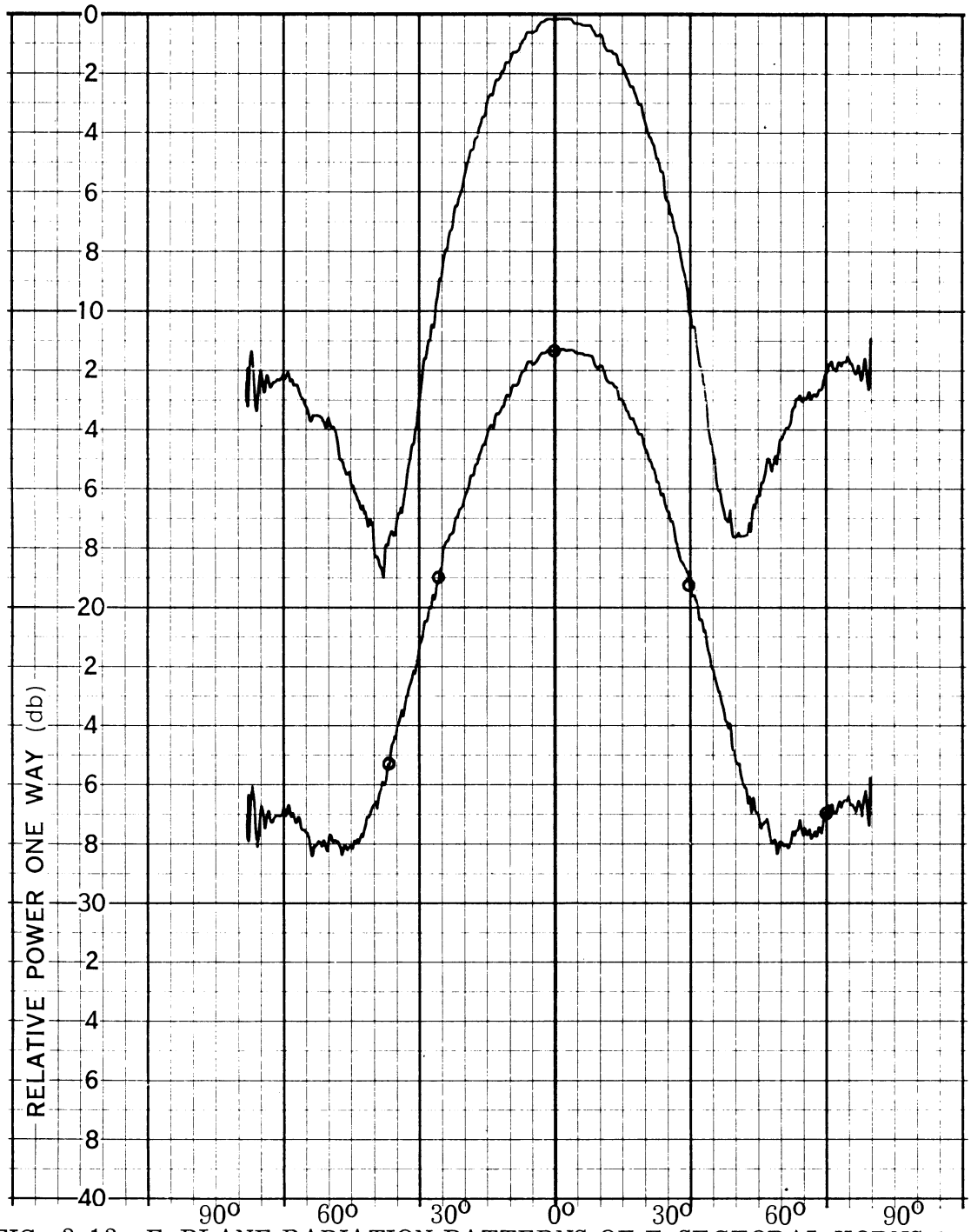

FIG. 3-13: E-PLANE RADIATION PATTERNS OF E-SECTORAL HORNS,* (0—) Flare angle 20^{o}; (-o-) Flare angle 45^{o} reduced to 20^{o} by the use of absorber wedges, * at 10.030 GHz.

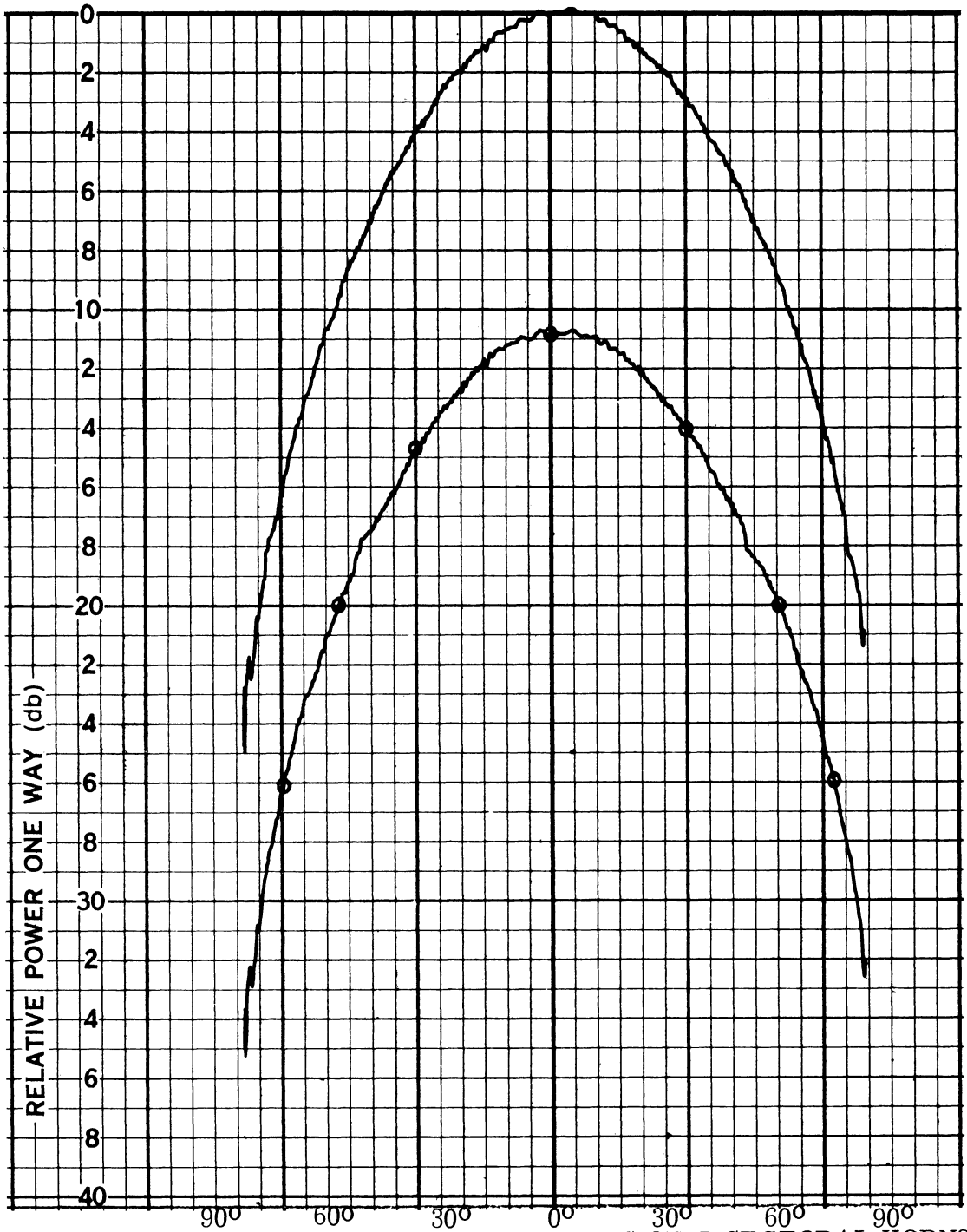

FIG. 3-14: H-PLANE RADIATION PATTERNS OF E-SECTORAL HORNS AT 10.030 GHz. FLARE ANGLE: (——) 20°; (-o-) 45° REDUCED TO 20° BY THE USE OF ABSORBER WEDGES.

change in the antenna directivity. It should be noted that the decoupling obtained in this case, 31 db for the transmitter-receiver system or 16.5 db per antenna, is still greater than the loss in maximum gain, i.e. the sidelobe reduction is greater than that of the mainlobe. Similar results were observed at 12.03 GHz; however, at 8.23 GHz the mainlobe was reduced more than the sidelobes (approximately 2 db).

A second approach to decouple E-sectoral horns is by placing a slab of absorbing material on the ground plane between the two horns. Different sizes of absorber pieces were used. The horns used in this case had a flare angle of 20^{o} and were located at a center-to-center distance of 11.43 cm. The E-plane coupling was reduced from -39 db to -63 db accompanied by a reduction in maximum gain of only 0.5 db. The E-plane radiation pattern showed an elimination of the sidelobe in the direction of the absorbing material while the main lobe shape was practically unaffected for a scan angle $-45^{o} < \theta < +45^{o}$.

The H-plane coupling was reduced from -48 db to -62 db. For this case a larger slab was used resulting in a reduction of maximum gain by 1.5 db. The shape of the E-plane radiation pattern showed a small decrease in the sidelobe levels while the H-plane pattern showed some assymmetry.

A metal object of the same dimensions as the absorber slab was placed on the ground plane and at the same positions as before. The radiation patterns taken were very similar to those with the absorber except that the maximum gain was usually somewhat higher (0.5 db) than that measured without any obstacle. So it can be concluded that the changes in the radiation pattern in the presence of a non-flush-mounted absorber slab are mainly due to reflection and refraction of the electromagnetic waves rather than absorption.

Due to the fact that in these experiments the flush-mounting requirement was not met (absorber protruding 1.8 cm above ground plane) more detailed results and

radiation patterns are not presented. The results obtained, however, are now being used for the design of a modified horn antenna which will hopefully exhibit the same high-isolation levels as the ones mentioned and at the same time meet the flush-mounting requirement.

3.3 VSWR of a Slot Antenna in the Presence of an Obstacle on the Ground Plane

When a wave is propagating through a waveguide terminated at a slot, reflections occur at the point of discontinuity giving rise to a standing wave in the transmission line. Let E_i be the incident wave component and $E_{r,1}$ the reflected wave component. Then the reflection coefficient is:

$$\rho_1 = \frac{E_{r,1}}{E_i} \tag{3.1}$$

The presence of an obstacle on the ground plane in the near field of the slot creates additional reflections, the amplitude of which depends upon the size and conductivity of the obstacle as well as the distance R_λ from the slot, (distance expressed in wavelengths). Let this be denoted by $E_{r,2}(R_\lambda)$. The phase of $E_{r,2}$ is varying with respect to $E_{r,1}$ with a period of 0.5λ, therefore it can be expressed as

$$E_{r,2}(R_\lambda) \cos\left(2\pi \frac{R}{0.5\lambda} + \phi\right) = E_{r,2}(R_\lambda) \cos(4\pi R_\lambda + \phi) \tag{3.2}$$

where ϕ is a reference phase angle. Thus the reflection coefficient becomes:

$$\rho_t = \frac{E_{r,1} + E_{r,2}(R_\lambda) \cos(4\pi R_\lambda + \phi)}{E_i} \tag{3.3}$$

The corresponding standing wave ratio is:

$$S_t = \frac{1 + |\rho_t|}{1 - |\rho_t|} \tag{3.4}$$

If an impedance matching device is used between the transmission line and the slot, when no obstacle is present, $E_{r,1}$ can be made practically zero and then one can obtain ρ_2 and $E_{r,2}(R_\lambda)$ according to Eq. 3.3.

This approach has been used in an experiment. Since in applications the SWR is used more often this is the quantity that has been measured and which is presented in Fig. 3-15. The size and location of the obstacle is shown in the same figure. The reflection coefficient for the slot only is:

$$\rho_1 = \frac{S_1 - 1}{S_1 + 1} = \frac{0.625}{2.625} = 0.238 \tag{3.5}$$

Then one has:

$$\rho_t = 0.238 + \rho_2 \cos(4\pi R_\lambda + \phi) \tag{3.6}$$

E.g. At the first maximum there is

$$\rho_2 = \frac{S_2 - 1}{S_2 + 1} = \frac{0.13}{2.13} = 0.061$$

$$\rho_t = \frac{S_t - 1}{S_t + 1} = \frac{0.85}{2.85} = 0.298$$

in agreement with Eq. (3.6).

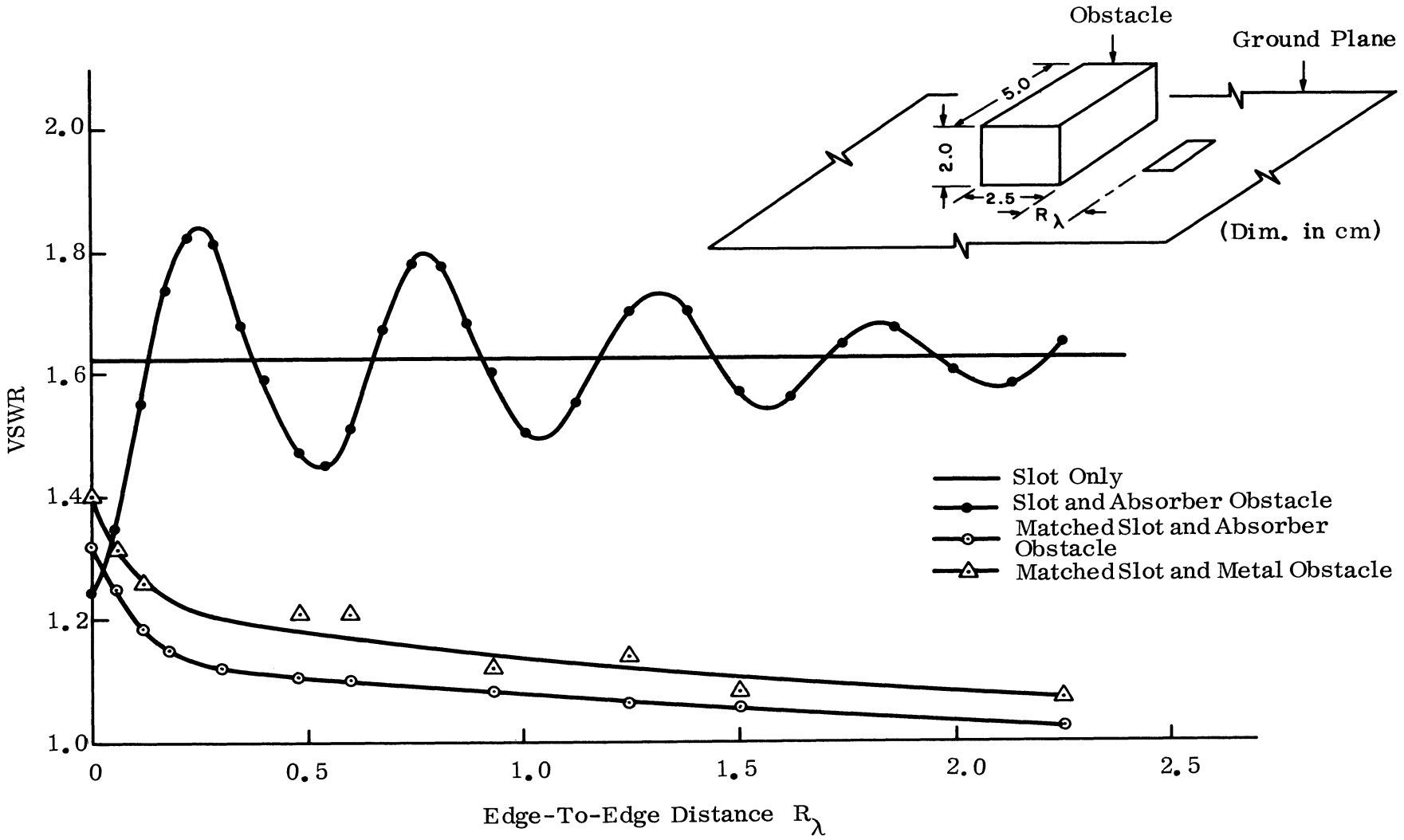

FIG. 3-15: VARIATION IN THE VSWR OF A SLOT ANTENNA IN THE PRESENCE OF AN OBSTACLE ON THE GROUND PLANE. EDGE-TO-EDGE DISTANCE MEASURED IN (FREE SPACE) WAVELENGTHS. f = 9.00 GHz

3.4 Isolation by Ribbed Surface

Ribbed or corrugated structures which have an end view appearance like a comb were investigated. Although such a structure would only be seriously considered as an isolation or decoupling device if it did not protrude, yet the cases of the structure standing out from the metal ground surface as well as being flush-mounted are considered. The ground surface contains the two slot antennas of two systems. Fig. 3.16 shows the experimental set-up.

3.4.1 Ribbed Structure Standing on the Ground Plane

A set of experiments has been performed with a corrugated or ribbed impedance put over the ground plane between the two slots as shown in Fig. 3-17 where:

f = frequency

D = separation between slots center-to-center

δ = the distance between edge of transmitter slot and the corrugation

t = separation between corrugation lines

d = depth of the corrugation

l = length of the corrugation

h = width of the corrugation

Figures 3-18 to 3-22 are graphs for angle versus coupling for different frequencies with and without the corrugated surface.

From this set of coupling experiments these points were noticed.

a) The decoupling between the two slots was very much dependent on frequency. (Figs. 3-18 to 3-22)

b) For the specific dimensions of the corrugated strip and its location between the two slots the decoupling attained was as high as 19 db.

c) The decoupling was higher than that when the width of the corrugation h was more than 5.4 cm (approximately 5.9 cm); then the decoupling reached

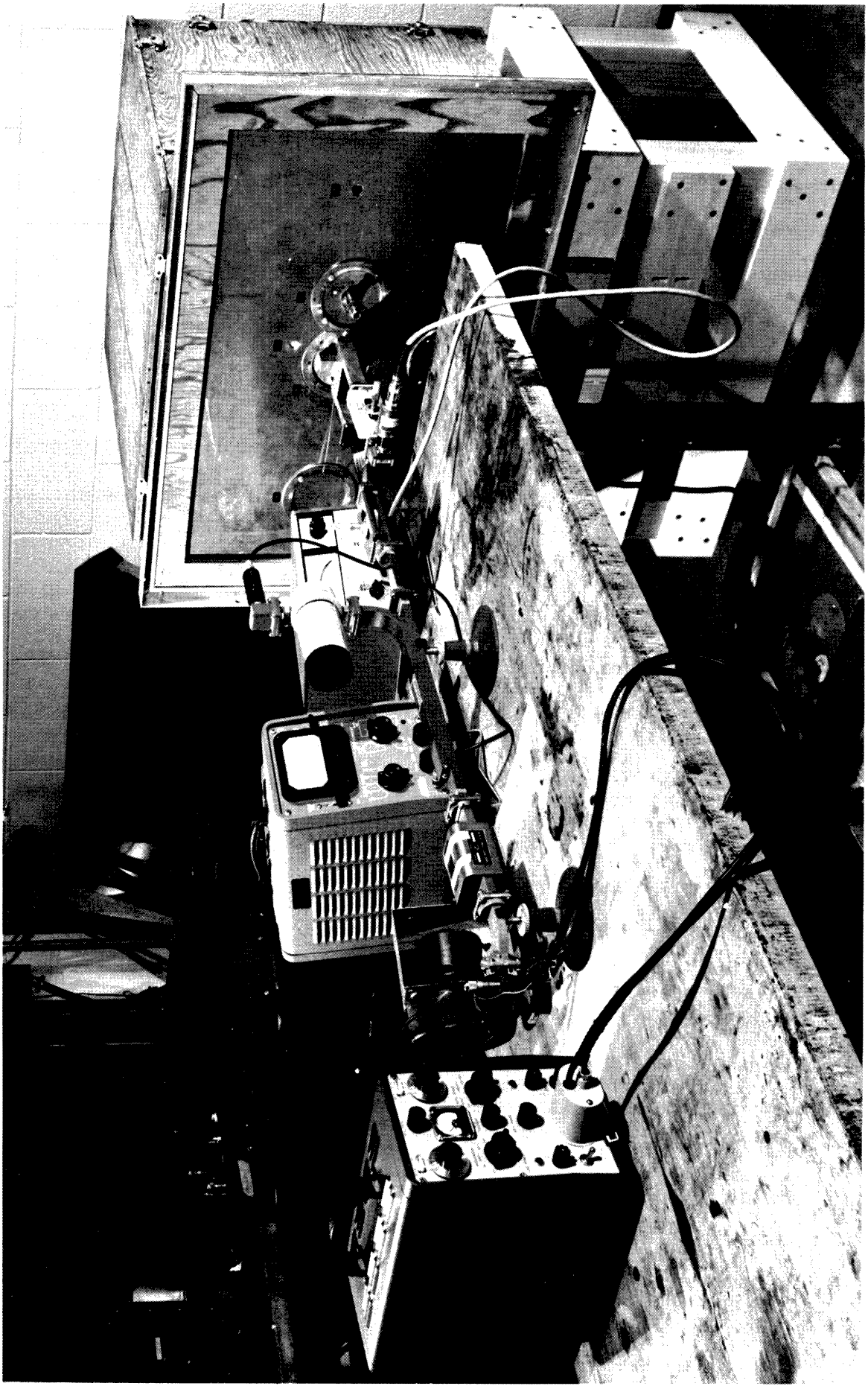

FIG. 3-16: EXPERIMENTAL SETUP WITH MINIATURE ANECHOIC CHAMBER

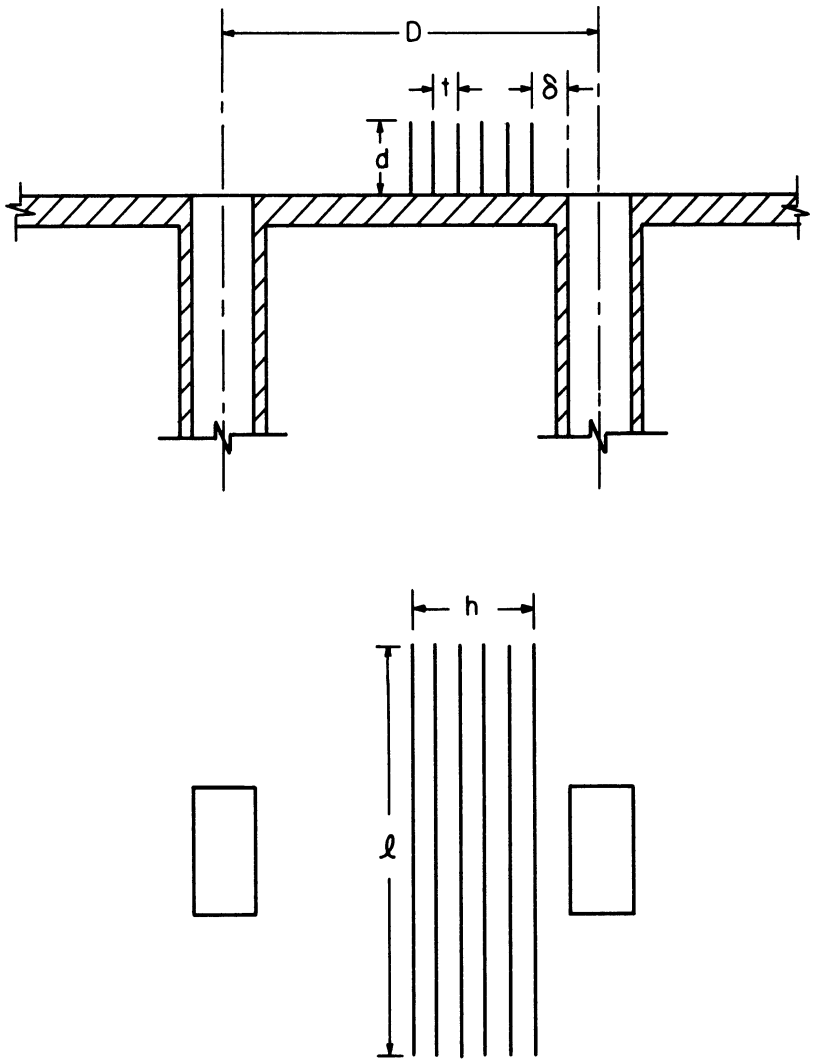

FIG. 3-17: TWO SLOTS WITH CORRUGATED STRUCTURE INBETWEEN

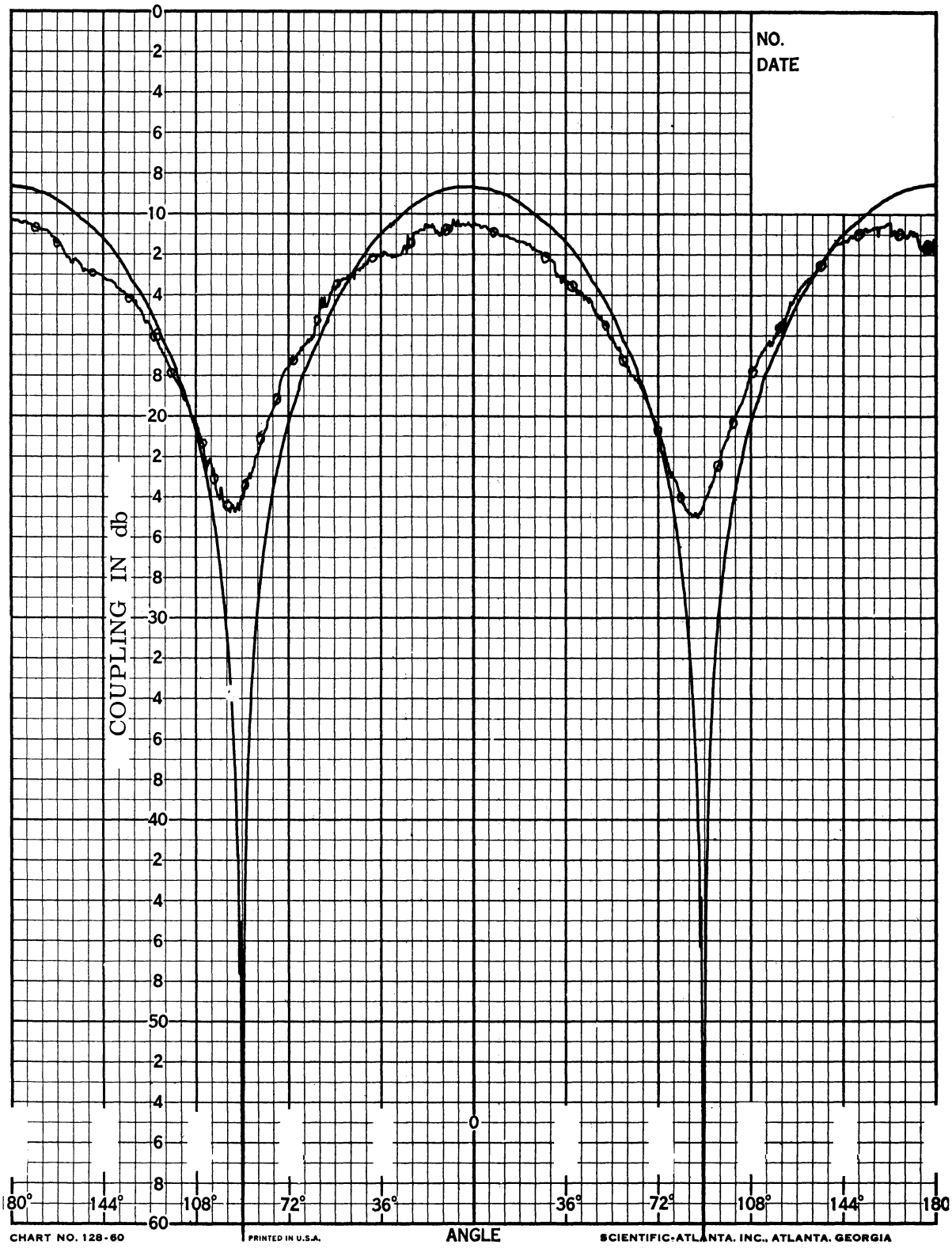

FIG. 3-18: E-PLANE COUPLING FOR SLOTS; f = 8.23 GHz; D = 11.4 cm; 0 = -20 db; (—) No corrugation; (-o-) With corrugation; t = 2.1 mm; ℓ = 9 cm; d = 0.9 cm; h = 5.4 cm; 8 = 1.2 cm

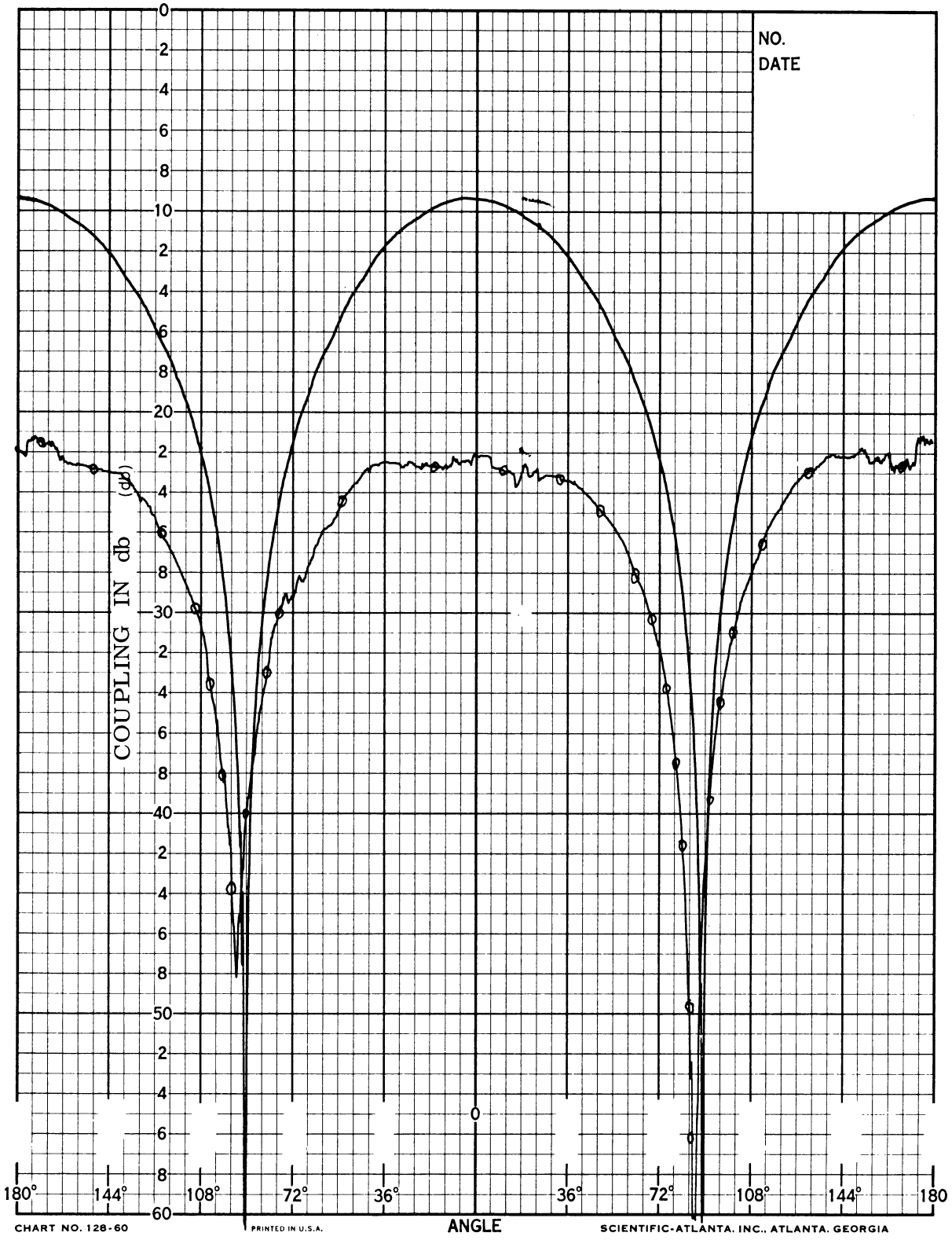

FIG. 3-19: E-PLANE COUPLING FOR SLOTS; f = 9.03 GHz; D = 11.4 cm; 0 = -20 db; (—) No corrugation; (-o-) With corrugation; t = 2.1 mm; ℓ = 9 cm d = 0.9 cm; h = 5.4 cm; δ = 1.2 cm

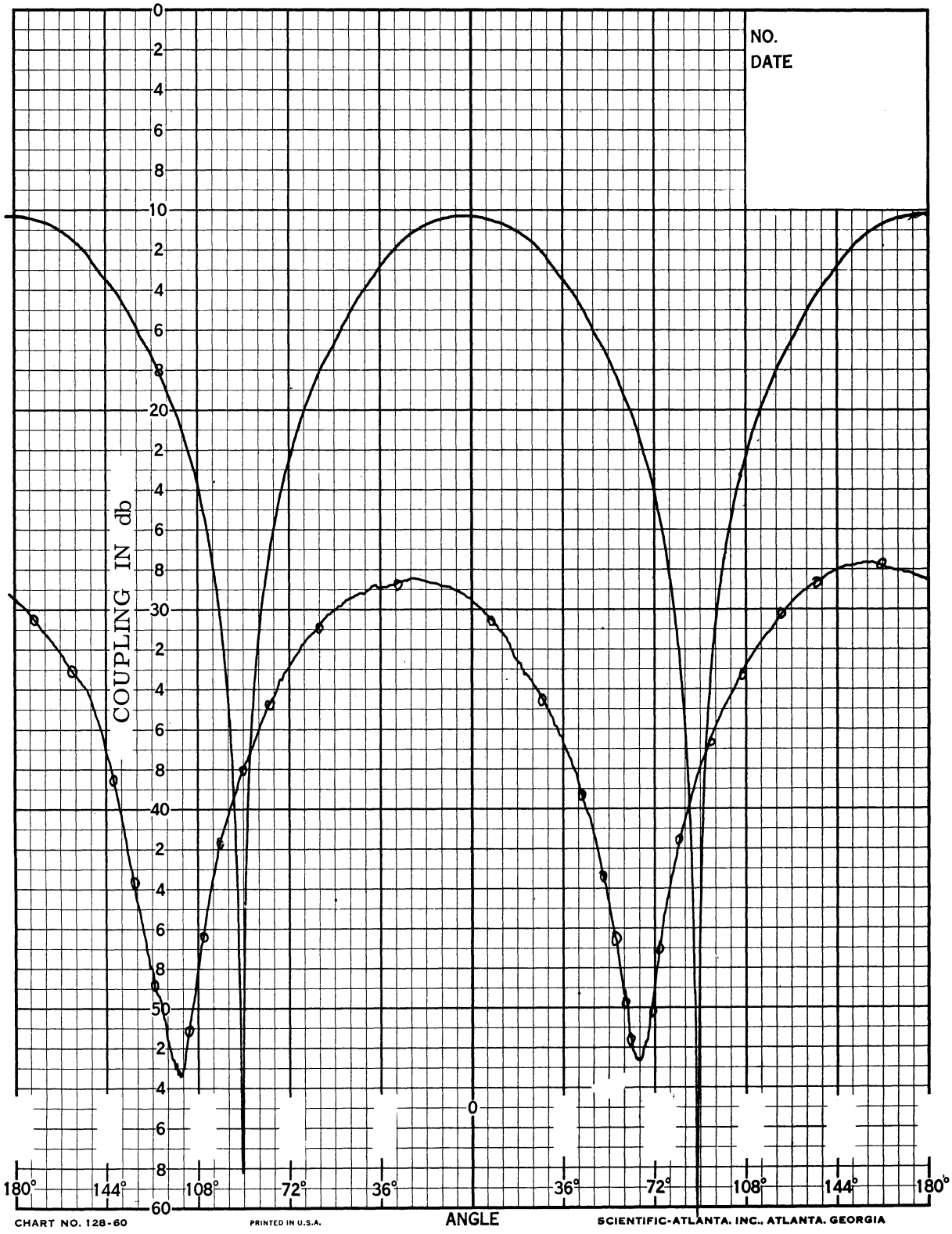

FIG. 3-20: E-PLANE COUPLING FOR SLOTS; f = 10.03 GHz; D = 11.4 cm; 0 = -20 db; (—) No corrugation; (-o-) With Corrugation; t = 2.1 cm; ℓ = 9 cm; d = 0.9 cm; h = 5.4 cm; δ = 1.2 cm

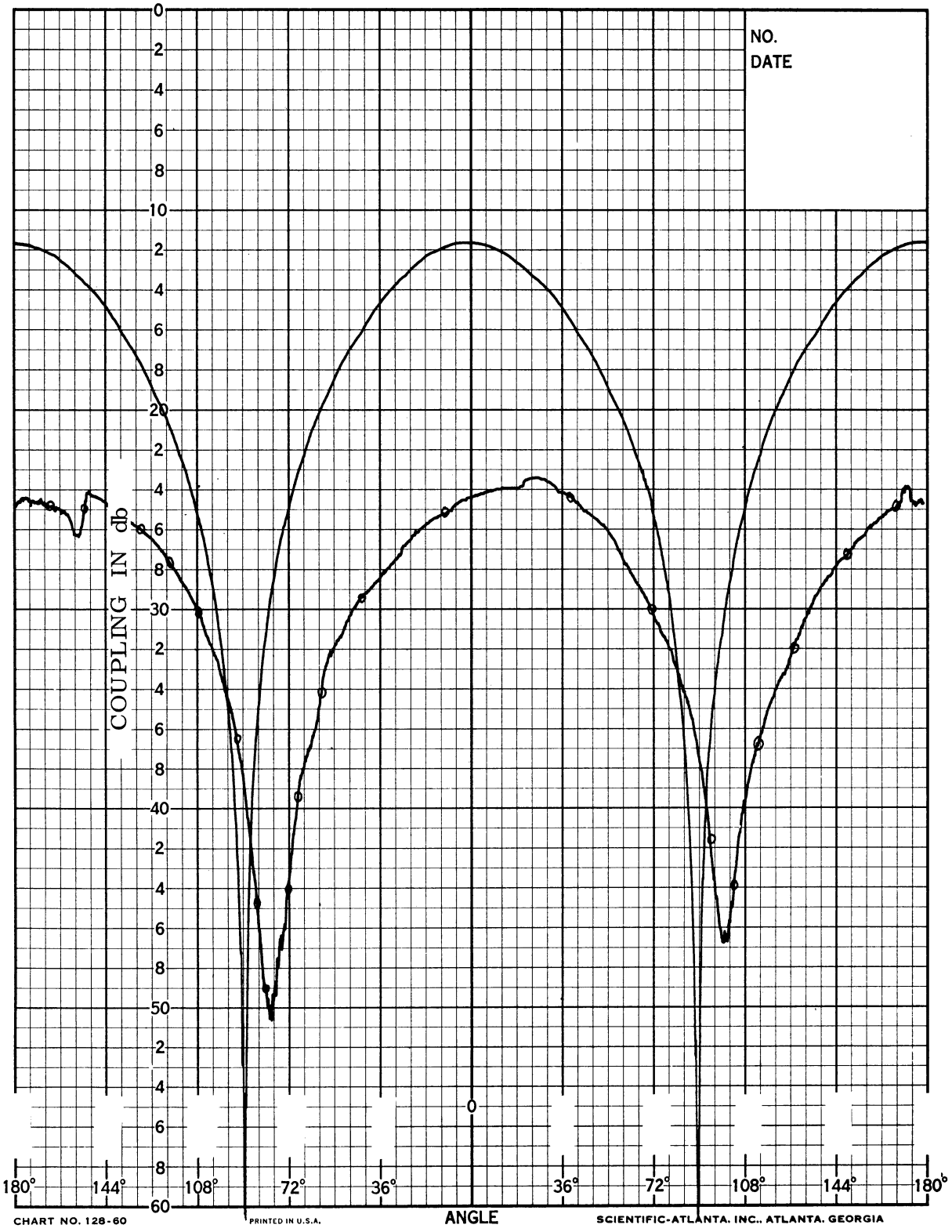

FIG. 3-21: E-PLANE COUPLING FOR SLOTS; f = 11.03 GHz; D = 11.4 cm; 0 = -20 db; (—) No corrugation; (-o-) With corrugation; t = 2.1 mm; ℓ = 9 cm; d = 0.9 cm; h = 5.4 cm; δ = 1.2 cm

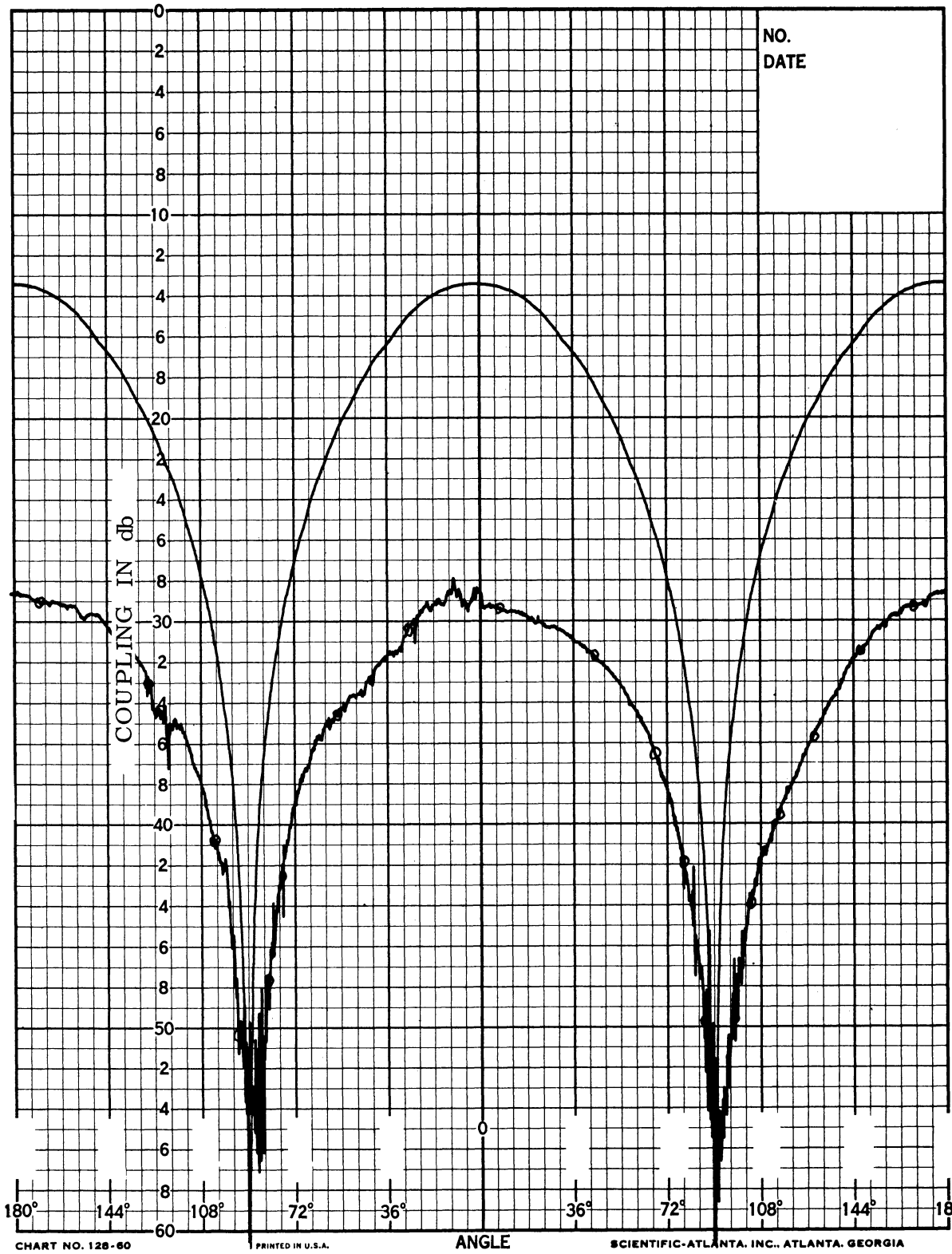

FIG. 3-22: E-PLANE COUPLING FOR SLOTS; f = 12.03 GHz; D = 11.4 cm; 0 = -20 db; (—) No corrugation; (-o-) With corrugation; t = 2.1 mm; ℓ = 9 cm; d = 0.9 cm; h = 5.4 cm; δ = 1.2 cm

a as high as 24 db.

d) The resonant frequency of the decoupling is expected to depend very much on the separation and depth.

e) The decoupling was sensitive to the position of the corrugation between the two slots or depends on δ .

f) For the case of H-plane coupling the coupling with the corrugated surface was higher than without the corrugated surface.

3.4.2 Radiation Patterns for Slot in the Presence of Free Standing Ribbed Structure

A set of experiments was performed to measure the field patterns (E-plane and H-plane) of a slot antenna with and without the existence of the corrugated surface in the neighborhood.

From this set of experiments the following observations were made:

a) For the case of E-plane patterns the pattern was affected as shown for different frequencies and for different locations of the corrugated strip with respect to the slot. (Figs. 3-23 to 3-27)

b) For the case of H-plane patterns it was noticed that the pattern with corrugated strip was not as much affected as the case without corrugation but still it was sensitive to the location of the strip with respect to the slot.

3.4.3 Ribbed Structure Flush-Mounted

Slot antennas were arranged with a cavity in between. This construction permitted the use of either a corrugated surface or absorbing material between the two slots for the flush-mounted case. (Figs. 3-28 to 3-30)

This coupling experiment was for E-plane or strong coupling versus frequency.

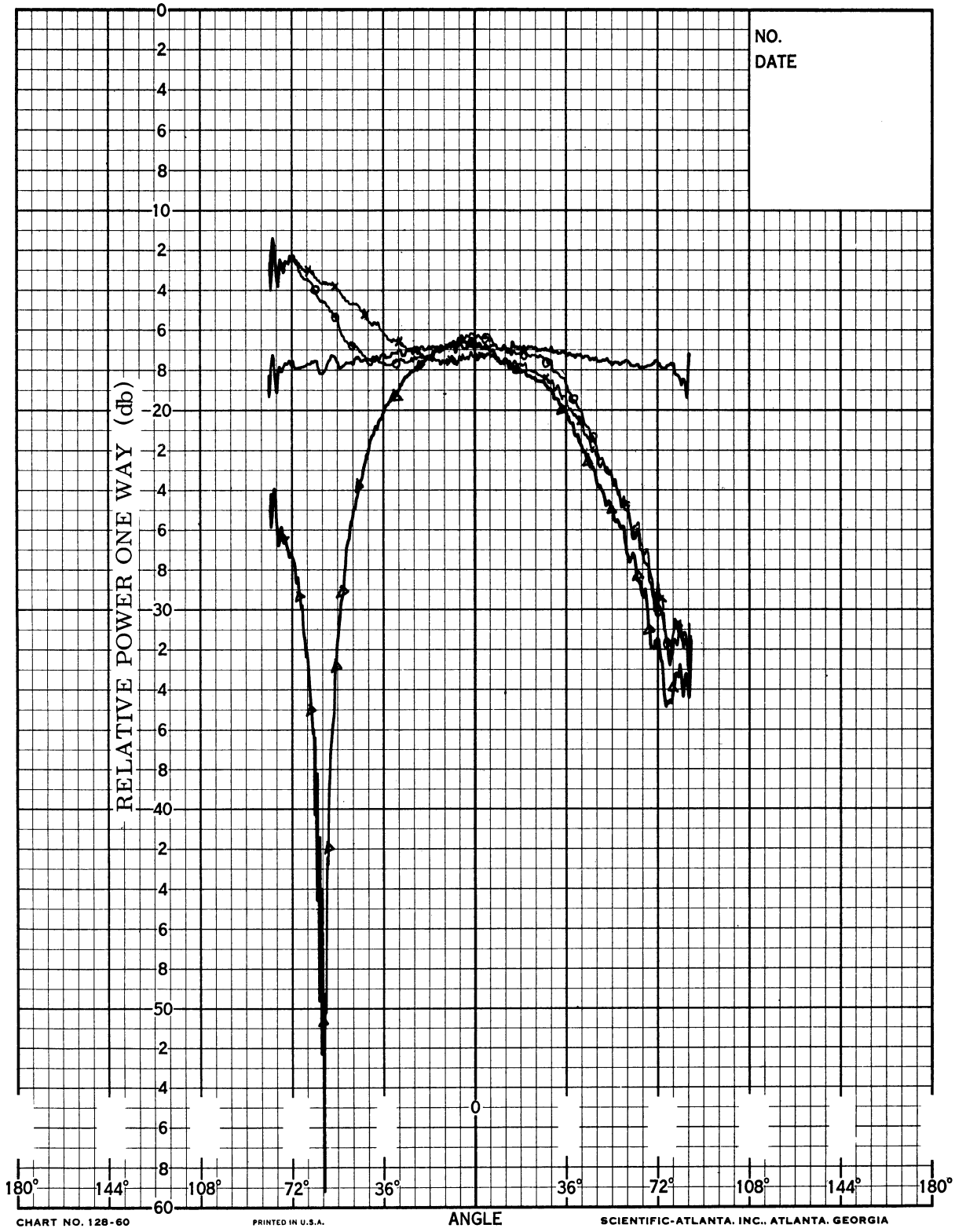

FIG. 3-23: E-PLANE RADIATION PATTERN FOR SLOT; f = 8.23 GHz; (—) No corrugation; (-△-) δ = 0.7 cm; (-o-) δ = 1.2 cm; (-x-) δ = 1.6 cm; t = 2.1 mm; ℓ = 9 cm; d = 0.9 cm; h = 5.4 cm

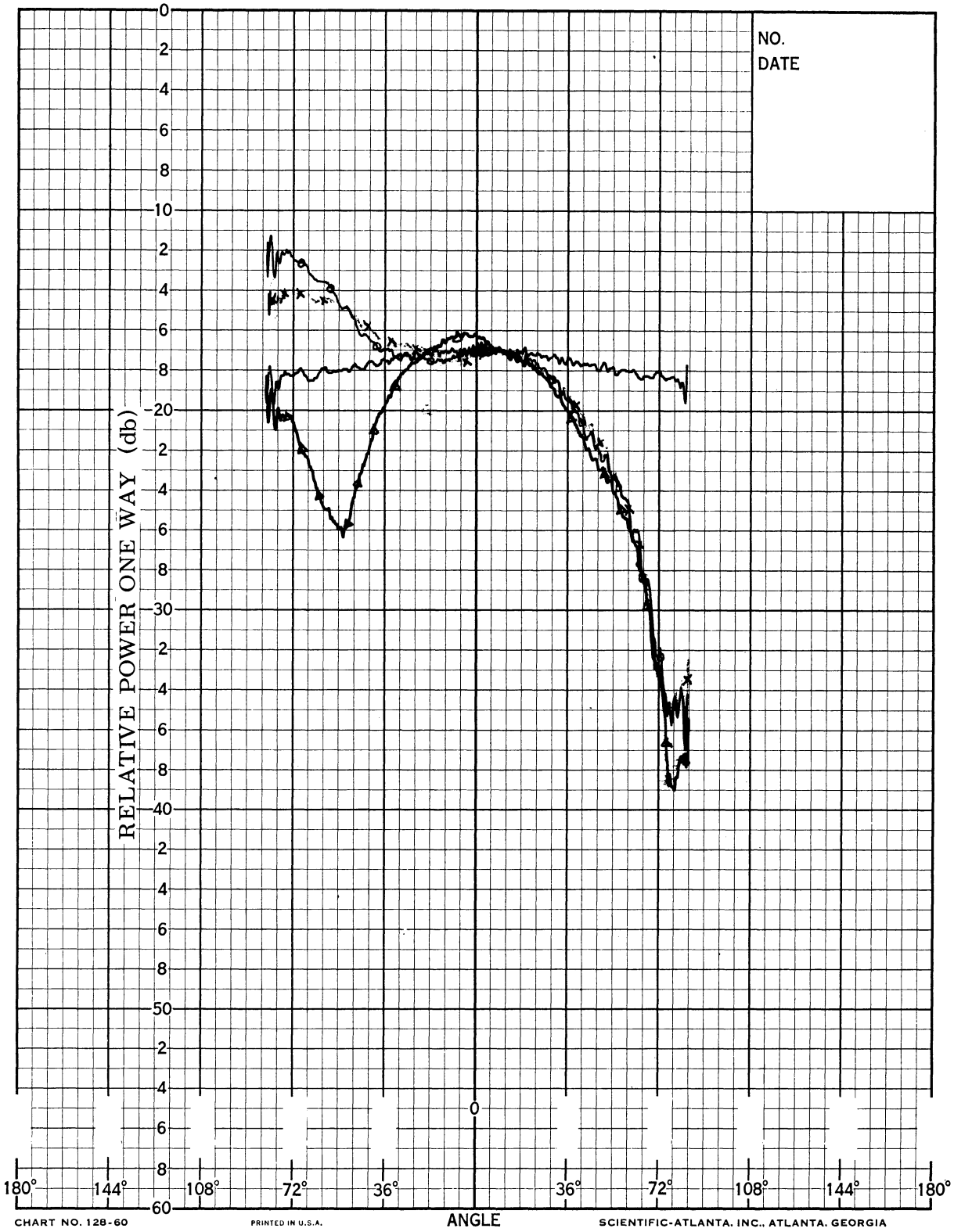

FIG. 3-24: E-PLANE RADIATION PATTERN FOR SLOT; f = 9.03 GHz; (—) No corrugation; (—△—) δ = 0.7 cm; (—o—) δ = 1.2; (—x—) δ = 1.6 cm; t = 2.1 mm; ℓ = 9 cm; d = 0.9 cm; h = 5.4 cm

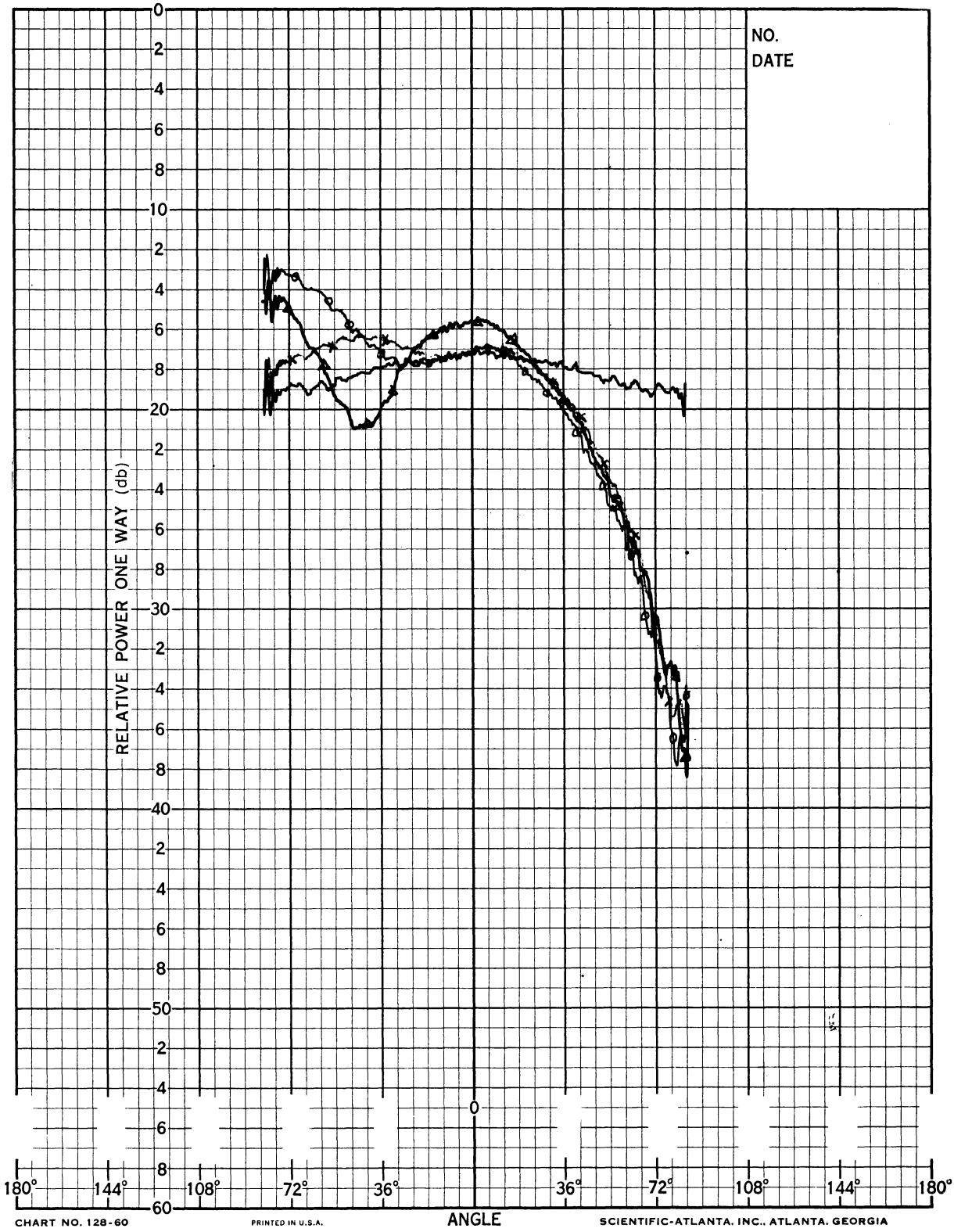

FIG. 3-25: E-PLANE RADIATION PATTERN FOR SLOT; f = 10.03 GHz; (—) No corrugation; (-△-) δ = 0.7 cm; (-o-) δ = 1.2 cm; (-x-) δ = 1.6 cm; t = 2.1 mm; ℓ = 9 cm; d = 0.9 cm; h = 5.4 cm

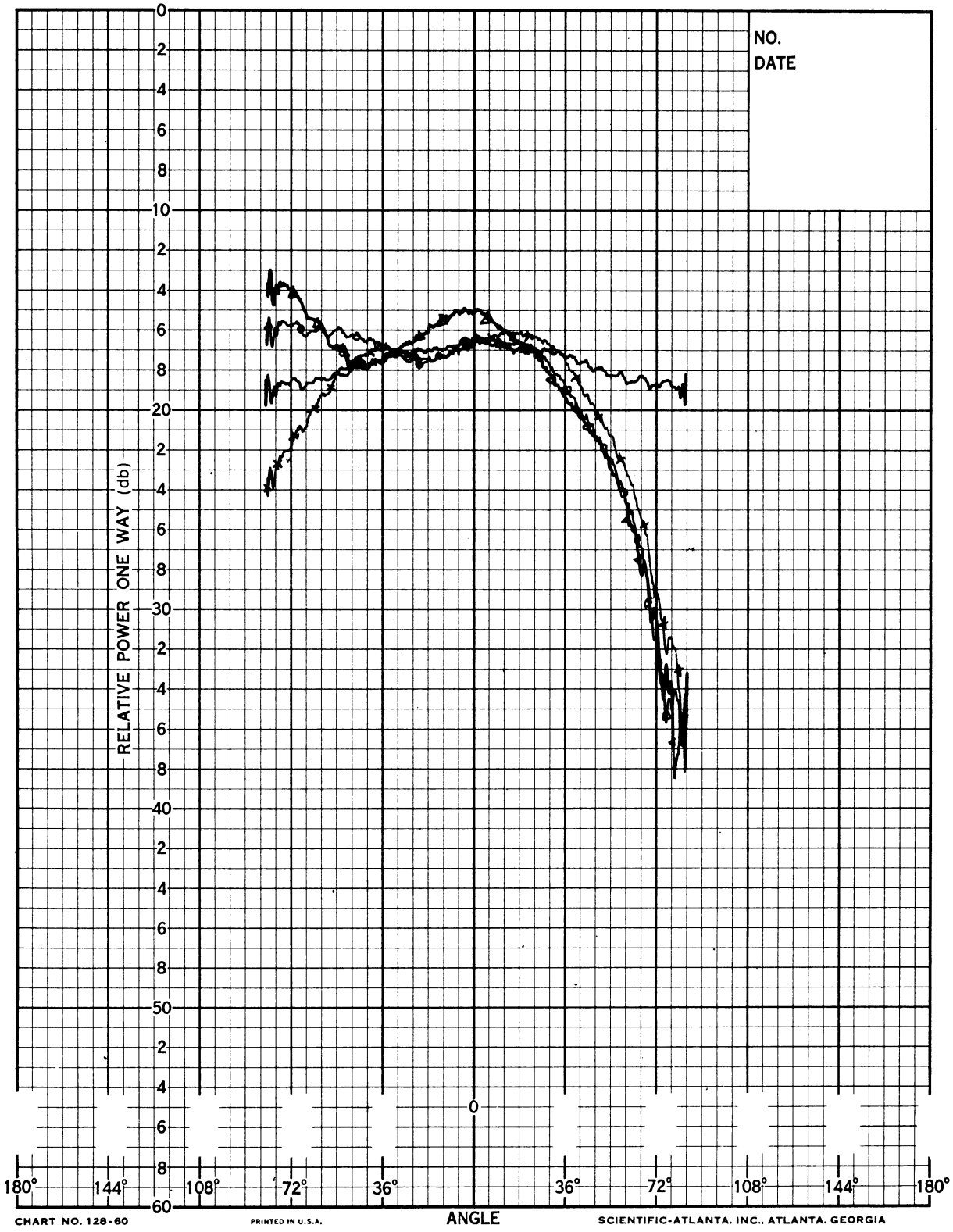

FIG. 3-26: E-PLANE RADIATION PATTERN FOR SLOT; f = 11.03 GHz; (—) No corrugation; (-△-) δ = 0.7 cm; (-o-) δ = 1.2 cm; (-x-) δ = 1.6 cm; t = 2.1 mm; ℓ = 9 cm; d = 0.9 cm; h = 5.4 cm

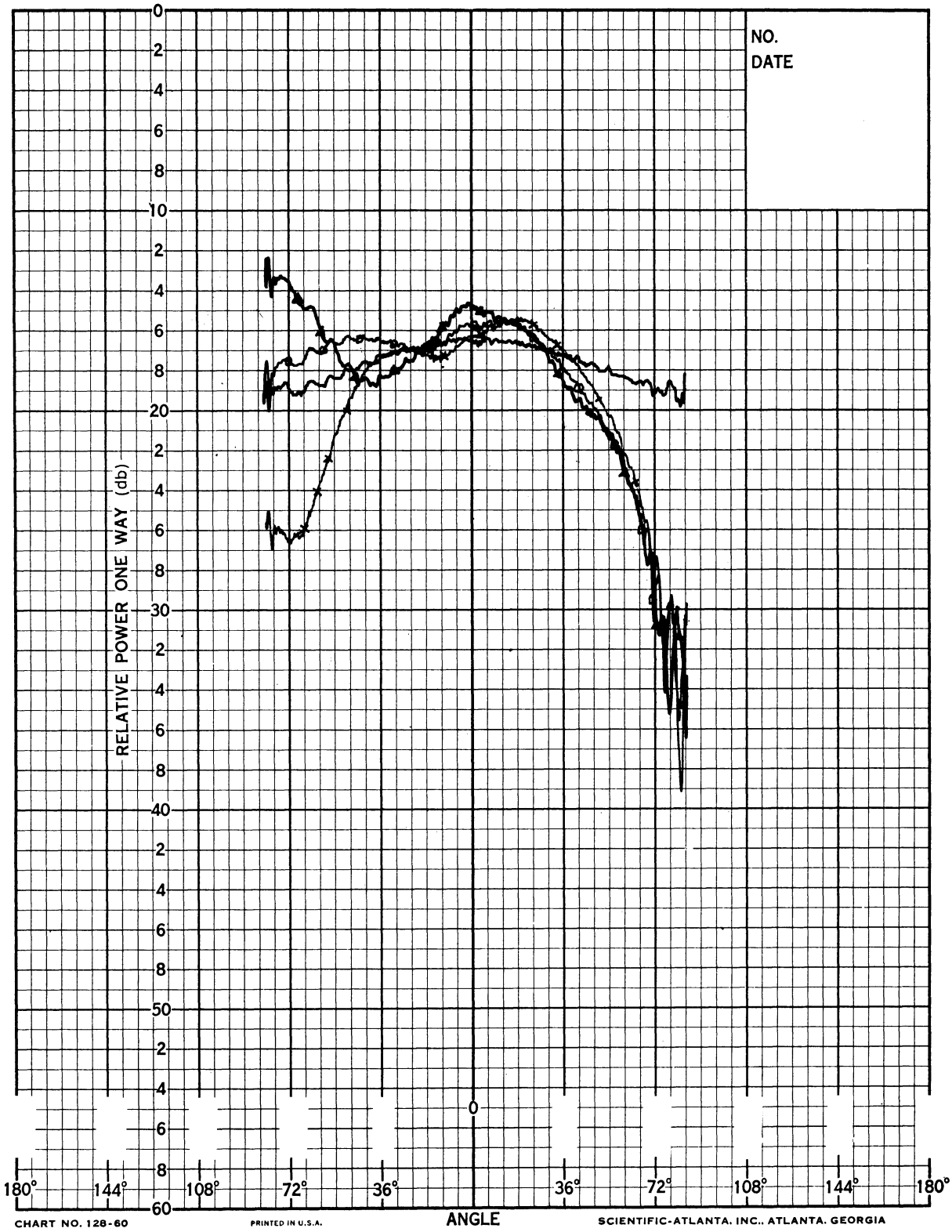

FIG. 3-27: E-PLANE RADIATION PATTERN FOR SLOT; f = 12.03 GHz; (—) No corrugation; (△) δ = 0.7 cm; (⊖) δ = 1.2 cm; (✕) δ = 1.6 cm; t = 2.1 mm; ℓ = 9 cm; d = 0.9 cm; h = 5.4 cm

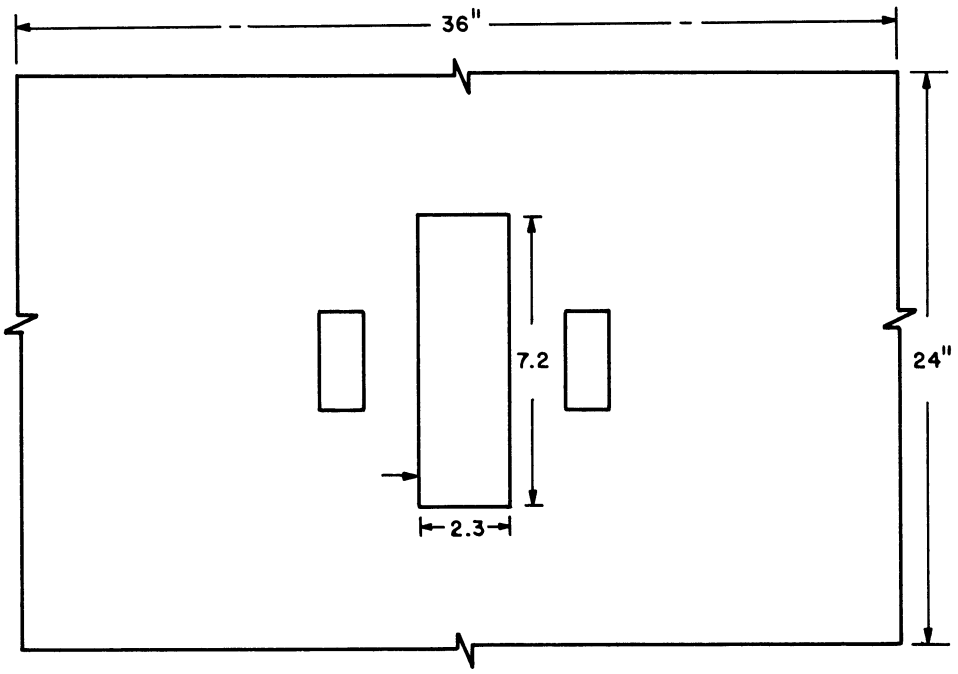

FRONT VIEW

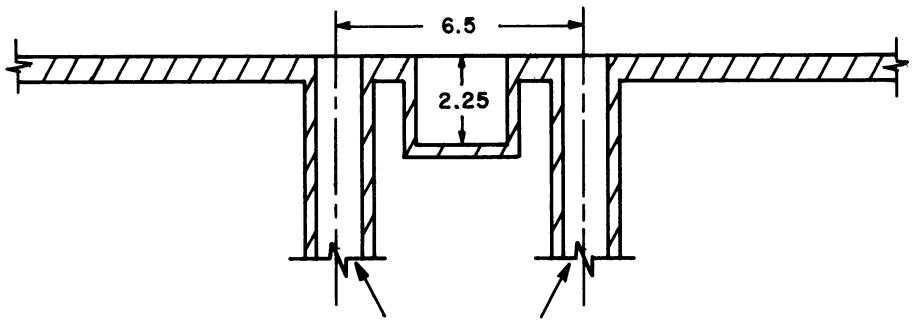

X-BAND WAVE GUIDE

FIG. 3-28: GEOMETRY OF SLOTS WITH CAVITY INBETWEEN

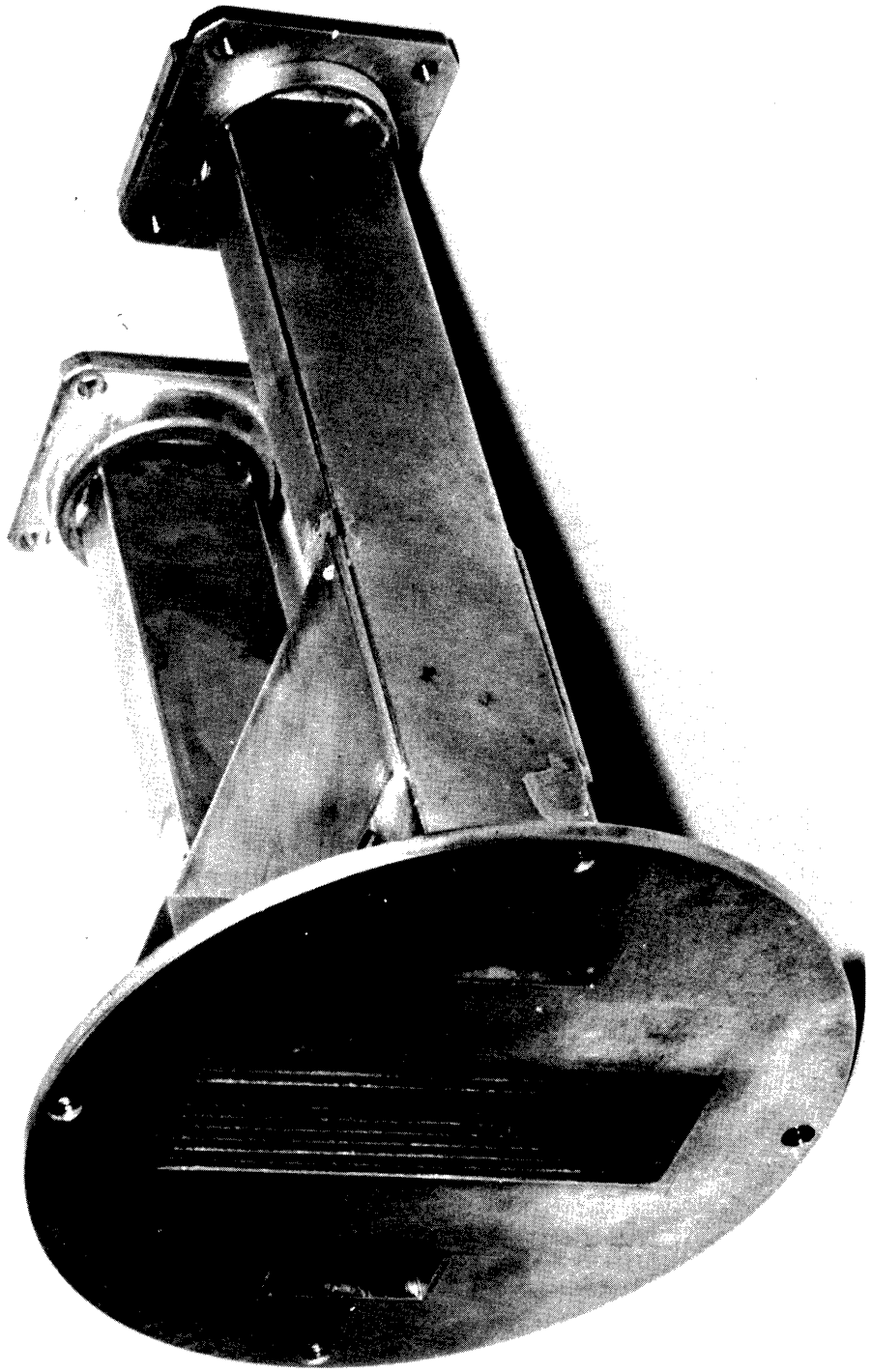

FIG. 3-29: PHOTOGRAPH OF THE FLUSH MOUNTED CORRUGATED STRUCTURE

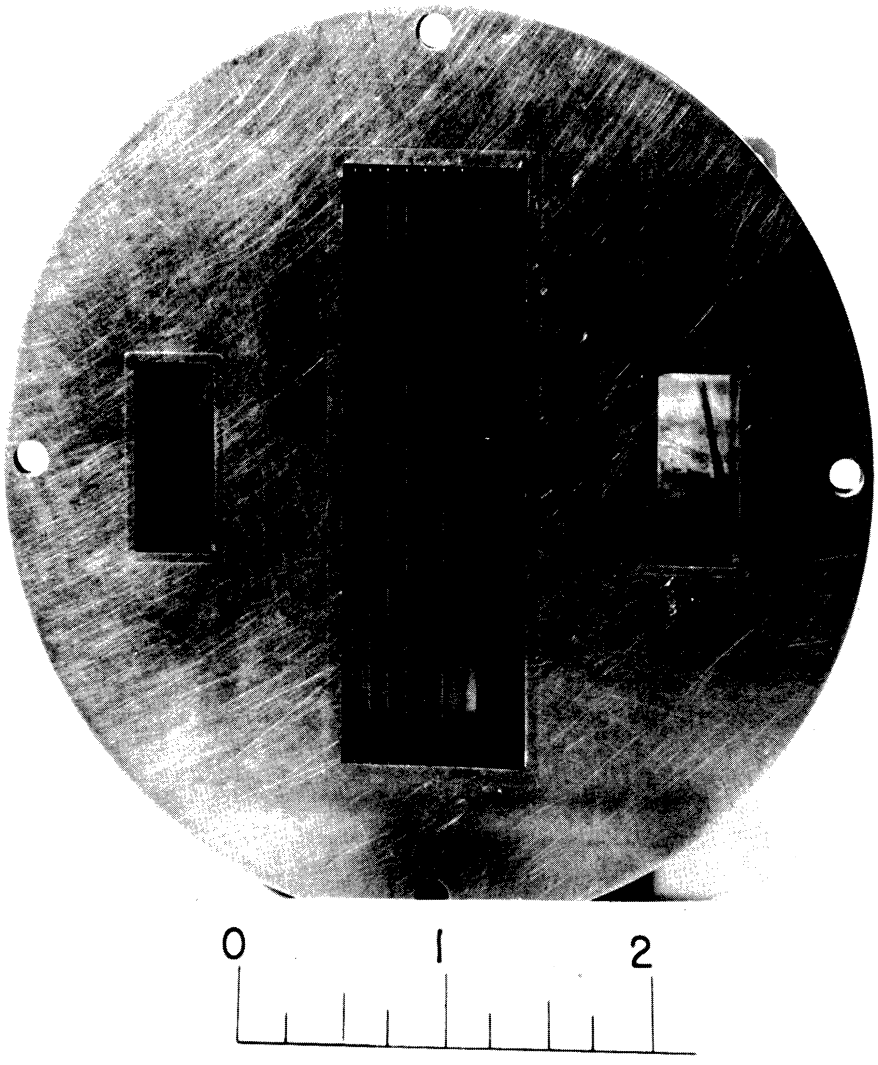

FIG. 3-30: FRONT VIEW OF THE FLUSH MOUNTED CORRUGATED STRUCTURE

It was noticed that:

a) The decoupling by means of the flush-mounted ribbed structure was less than the decoupling with the same piece of corrugation put over the ground plane (Fig. 3-31).

b) The decoupling in this case was not as high as the decoupling obtained from the case of section 3.4.1 because the width of the ribbed structure was less and as mentioned before this has great effect on coupling reduction.

e) The dimensions of the corrugations were not changed but obviously should be to find the optimum decoupling.

d) E-plane patterns at different frequencies with corrugations and without corrugations are given (Figs. 3-31 to 3-33).

e) H-plane patterns at different frequencies with the corrugations placed in between the two slots are compared with patterns taken with the cavity covered (Figs. 3-34 and 3-35)

3.5 Flush-Mounted Absorbing Material

A set of experiments similar to the case in section 3.4.3 has been performed. The cavity in this case was filled with either B.F. Goodrich RF - material, or Emerson-Cuming Incorporated Ecco-Sorb CR material.

It was noticed that:

a) There is a very large difference in the reduction of coupling for the flush-mounted case as compared with the absorber slab over the ground plane (see Figs. 3-36 to 3-38).

b) A set of curves for the E-plane radiation pattern was obtained for different frequencies (see Figs. 3-39 and 3-40).

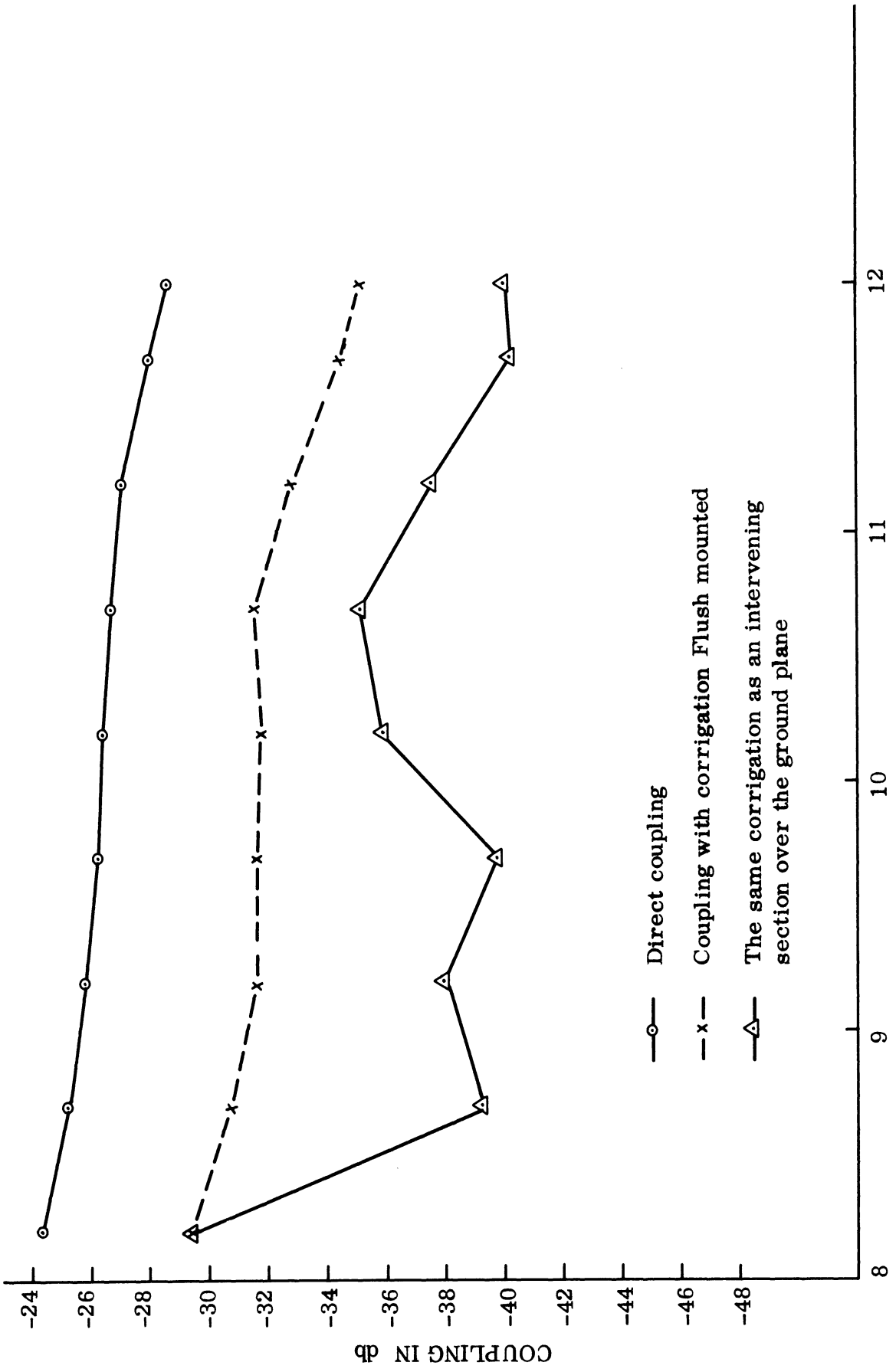

FIG. 3-31: E-PLANE FREQUENCY VS. COUPLING FOR CORRUGATED STRUCTURE
Dimensions: length 7.2 cm; depth 1 cm; fin separation 2.1 mm; total width 2.3 cm

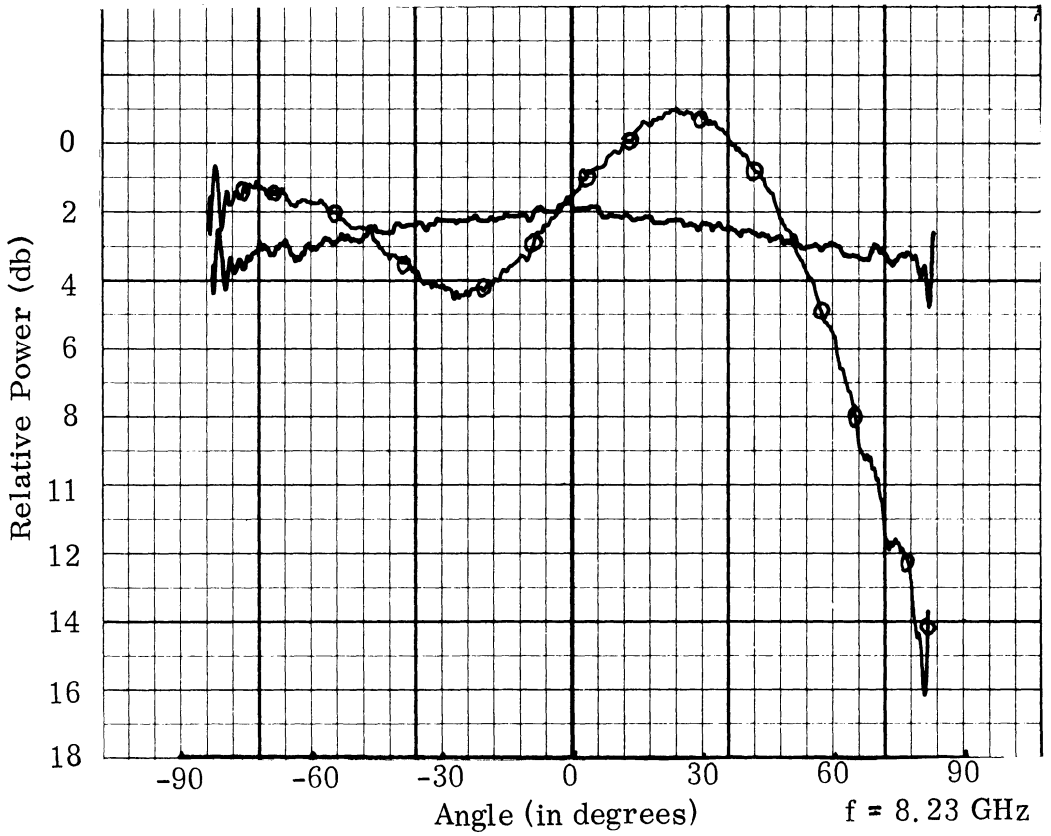

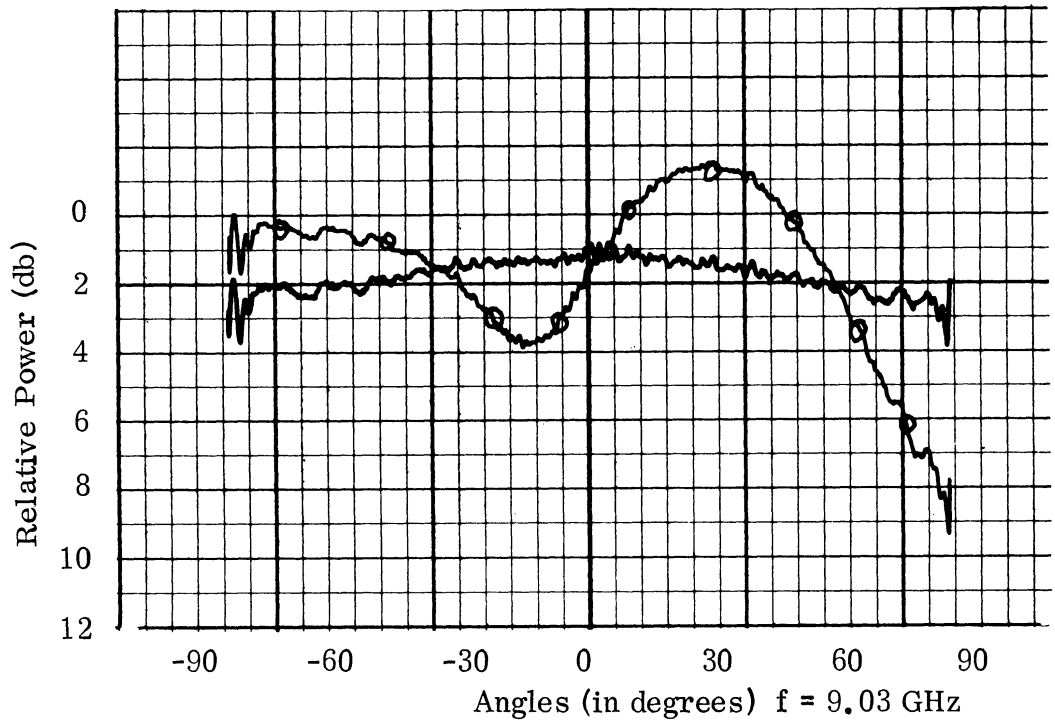

FIG. 3-32: E-PLANE RADIATION PATTERN FOR SLOT, (——) No corrugation or cavity covered, (-o-) With Flush-mounted corrugation, t = 2.1 mm, ℓ = 7.2 cm, d = 0.9 cm, h = 2.3 cm.

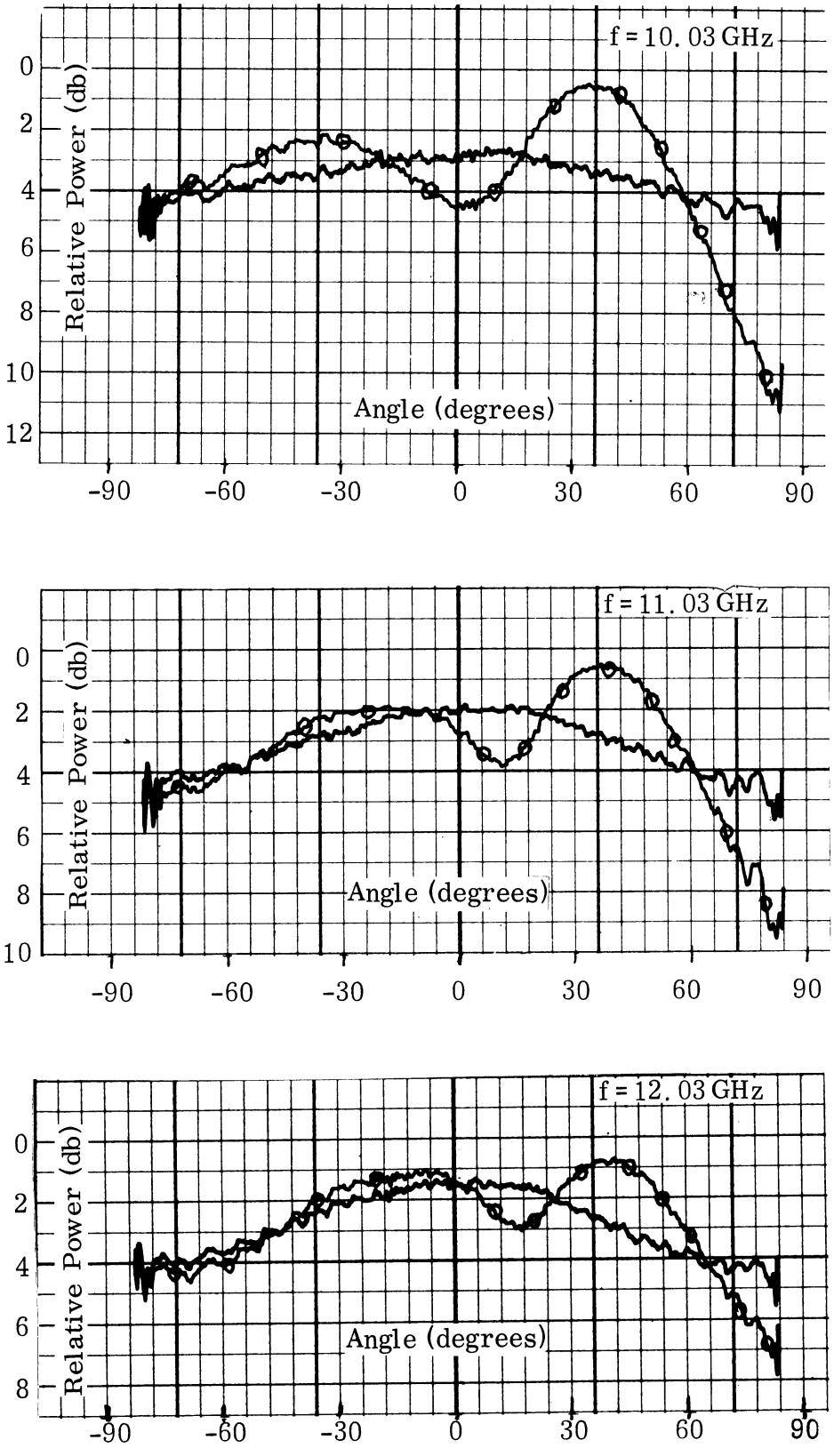

FIG. 3-33: E-PLANE RADIATION PATTERN FOR SLOT; (—) Cavity covered; (-⊕-) With Flush mounted corrugation; t = 2.1 mm; ℓ = 7.2 cm; d = 0.9 cm; h = 2.3 cm

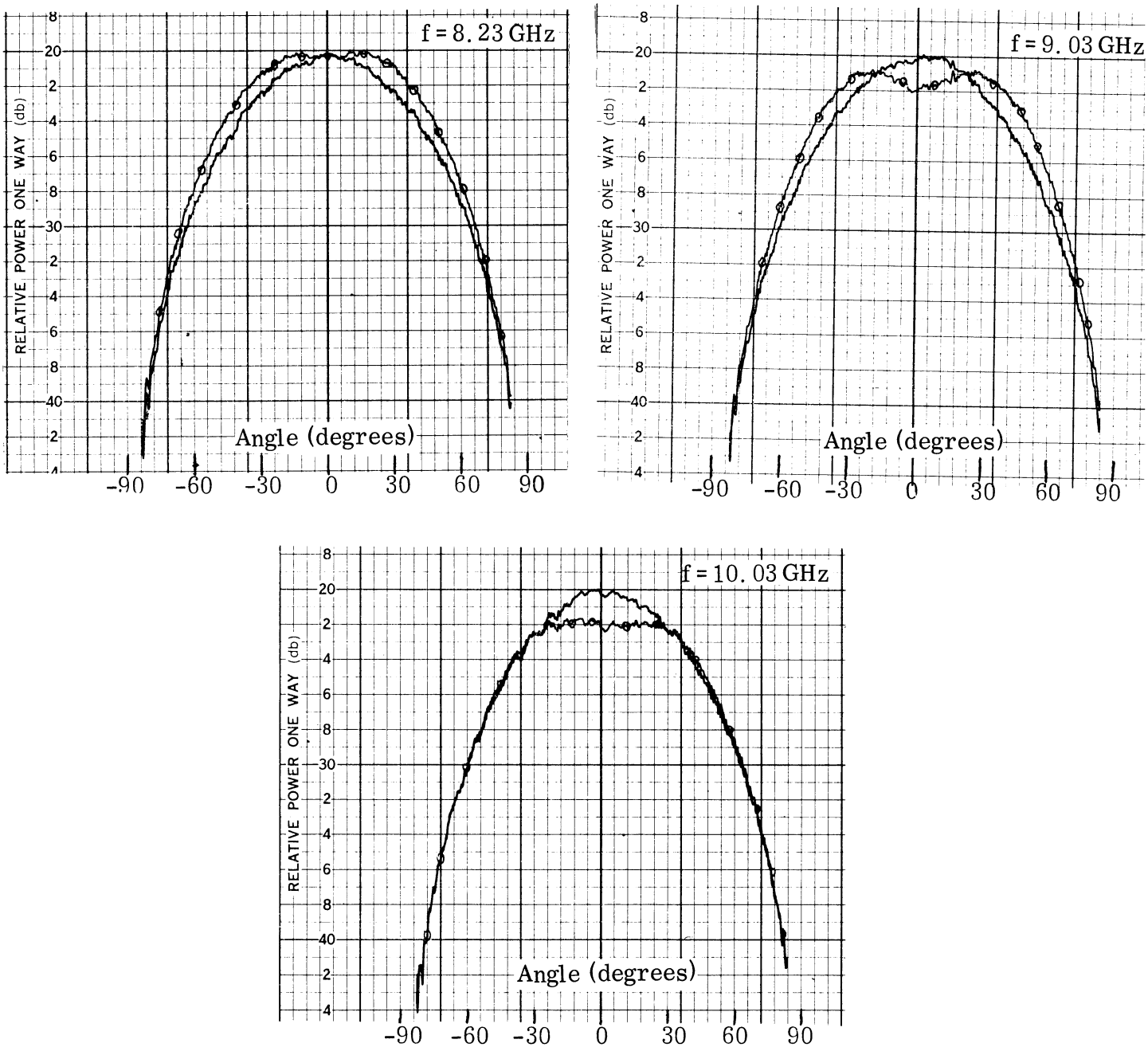

FIG. 3-34: H-PLANE RADIATION PATTERN FOR SLOT; (—) Cavity covered; (-o-) With Flush Mounted corrugation; t = 2.1 mm; ℓ = 7.2 cm; d = 0.9 cm; h = 2.3 cm

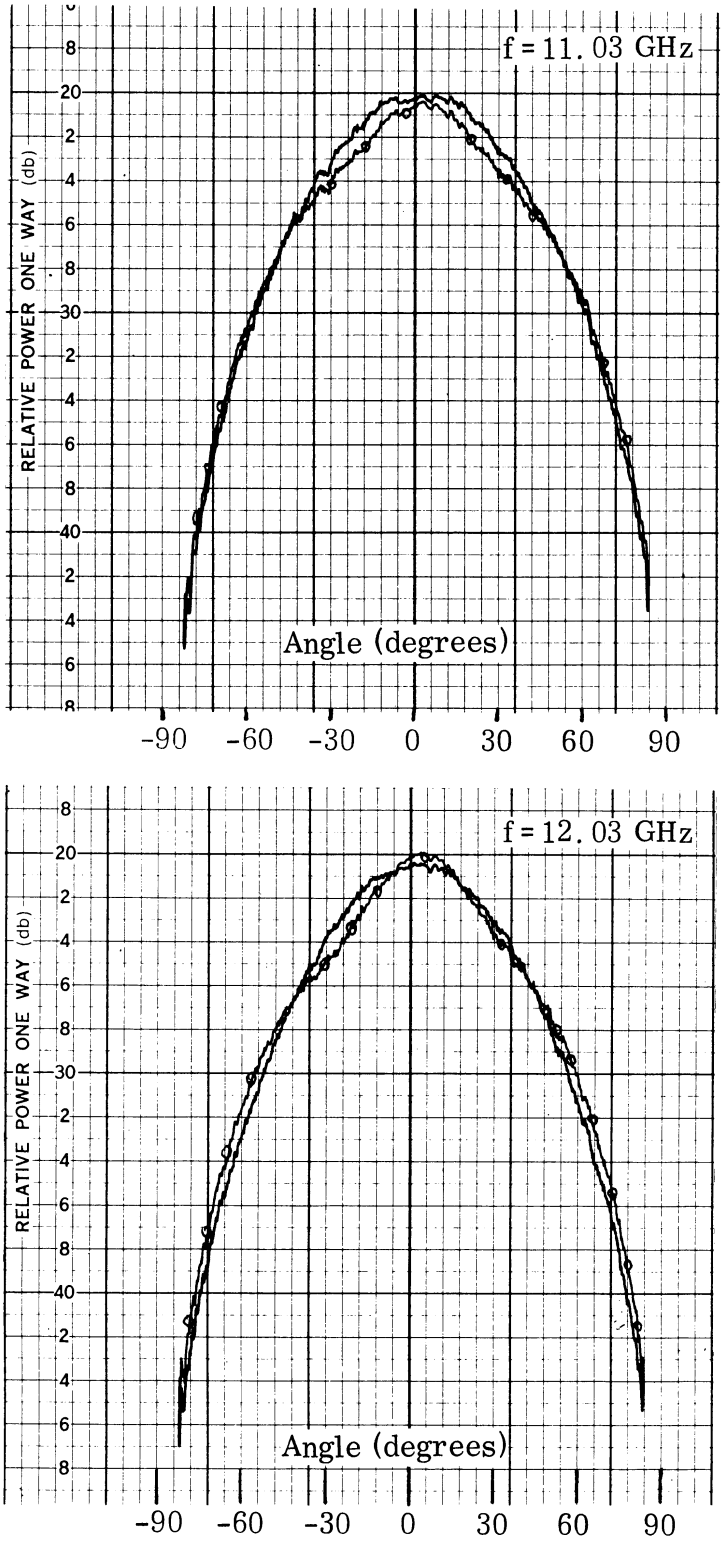

FIG. 3-35: H-PLANE RADIATION PATTERN FOR SLOT; (—) Cavity covered; (-o-) With flush mounted corrugation; t = 2.1 mm; ℓ = 7.2 cm; d = 0.9 cm; h = 2.3 cm

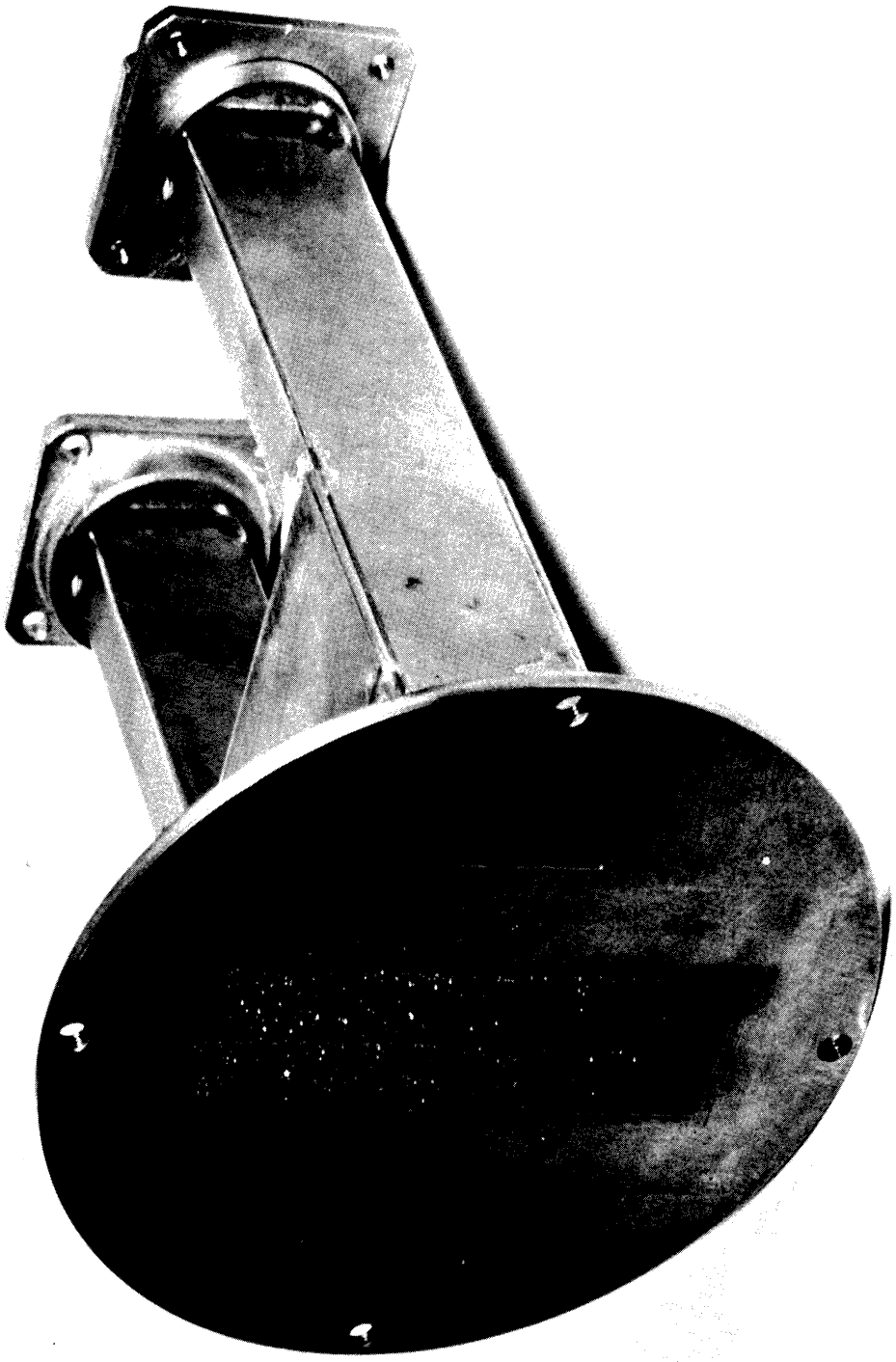

FIG. 3-36: CAVITY FILLED WITH ABSORBING MATERIAL

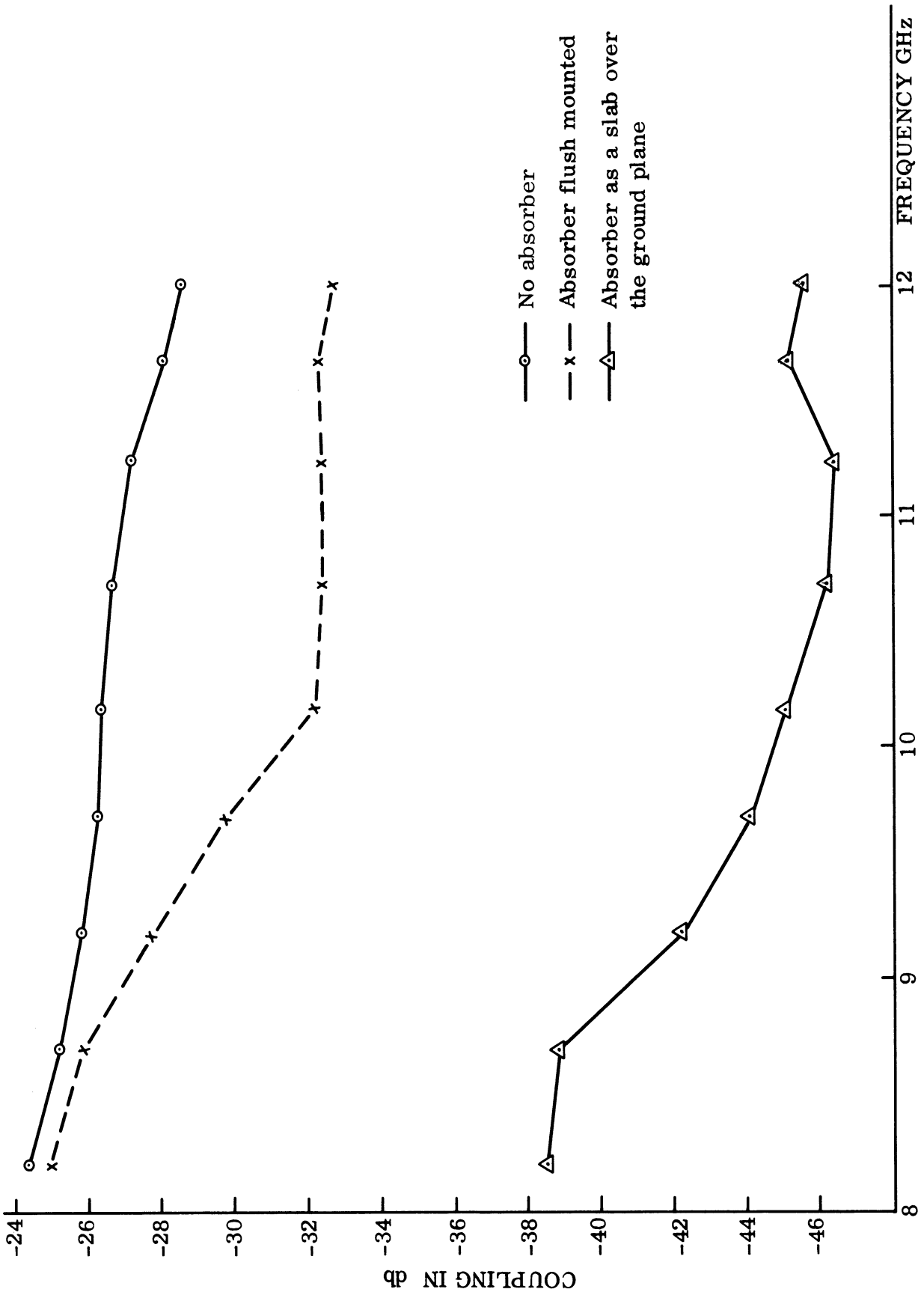

FIG. 3-37: E-PLANE COUPLING VS. FREQUENCY FOR SLOTS WITH CAVITY INBETWEEN B. F. Goodrich RF-X with slot separation 6.5 cm and in the middle a cavity with dimensions length 7.2, width 2.3, depth 2.25

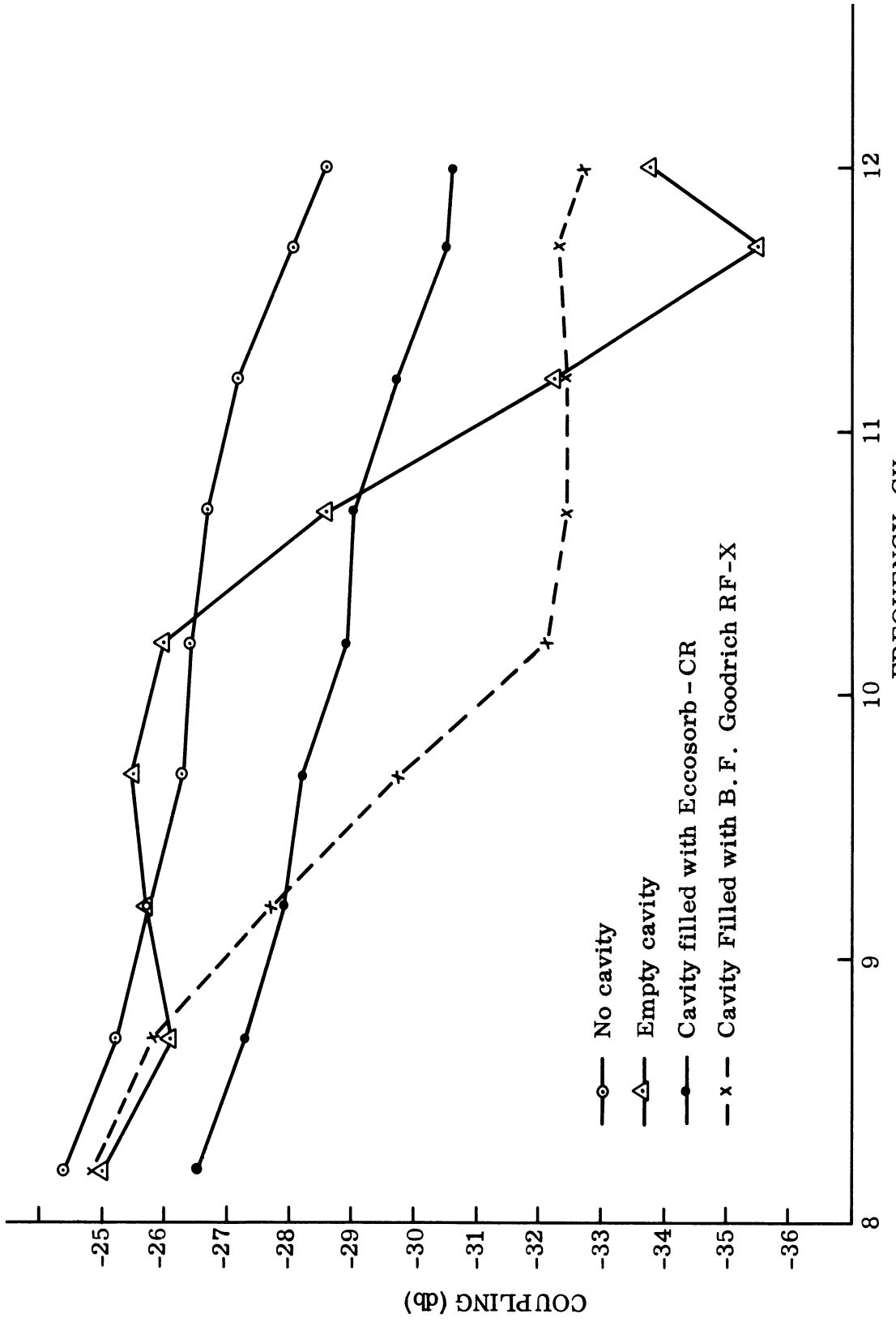

FIG. 3-38: E-PLANE COUPLING VS. FREQUENCY FOR TWO SLOTS WITH CAVITY INBETWEEN; D = 6.5 cm

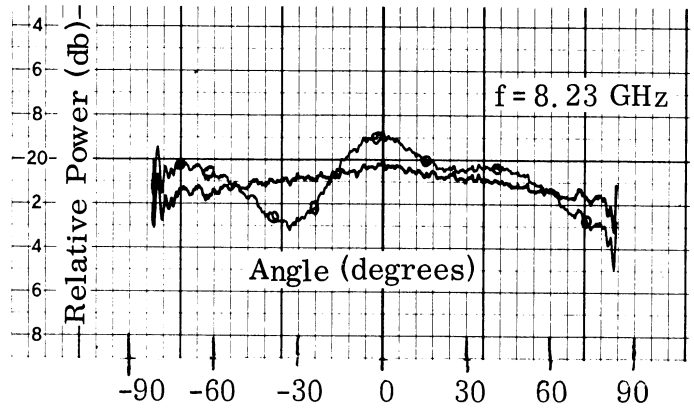

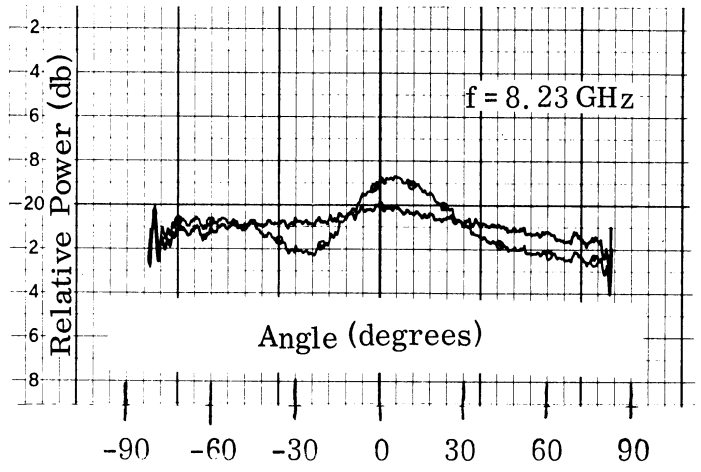

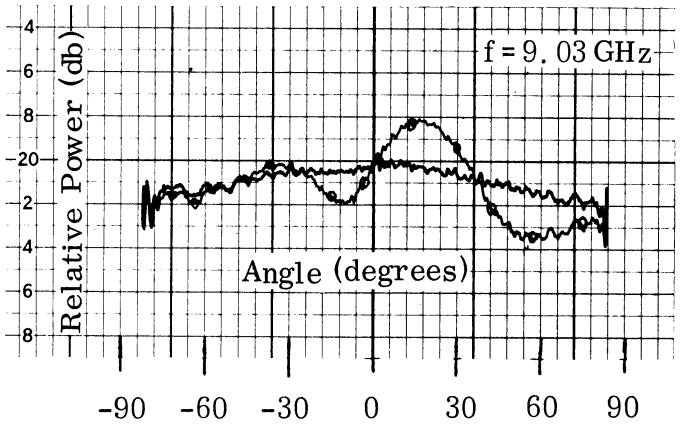

FIG. 3-39: E-PLANE RADIATION PATTERN FOR SLOT

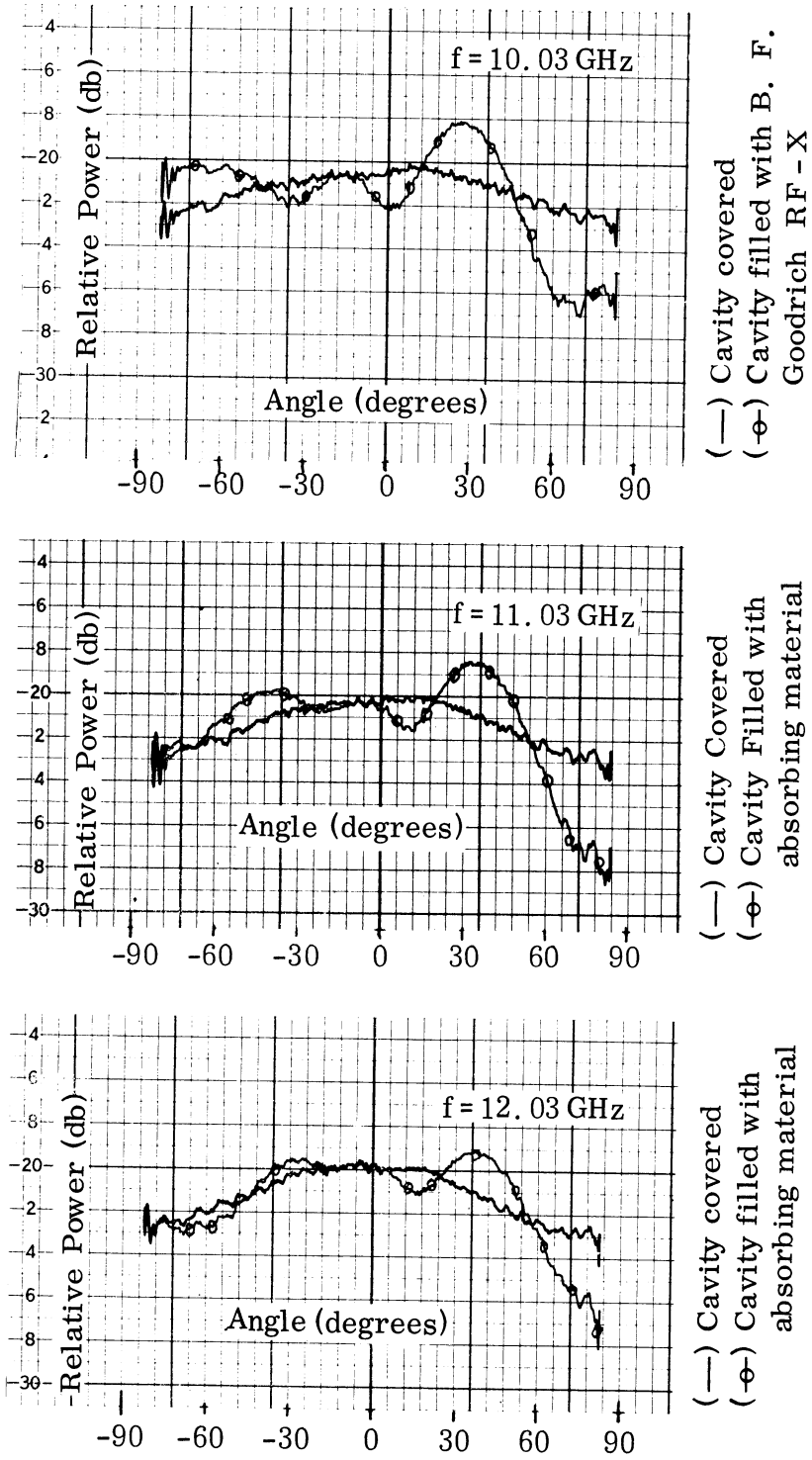

FIG. 3-40: E-PLANE RADIATION PATTERN FOR SLOT

IV

ABSORBING MATERIALS

A task of preparation and evaluation of absorbing materials has been initiated. The requirements which these materials must meet are high dielectric and magnetic loss factors and an intrinsic impedance nearly that of free space. These requirements are imposed by the fact that these materials are to be used as flush-mounted absorbers between two slot antennas with the intention of increasing their isolation. A preliminary investigation and procedure for preparation and testing of these materials is already in progress. Several compositions by weight of wax, iron powder, aluminum powder and carbon black have been produced by heating of the components. The resulting mixtures, after they are allowed to cool have been machined to proper toroid sizes so that they can be tested for their μ and ϵ characteristics. The measurement techniques have been previously reported by this laboratory.

Twelve mixtures have been prepared altogether. Permeability and magnetic Q measurements have been taken so far for compositions 7, 8, 9, 10, 11 at a frequency range between 75 and 400 MHz. The data are reported in Table IV-1 and plotted in Figs. 4-1 a, b, c, d and e and Figs. 4-2 a, b, c, d and e. From the loss tangent graphs in Fig. 4-2 it is clear that the mixtures appear to be rather promising from the aspect of high magnetic Q factor near the 300-400 MHz range. Any conclusions for the applicability of these mixtures however cannot be drawn as yet. There still is need to measure the dielectric properties and then it is expected that a satisfactory composition will be found by interpolation of the data for the mixtures on hand. In the next report there will be a complete table of μ'/ϵ' ratios and magnetic and dielectric loss factors. It is anticipated that new mixtures will be provided for testing by then. Emphasis will be placed on the finding of a better binder instead of wax.

TABLE IV-1
(a)

f (MHz)	Q_{m_7}	$\tan\delta_{m_7}$	Q_{m_8}	$\tan\delta_{m_8}$	Q_{m_9}	$\tan\delta_{m_9}$	$Q_{m_{10}}$	$\tan\delta_{m_{10}}$	$Q_{m_{11}}$	$\tan\delta_{m_{11}}$
75	5.68	0.177	6.5	0.154	4.5	0.222	12.2	0.082	5.68	0.176
100	8.15	0.121	7.65	0.131	7.1	0.141	230	0.00435	11.4	0.0878
125	10.75	0.0915	3.86	0.259	3.18	0.314	4.0	0.25	23.0	0.0435
150	2.74	0.359	3.16	0.316	1.92	0.520	4.5	0.222	4.95	0.22
200	5.78	0.171	2.74	0.365	1.95	0.5125	3.735	0.268	3.73	0.268
250	6.32	0.156	2.145	0.465	1.07	0.925	2.92	0.342	4.48	0.223
300	14.3	0.069	2.14	0.467	1.14	0.88	1.92	0.52	3.18	0.315
350	2.14	0.46	1.43	0.70	1.565	0.64	1.665	0.6	2.36	0.425
400	3.74	0.263	1.035	0.965	1.915	0.5225	1.19	0.84	1.54	0.650

(b)

Composition	Al (gr)	Fe (gr)	Wax (gr)	Carbon Black (gr)
7	30	30	20	—
8	30	30	20	5
9	20	20	15	10
10	20	10	20	10
11	20	10	30	10

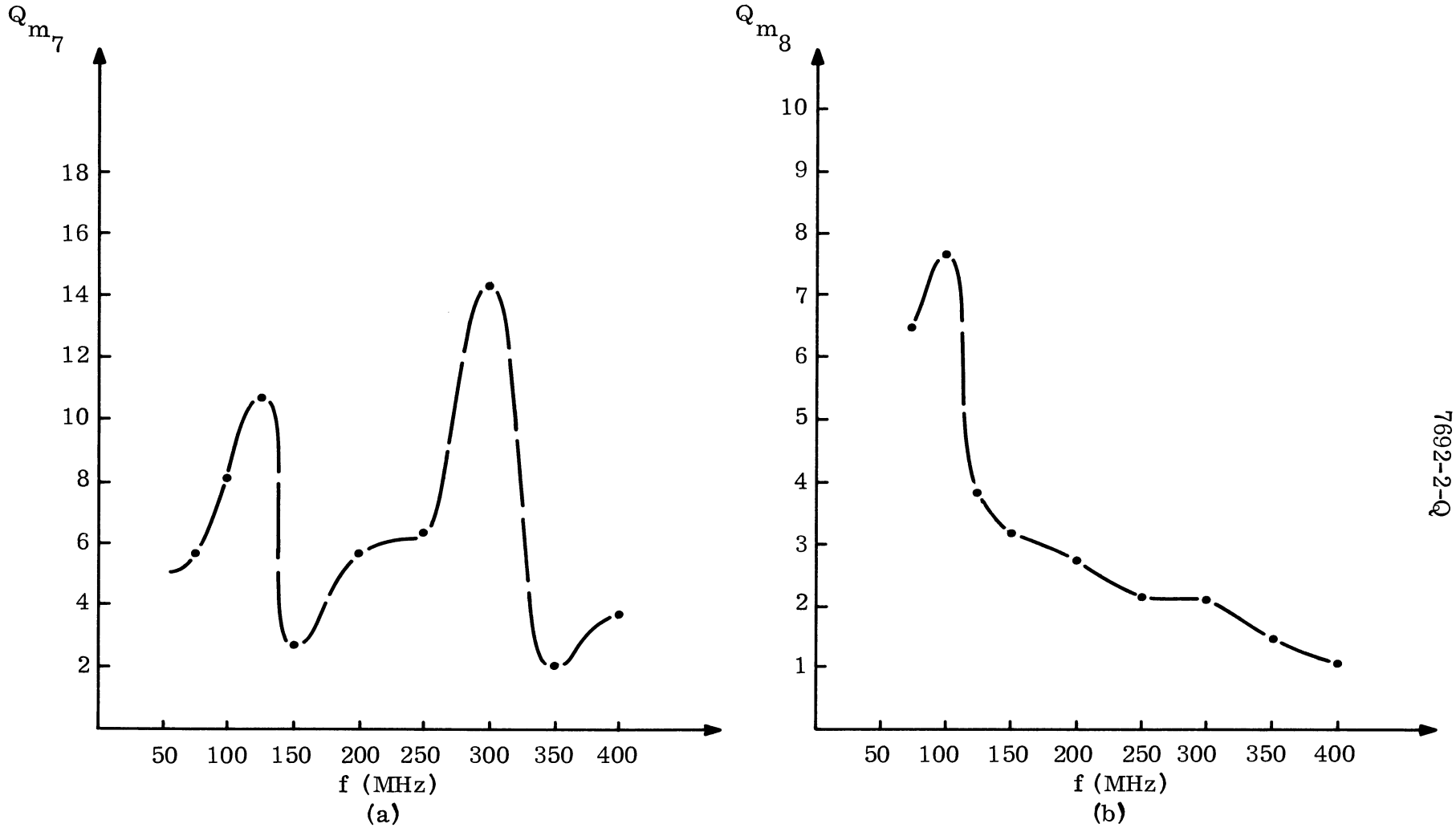

FIG. 4-1: SPECIMEN MAGNETIC Q VERSUS FREQUENCY

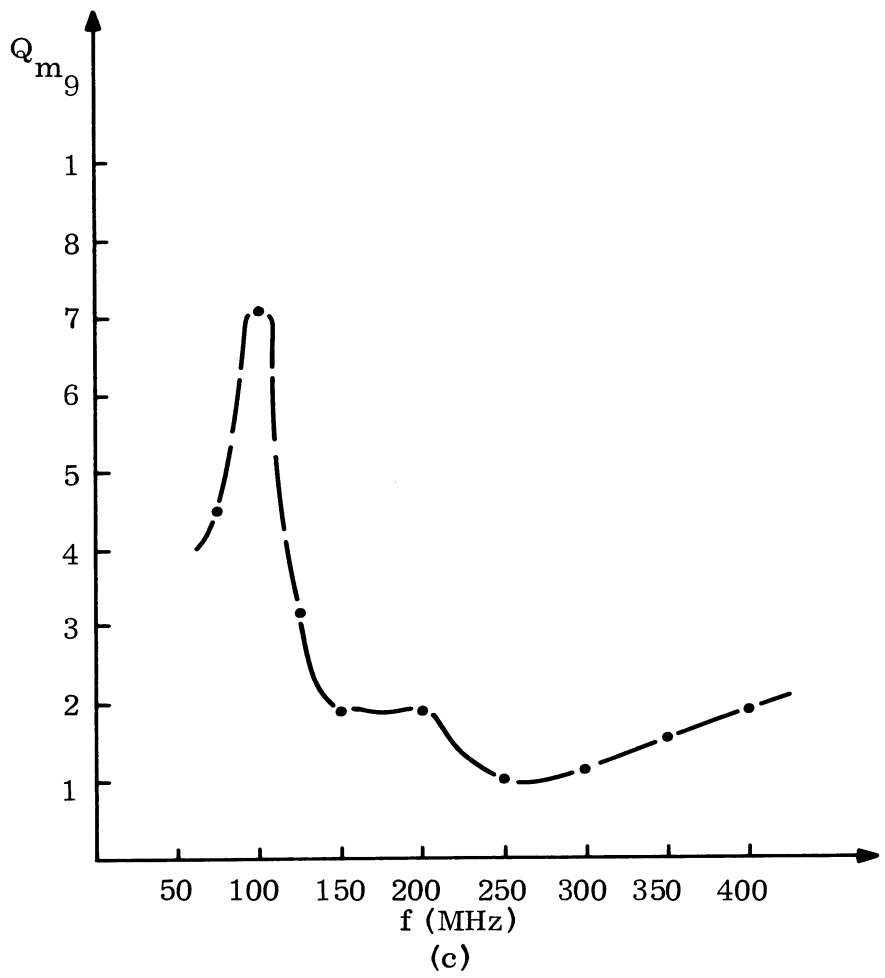

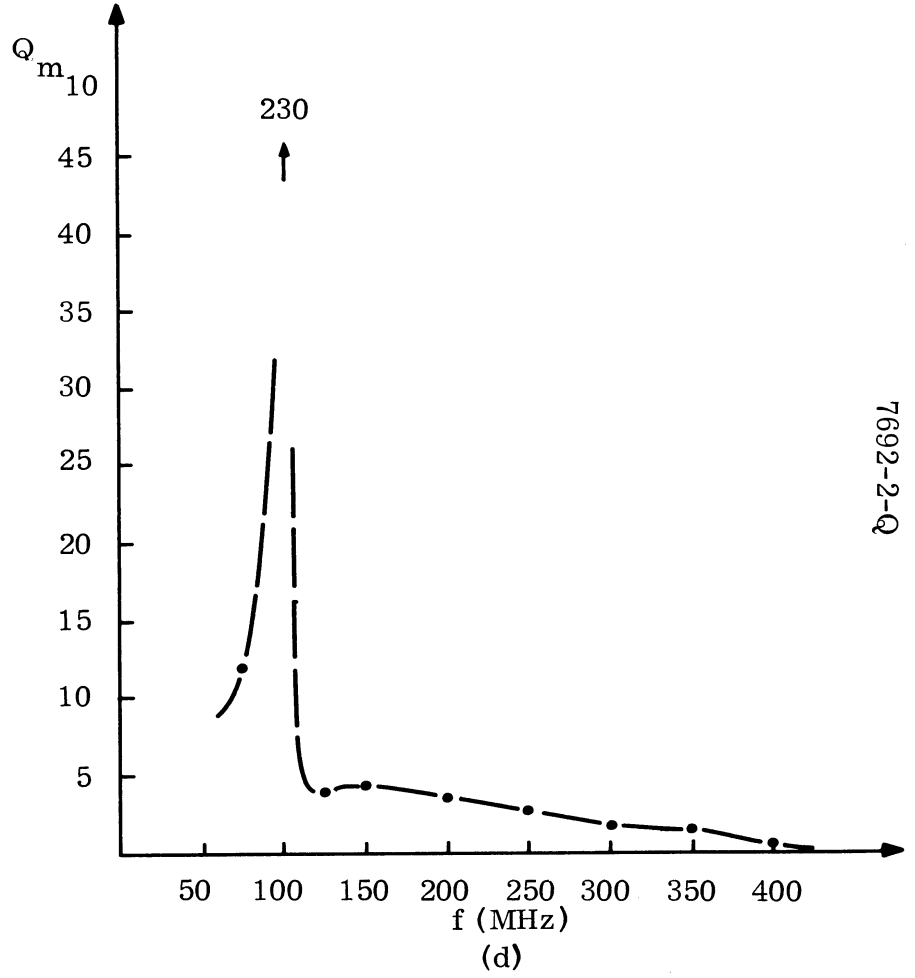

FIG. 4-1: SPECIMEN MAGNETIC Q VERSUS FREQUENCY

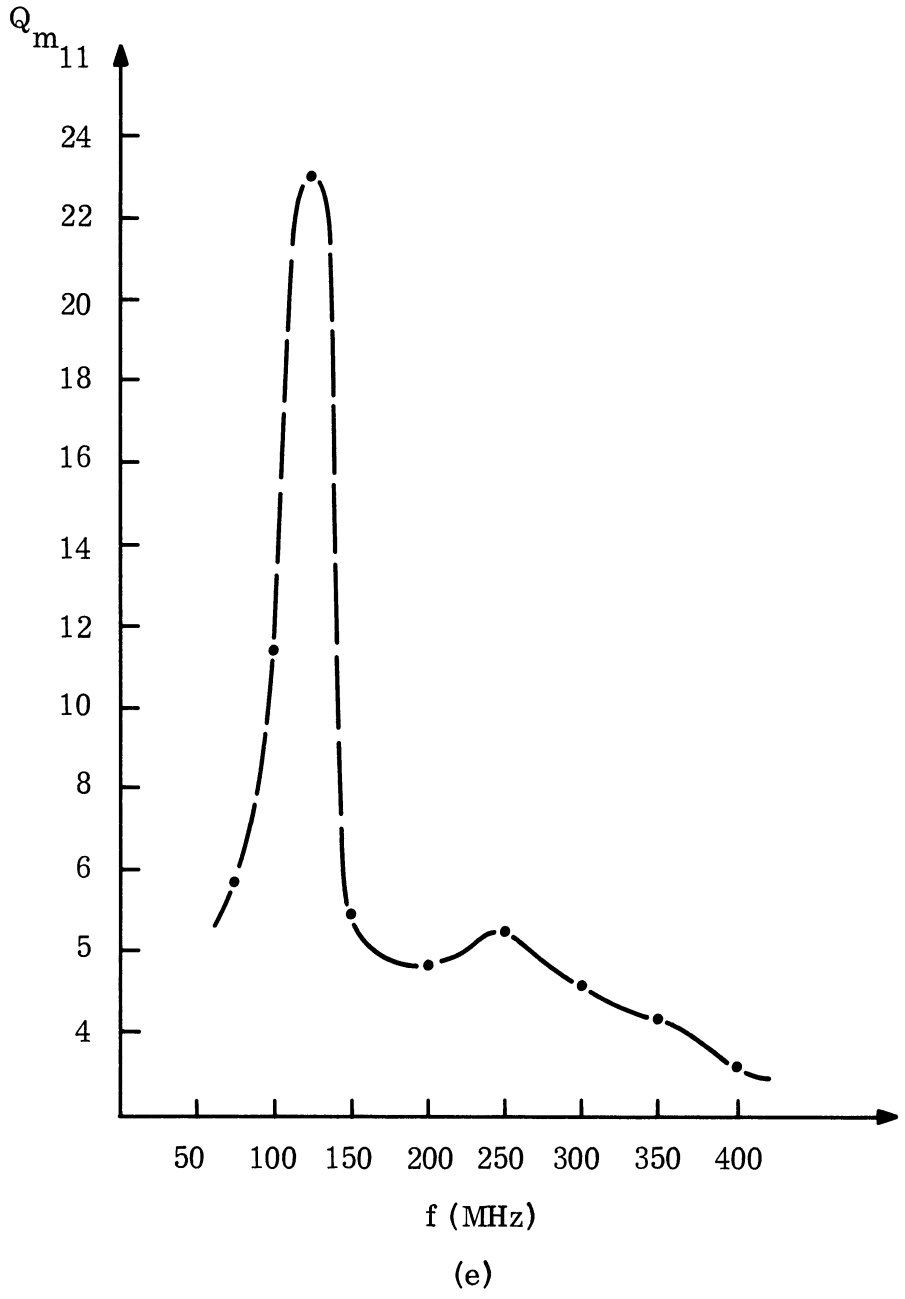

FIG. 4-1: SPECIMEN MAGNETIC Q VERSUS FREQUENCY

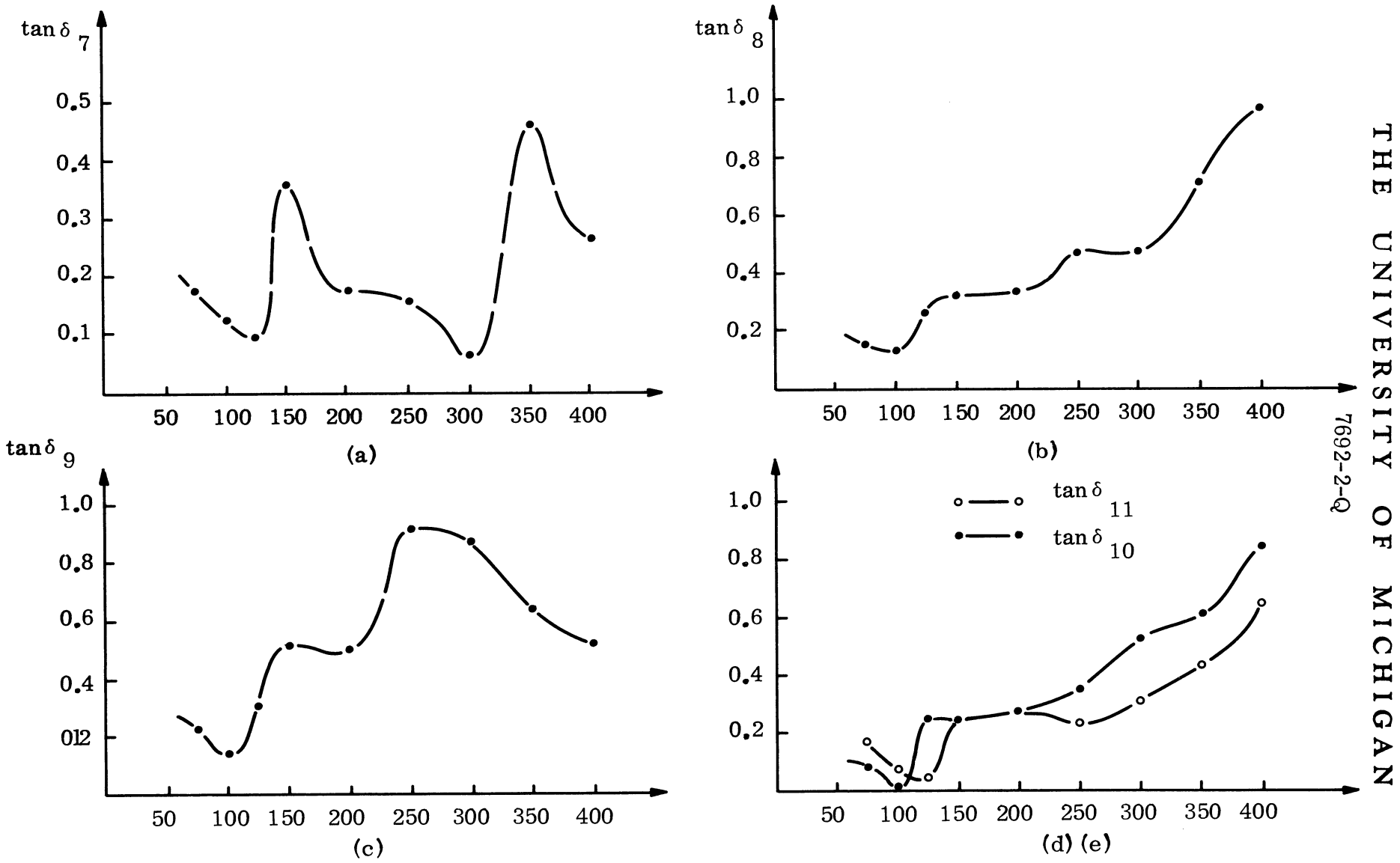

FIG. 4-2: SPECIMEN MAGNETIC LOSS TANGENT VERSUS FREQUENCY

V

CONCLUSIONS

The effort on increasing the isolation, to date, gives strong indications that merely having an intervening flush-mounted slab of lossy material is not a completely satisfactory solution. Only modest changes in coupling can be accomplished by such a slab. It is believed that the corrugated surface combined with the possibility of varying the depths of corrugation as well as the widths of corrugations will be effective. Also further combining this type of construction by loading with lossy material may prove a better solution in the decoupling problem. It is expected that the work on materials will be helpful in obtaining more optimal designs of any decoupling methods.

Early work indicates that the use of parasitic periodic elements offers some promise. It has further been observed that the depth of parasitic cavities or slots is very important as far as the dependence of coupling on frequency.

VI

FUTURE EFFORT

The effort planned for the future will include the use of RF bridge methods which will be adapted to broadband work. It is expected that several links will be made between two antenna systems each one of which will be suitable for one selected frequency. Such a system depends upon the destructive interference of the unwanted signal by feeding a certain portion of this signal around by a separate path. Properly proportioning these paths will enable each path to be optimized for a given frequency. In this way, it will be possible to make the decoupling have a stagger tuned characteristic much like that which is obtained in intermediate frequency amplifiers. It is expected that this technique will be helpful in the broadband decoupling which is very much needed.

Future effort will utilize the catalogue of materials which will show how needed electrical characteristics can be reasonably obtained through the use of simple mixes of materials. There appears to be little or no need for further effort on new material mixes.

A continuation of effects of corrugated metal surfaces will be made. Emphasis will be entirely on flush-mounted surfaces. A detailed study will be made of the depth and the width of the corrugations as well as of the cases where the corrugations are filled with lossy dielectric or ferrite materials.

Analytical work has been planned for the future dealing with the use of parasitic antenna elements as a means of increasing the isolation between two antenna systems. So far, parasitics have been studied entirely from an experimental viewpoint. It is believed that analytical work is necessary in order to more nearly approach expected optimum conditions for decoupling.

It is anticipated that the use of circumferential grooves and trenches will be extended. A new slot antenna with four such trenches has been fabricated; tests on this type of structure will be made in the near future.

ACKNOWLEDGEMENTS

Mr. Edward J. Rohan of The University of Michigan, Institute of Science and Technology, obtained part of the data on the coupling between two slots with ribbed structure between them.

REFERENCES

Elliott, R.S. (April, 1954), "On the Theory of Corrugated Plane Surfaces," IRE Trans. on Antenna and Propagation, Vol. AP-2, pp. 71-81.

Hurd, R.A. (December, 1954), "The Propagation of an Electromagnetic Wave Along an Infinite Corrugated Surface," Canadian Journal of Physics, 32, pp. 727-734.

UNCLASSIFIED

Security Classification

DOCUMENT CONTROL DATA - R&D

(Security classification of title, body of abstract and indexing annotation must be entered when the overall report is classified)

1. ORIGINATING ACTIVITY *(Corporate author)*

The University of Michigan Radiation Laboratory
Department of Electrical Engineering

2a. REPORT SECURITY CLASSIFICATION
UNCLASSIFIED

2b. GROUP

3. REPORT TITLE

Electromagnetic Coupling Reduction Techniques

4. DESCRIPTIVE NOTES *(Type of report and inclusive dates)*
Second Quarterly Report 15 February 1966 - 14 May 1966

5. AUTHOR(S) *(Last name, first name, initial)*

Lyon, John A.M., Alexopoulos, Nicholas G., Brundage, Donald R., Cha, Alan G.T., Digenis, Constantine, J., Ibrahim, Medhat A.H. and Kwon, Yong-Kuk.

6. REPORT DATE	7a. TOTAL NO. OF PAGES	7b. NO. OF REFS
May 1966	84	2

8a. CONTRACT OR GRANT NO.
AF 33(615)-3371

b. PROJECT NO.
4357

c.
Task 435709

d.

9a. ORIGINATOR'S REPORT NUMBER(S)
7692-2-Q

9b. OTHER REPORT NO(S) *(Any other numbers that may be assigned this report)*

10. AVAILABILITY/LIMITATION NOTICES Qualified requestors may obtain copies of this report from DDC This document is subject to special export controls and each transmittal to foreign governments or foreign nationals may be made only with prior approval of AFAB(AVPT), Wright-Patterson AFB, Ohio.

11. SUPPLEMENTARY NOTES

12. SPONSORING MILITARY ACTIVITY
Air Force Avionics Laboratory, USAF AFSC
Wright-Patterson AFB, Ohio 45433

13. ABSTRACT A detailed analysis is presented of a flush-mounted impedance strip which lies between a magnetic line source and a field point locating the aperture of a receiving antenna. In this analysis, the assumption has been made that the line source, and the impedance strip are each of infinite length. This analysis shows the influence of the surface impedance of the strip upon the coupling between the assumed magnetic source and a field point on the ground plane beyond the strip. The analysis clearly shows the desirability of having the surface impedance with a capacitive reactance characteristic. Some verification of this analysis has been obtained experimentally through the use of a flush-mounted corrugated metal obstacle between two antennas.

In this report, information is presented on the influence on radiation pattern of a given antenna, such as a slot or horn in the near presence of absorbing material. In some cases, the absorbing material is contained within the flare of the antenna. In other cases, the absorbing material is mounted flush in the surrounding ground plane. In still other cases, the absorbing material protrudes above the ground plane.

Results are reported upon a series of experiments using rectangular slot antennas where one or both of the antennas is surrounded by a choke trench. The trenches were circular in form. The depth of the trenches was chosen so as to offer a given type of reactance.

Work has continued during this period, on providing simple absorbing materials whose electrical characteristics can be varied according to specific need for isolation. A large number of mixes of absorbing materials were made and the electrical characteristics were obtained for each mix.

DD FORM 1 JAN 64 1473

UNCLASSIFIED

Security Classification

14. KEY WORDS	LINK A		LINK B		LINK C	
	ROLE	WT	ROLE	WT	ROLE	WT
Decoupling Absorbing Materials Corrugations						

INSTRUCTIONS

1. ORIGINATING ACTIVITY: Enter the name and address of the contractor, subcontractor, grantee, Department of Defense activity or other organization *(corporate author)* issuing the report.

2*a*. REPORT SECURITY CLASSIFICATION: Enter the overall security classification of the report. Indicate whether "Restricted Data" is included. Marking is to be in accordance with appropriate security regulations.

2*b*. GROUP: Automatic downgrading is specified in DoD Directive 5200.10 and Armed Forces Industrial Manual. Enter the group number. Also, when applicable, show that optional markings have been used for Group 3 and Group 4 as authorized.

3. REPORT TITLE: Enter the complete report title in all capital letters. Titles in all cases should be unclassified. If a meaningful title cannot be selected without classification, show title classification in all capitals in parenthesis immediately following the title.

4. DESCRIPTIVE NOTES: If appropriate, enter the type of report, e.g., interim, progress, summary, annual, or final. Give the inclusive dates when a specific reporting period is covered.

5. AUTHOR(S): Enter the name(s) of author(s) as shown on or in the report. Enter last name, first name, middle initial. If military, show rank and branch of service. The name of the principal author is an absolute minimum requirement.

6. REPORT DATE: Enter the date of the report as day, month, year; or month, year. If more than one date appears on the report, use date of publication.

7*a*. TOTAL NUMBER OF PAGES: The total page count should follow normal pagination procedures, i.e., enter the number of pages containing information.

7*b*. NUMBER OF REFERENCES: Enter the total number of references cited in the report.

8*a*. CONTRACT OR GRANT NUMBER: If appropriate, enter the applicable number of the contract or grant under which the report was written.

8*b*, 8*c*, & 8*d*. PROJECT NUMBER: Enter the appropriate military department identification, such as project number, subproject number, system numbers, task number, etc.

9*a*. ORIGINATOR'S REPORT NUMBER(S): Enter the official report number by which the document will be identified and controlled by the originating activity. This number must be unique to this report.

9*b*. OTHER REPORT NUMBER(S): If the report has been assigned any other report numbers *(either by the originator or by the sponsor)*, also enter this number(s).

10. AVAILABILITY/LIMITATION NOTICES: Enter any limitations on further dissemination of the report, other than those imposed by security classification, using standard statements such as:

(1) "Qualified requesters may obtain copies of this report from DDC."

(2) "Foreign announcement and dissemination of this report by DDC is not authorized."

(3) "U. S. Government agencies may obtain copies of this report directly from DDC. Other qualified DDC users shall request through

_____."

(4) "U. S. military agencies may obtain copies of this report directly from DDC. Other qualified users shall request through

_____."

(5) "All distribution of this report is controlled. Qualified DDC users shall request through

_____."

If the report has been furnished to the Office of Technical Services, Department of Commerce, for sale to the public, indicate this fact and enter the price, if known.

11. SUPPLEMENTARY NOTES: Use for additional explanatory notes.

12. SPONSORING MILITARY ACTIVITY: Enter the name of the departmental project office or laboratory sponsoring *(paying for)* the research and development. Include address.

13. ABSTRACT: Enter an abstract giving a brief and factual summary of the document indicative of the report, even though it may also appear elsewhere in the body of the technical report. If additional space is required, a continuation sheet shall be attached.

It is highly desirable that the abstract of classified reports be unclassified. Each paragraph of the abstract shall end with an indication of the military security classification of the information in the paragraph, represented as *(TS)*, *(S)*, *(C)*, or *(U)*.

There is no limitation on the length of the abstract. However, the suggested length is from 150 to 225 words.

14. KEY WORDS: Key words are technically meaningful terms or short phrases that characterize a report and may be used as index entries for cataloging the report. Key words must be selected so that no security classification is required. Identifiers, such as equipment model designation, trade name, military project code name, geographic location, may be used as key words but will be followed by an indication of technical context. The assignment of links, rules, and weights is optional.